# ASSESSING LONG-TERM AND SHORT-TERM SHORELINE CHANGE OF COCKSPUR ISLAND IN THE SAVANNAH RIVER ESTUARY

by

#### COLBY T. PEFFER

(Under the Direction of Clark Alexander)

#### **ABSTRACT**

The shorelines of Cockspur Island, GA are constantly responding to natural and anthropogenic forces. In the fall of 2015, dredge spoil was placed on the north shore to protect cultural resources from rapid erosion. This study assessed both long-term and short-term shoreline change trends occurring on the island and at the experimental beneficial-use dredge spoil site, using GIS and sUAV surveying, to inform adaptive management strategies. The north and south shorelines were dominantly erosional over 85 years, at rates of -0.47 m yr<sup>-1</sup> and -0.2 m yr<sup>-1</sup>, respectively, and the east shoreline was accretionary at +3.79 m yr<sup>-1</sup>. Based on a 0.5% per month volume loss rate over the 40-month period, the lifetime of dredge spoil placement is 14 years. However, because the elevation of the berm is decreasing as the deposit erodes landward, a shorter effective lifespan of 8 years is more likely.

INDEX WORDS: Shoreline change, beneficial-use, dredge spoil, UAV, shoreline nourishment, shoreline stabilization, cultural resource protection, Cockspur Island, Fort Pulaski National Monument, AMBUR

# ASSESSING LONG-TERM AND SHORT-TERM SHORELINE CHANGE OF COCKSPUR ISLAND IN THE SAVANNAH RIVER ESTUARY

By

## COLBY T. PEFFER

B.S., Humboldt State University, 2017

A Thesis Submitted to the Graduate Faculty of The University of Georgia in Partial Fulfillment of the Requirements for the Degree

MASTER OF SCIENCE

ATHENS, GEORGIA

2019

© 2019

Colby T. Peffer

All Rights Reserved

# ASSESSING LONG-TERM AND SHORT-TERM SHORELINE CHANGE OF COCKSPUR ISLAND IN THE SAVANNAH RIVER ESTUARY

By

COLBY T. PEFFER

Major Professor: Clark Alexander

Committee: Merryl Alber

Steven M. Holland Sergio Bernardes

Electronic Version Approved:

Ron Walcott Interim Dean of the Graduate School The University of Georgia December 2019

#### **ACKNOWLEDGEMENTS**

I would like to thank my advisor, Clark Alexander firstly, for the opportunity to intern for the summer in his lab at Skidaway Institute of Oceanography, and secondly, for the opportunity to come back as a graduate student, and further explore my passion for coastal science. This experience has set me on a path that I hope I will continue to enjoy and grow with throughout my career. Next, thank you to my committee members: Merryl Alber, Steven M. Holland, and Sergio Bernardes. My research project was much improved and expanded by their thoughtful feedback and guidance. Also, thank you so much to the Alexander lab, Claudia, Mike, Karrie and Christine. The hours of field work and analysis would have been impossible without them. And lastly, thank you to my family: Mom, Dad, Nick, and to my grandparents, without them cheering me on, I would not be here today.

## TABLE OF CONTENTS

Pa	ıge
ACKNOWLEDGEMENTS	iv
LIST OF TABLES	vii
LIST OF FIGURESv	⁄iii
NTRODUCTION AND LITERATURE REVIEW	. 1
1.1 Introduction	. 1
1.2 Literature Review	10
1.3 Thesis Objectives	11
METHODOLOGY	14
2.1 Study Sites	14
2.2 Historical Shoreline Change	17
2.3 Short-Term Nourished Shoreline Change	20
2.4 Drone Surveying and Processing	22
2.5 Areal Elevation Change	24

2.6	Shoreline Profile Change	24
2.7	Volume Change	25
2.8	Sediment Grain Size	26
RESULTS		28
3.1	Historical Shoreline Change	28
3.2	Short-term Nourished Shoreline Areal Elevation Change	30
3.3	Short-term Nourished Shoreline Profile Change	32
3.4	Short-term Nourished Shoreline Volume Change	35
3.5	Sediment Grain Size	37
DISCUSSI	ON	40
CONCLUS	SIONS	50
REFEREN	CES	52
TABLES A	ND FIGURES	57

## LIST OF TABLES

Page	•
Table 1: Digitized shoreline information for Cockspur Island, including imagery types, imagery	
source, digitizing and total shoreline error values57	7
Table 2: UAV flight parameters used in Pix4Dcapture iOS application58	3
Table 3: Results for shoreline change analysis using AMBUR transect data showing percent	
erosional and accretionary transects and shoreline change statistics	)
Table 4: Tidal datums and extreme water levels observed at Fort Pulaski	)
Table 5: Areal elevation change of the nourished northern shoreline of Cockspur Island from	
April 2015 to March 201961	l
Table 6: Volume change of the nourished northern shoreline of Cockspur Island from April 2015	
to March 201962	2
Table 7: Subsection A volume change of the nourished northern shoreline of Cockspur Island	
from April 2015 to March 201963	3
Table 8: Subsection B volume change of the nourished northern shoreline of Cockspur Island	
from April 2015 to March 2019.	1
Table 9: Subsection C volume change of the nourished northern shoreline of Cockspur Island	
from April 2015 to March 201965	5

## LIST OF FIGURES

Page
Figure 1. Map of Cockspur Island. Inset map (bottom left) shows location of Cockspur Island
relative to the Georgia coast66
Figure 2. Map of Cockspur Island AMBUR shoreline subregions
Figure 3. Map of Cockspur Island's nourished northern shoreline, with overlaid analysis, divided
into subsections A, B, and C68
Figure 4. AMBUR transects for Cockspur Island northern shoreline
Figure 5. End point rate (EPR) values for each transect of the northern shoreline, plotted by
shoreline analysis group70
Figure 6. AMBUR transects for Cockspur Island southern shoreline71
Figure 7. AMBUR end point rate (EPR) values for southern shoreline transects between 1933 to
201872
Figure 8. AMBUR transects for Cockspur Island eastern shoreline
Figure 9. AMBUR end point rate (EPR) values for eastern shoreline transects between 1933 to
2018

Figure 10.	Elevation change of the nourished northern shoreline of Cockspur Island comparing
	April 2015 to November 2015
Figure 11.	Elevation changes for the nourished northern shoreline of Cockspur Island from
	November 2015 to June 201776
Figure 12.	Elevation changes for the nourished northern shoreline of Cockspur Island from June
	2017 to July 2018
Figure 13.	Elevation Changes for the nourished northern shoreline of Cockspur Island from July
	2018 to August 2018
Figure 14.	Elevation changes for the nourished northern shoreline of Cockspur Island from
	August 2018 to September 201879
Figure 15.	Elevation changes for the nourished northern shoreline of Cockspur Island from
	September 2018 to October 2018
Figure 16.	Elevation changes for the nourished northern shoreline of Cockspur Island from
	October 2018 to December 201881
Figure 17.	Elvation changes for the nourished northern shoreline of Cockspur Island December
	2018 to February 2019
Figure 18.	Elevation changes for the nourished northern shoreline of Cockspur Island from
	February 2019 to March 201983
Figure 19.	Elevation changes for the nourished northern shoreline of Cockspur Island from
	November 2018 to March 2019

Figure 20. Map of elevation profile transect locations for Cockspur Island's nourished northern	
shoreline8	5
Figure 21. Elevation Profile Transect 18	6
Figure 22. Elevation Profile Transect 28	7
Figure 23. Elevation Profile Transect 38	8
Figure 24. Elevation Profile Transect 48	9
Figure 25. Elevation Profile Transect 59	0
Figure 26. Elevation Profile Transect 69	1
Figure 27. Elevation Profile Transect 79	2
Figure 28. Map of mean grain size, in phi, of the nourished northern shoreline on Cockspur	
Island, for January 20189	3
Figure 29. Map of grain size sorting of the nourished northern shoreline on Cockspur Island, for	
January 20189	4
Figure 30. Map of mean grain size, in phi, of the nourished northern shoreline on Cockspur	
Island, for December 20189	5
Figure 31. Map of grain size sorting of the nourished northern shoreline on Cockspur Island, for	
December 20189	6

Figure 32. Comparison of January and December 2018 sediment sample mean grain size at
reoccupied stations97
Figure 33. Change in mean grain size, in phi, on the nourished northern shoreline of on Cockspur
Island98
Figure 34. Change in grain size sorting on the nourished northern shoreline of Cockspur Island.
99
Figure 35. January 2018 sediment sample sorting values plotted against December 2018
sediment sample sorting values at the same location

### INTRODUCTION AND LITERATURE REVIEW

#### 1.1 INTRODUCTION

### Shoreline Change

Shorelines are the interface between terrestrial and marine environments. The position of a shoreline is dynamic because of the conditions that shorelines experience (*Boak and Turner*, 2005). Shorelines that are not currently in a state of equilibrium are evolving towards equilibrium (*Carter*, 1988). At this equilibrium, energy dispersion across the shoreline can be maximized. Processes that contribute to shoreline change include waves, winds, currents, bioerosion, sediment transfer, and changes in sea level (*Davis and Fitzgerald*, 2009). Wave and wind energies are increased during storm events, heightening the potential for changes in the shoreline. Estuarine shorelines develop in response to the additional forces of channelized river flow, expansion of residential and industrial development and their related infrastructures, and vessel wakes related to boating, shipping, and fishing (*Pye and Allen*, 2000). The aforementioned influences all affect the estuarine shorelines of the Georgia coast.

Shorelines can erode and accrete laterally and vertically, changing the elevation or extent of coastal habitats (*Cowart et al.*, 2010). Rates of erosion can be especially sensitive to changes in local sediment flux (*Carter*, 1988; *Doody*, 1996). Sea-level rise, which in the Savannah area of the Georgia coast is 3.25 mm yr<sup>-1</sup> (*National Oceanic and Atmospheric Administration*, 2018a), can also alter the extent of wave and tide energies, and is a key factor in determining the historical and future extent of a shoreline (*Doody*, 1996).

Shoreline extent is also influenced by direct anthropogenic modification. In areas of coastal development, a shoreline is often perceived by upland stakeholders as an inflexible line needing to be maintained as coastal development increases. The options available to maintain

these estuarine shorelines fall under a few different categories: strengthening shoreline defenses; accretion enhancement in front of the line; or redefining management strategies (*Doody*, 1996). Many of these options affect the sediment budget or the energy reaching the shoreline, or both (*Carter*, 1988). For example, armoring a shoreline can both stop the transfer of sediment and alter wave energy as it dissipates or reflects against a bulkhead, groin, or jetty.

Anthropogenic influences can also indirectly modify shorelines by humans changing the sediment supply. These changes include altering sediment loads in runoff from agriculture or upland development, modifying river flow through damming or removal of dams, or dredging channels (*Juliean*, 1995; *National Research Council*, 1995). Agricultural modification of forested land can decrease soil stability, increasing sediment runoff into watersheds. Dams and reservoirs are estimated to currently hold approximately 20% of the global sediment load, and prevent much of it from reaching estuaries and coasts, where it is necessary for building and maintaining marshes (*Kirwan and Megonigal*, 2013). Dredging and channel deepening can also increase suspended sediment concentrations within the water column and change tidal dynamics within an estuary, both of which vary rates of shoreline erosion or accretion (*van Maren et al.*, 2015). Vessel wake, ranging from small power boats to large cargo ships, and the creation of jetties, bulkheads, revetments, breakwaters and groins can also alter the wave energy experienced by the shoreline (*Carter*, 1988; *National Research Council*, 1995).

Large populations live in coastal regions for their aesthetics and economic value (*Davis and Fitzgerald*, 2009). According to the 2010 U.S. Census, over 1 million people, almost 11 % of the state's population, lived in Georgia's coastal counties (*U.S. Census Bureau*, 2010). With such a high coastal population, shoreline change can threaten coastal development and infrastructure needed in coastal municipalities such as residential and industrial buildings, roads,

waste treatment plants, and medical and emergency facilities. Further, it routinely threatens the existence of irreplaceable prehistoric, historic, and cultural sites. These threats present a need for comprehensive coastal zone management, where assessments of lateral shoreline change have "historically been a primary planning tool for coastal scientists, engineers and managers" to gain understanding of shoreline movement in natural and developed areas (*Dolan et al.*, 1991).

Shorelines can be delineated using a variety of sources including historical maps, aerial images, topographic surveys, light detection and ranging (LiDAR) surveys, and satellite imagery. Historical aerial imagery is most commonly used for historical shoreline change evaluations because of their widespread availability from federal and state agency survey efforts (*Boak and Turner*, 2005; *Cowart et al.*, 2010). Ideally, lateral shoreline movement is measured over the course of many years to achieve a rate of erosion or accretion that transcends seasonal or episodic changes (*Carter*, 1988). Erosional conditions also often vary along a shoreline due to alongshore composition differences and wave height variability, highlighting the importance of inter-regional documentation of shoreline character and change (*Alexander*, 2016; *Carter*, 1988).

## Beneficial Use of Dredge Material

Where sediments accumulate in response to natural and anthropogenic effects determines where navigation can safely occur. Safe and navigable channels leading to ports and harbors are essential for coastal economic sustainability. To retain the navigability of these channels, maintenance dredging is commonly performed. Typically, dredge spoils are disposed at sea or in upland sites. In estuarine systems, this management approach means valuable sediment is being permanently removed from the environment. Estuarine systems that lack a sufficient supply of sediment can experience increased loss of elevation and erosion of estuarine shorelines (*Kirwan and Megonigal*, 2013). Dredging is also seen in a negative light for other reasons such as habitat

disturbance and water column pollution by suspended sediment, heavy metals, or organic micropollutants (*Goossens and Zwolsman*, 1996; *van Maren et al.*, 2015). However, dredging is often unavoidable in today's economic and industrial environments.

As a method for preventing erosion on shorelines, beach nourishment is defined as a method of soft stabilization because it does not involve hard structures along a shoreline. Nourishment has a short lifetime as a shoreline protection method, as it will eventually erode away without continued maintenance, the speed of which varies by the size of the nourishment and the energy dynamics of the environment. Despite it being a non-permanent solution to shoreline erosion, it is now considered a primary method for shoreline protection (Dohner and Trembanis, 2017; National Research Council, 1995; Nordstrom, 2005). Beach nourishment is expensive, estimated to have cost over \$100 million annually on the East Coast alone in 1996, and the sand material itself is a valuable and difficult-to-obtain resource (Dohner and Trembanis, 2017). Between these two issues, finding alternatives to traditional beach nourishment sources is paramount to continuing shoreline maintenance (Dohner and Trembanis, 2017). If dredge spoil were to be treated as a resource for community benefit and as a more affordable source for soft stabilization, rather than as a disposable by-product of channel maintenance, beneficial-use renourishment projects could become more prevalent with further research and technology development (Dohner and Trembanis, 2017; McVeigh, 2018).

Key research pursuits for future beneficial-use dredge spoil projects include costfeasibility and effectiveness of the shoreline stabilization for specific projects. Within the focus of cost-feasibility, longevity of a nourishment and effectiveness of natural and cultural resource protection must be evaluated. Longevity is also important because stakeholders must be able to align the timeline of dredge-spoil supply and nourishment maintenance for projects to be beneficial and cost-saving for both the supplier as well as the receiver of dredge spoil (*U.S. Environmental Planning Agency, U.S. Army Corps of Engineers*, 2015).

## Shoreline Change Analysis

Shoreline change is typically studied using a transect-based methodology that evaluates lateral shoreline movement based on multi-year shoreline intersections with shore-perpendicular transects (*Crowell et al.*, 1991; *Dolan et al.*, 1991; *Romine et al.*, 2009). The analysis is affected by the following considerations: temporal variability of the shoreline; how many shoreline positions are used; the temporal proximity of shoreline measurements; the time period being analyzed; and the method used to calculate the rate of change (*Dolan et al.*, 1991).

A few Geographic Information Systems (GIS)-based programs have been created to automate the transect-based analysis of shoreline change. Digital Shoreline Analysis System (DSAS) is a ESRI ArcGIS extension available through the United States Geological Survey (USGS) that performed transect-based analysis of shorelines and computes rate of change statistics (*Thieler et al.*, 2009). BeachTools was created for ESRI's ArcView, and allowed for automatic delineation of shorelines and transect-based change analysis within a suite of other coastal feature analysis tools (*Hoeke et al.*, 2001). Simple Change Analysis of Retreating and Prograding Systems (SCARPS) is an extension written for ESRI's ArcView to analyze shoreline movement (*Jackson*, 2004). All the aforementioned programs required a license to ESRI's ArcGIS or another commercial GIS program at the time of their creation (*Jackson et al.*, 2012). Further, most were not capable of accurately assessing complex and highly curved shorelines.

Analyzing Moving Boundaries Using R (AMBUR) was created to provide an opensource shoreline change analysis option to succeed SCARPS (*Jackson et al.*, 2012). While the AMBUR package requires inputs of GIS-based file formats (shapefiles), these can be created in any GIS program, including open-source options such as GRASS and QGIS (*QGIS Development Team*, 2019; *GRASS Development Team*, 2017). The processing of the shoreline change is done in R, an open-source statistical computing software (*R Core Team*, 2017). Because the package tracks changes in boundary locations, it can be used to measure any sort of moving boundary, not just shorelines. AMBUR also fundamentally advanced shoreline change analysis through its ability to filter transects so they do not overlap; this technique has now been more widely implemented in other programs as well.

The first step in shoreline change with these programs is to digitize, or trace, the shorelines of different time periods from georeferenced, georectified aerial images or maps. The second is to establish seaward and landward baselines that encompass the entire shoreline set, which are created using the Buffer tool on the shoreline files using a GIS program. From these baselines, perpendicular transects are cast from the seaward baseline to the landward baseline. The intersections of the transects and shorelines are used to quantify values and statistics of shoreline change.

Several different metrics have been used in previous work to characterize shoreline change trends. The most common metric is the *net change* that has occurred during the time period being analyzed. In the context of determining *rates* of shoreline change, the end point rate (EPR) is the most common method (*Cowart et al.*, 2010; *Dolan et al.*, 1991; *Jackson et al.*, 2012; *Romine et al.*, 2009). The EPR is the shoreline change rate, typically in meters per year (m yr<sup>-1</sup>), assessed between the oldest shoreline and the youngest shoreline at each transect. The mean EPR is the mean of all transect EPRs along a shoreline. Because the mean net change and the mean EPR calculations average all of the transects along a shoreline, these metrics can be influenced by transects that alternate between erosion and accretion that cancel each other out. The rates for

armored sections, when averaged with change rates of natural shorelines sections, can also reduce the overall averages. This problem can be partially remedied by separating natural and anthropogenically modified shorelines and analyzing them independently.

## **Drone-based Shoreline Monitoring**

Because of the expense of flying manned aerial surveys and obtaining tasked satellite imagery, shoreline datasets are often acquired less frequently than needed to determine changes from episodic and storm events (*Clark*, 2017). This is not a problem when the short-term behavior of the shoreline is already known or not considered more important than long-term trends. However, to understand the short-term behavior of a newly created environment such as a nourished beach, the frequency of data collection must be high enough to capture episodic and storm events.

For renourishment sites, determining erosion and volume changes on seasonal and annual timescales is necessary to characterize the longevity and effectiveness of the nourishment.

Drone, or small unmanned aerial vehicle (sUAV), surveying is a fairly new method with which to monitor shoreline changes on these shorter timescales (*Casella et al.*, 2016).

Acquiring high frequency digital surface models (DSMs) from which to obtain volume and elevation changes over time requires collecting imagery that can be processed using a photogrammetric technique termed "Structure-from-Motion" (SfM). SfM uses overlapping, oblique images taken from a wide array of positions and motion signatures from the moving camera to resolve three-dimensional structure (*Lillesand et al.*, 2007; *Westoby* et al., 2012). These images are then processed using a bundle block adjustment, which identifies key features from the overlapping images and builds a point cloud of the feature. Ground control identified in the imagery serves the function of transforming and georeferencing the point cloud into real-

world object space (*Westoby et al.*, 2012). Surfaces created by drone surveying and processing of high-overlap, high-resolution images using SfM techniques, given adequate ground control, now surpasses the vertical accuracy of surfaces produced using manned aerial LiDAR, which is typically ± 15 cm elevation in relatively vegetation-free areas. In Clark (2017), quadcopters were able to survey a coastal cliff edge resulting in DEMs with vertical accuracies within less than 3 centimeters compared to GNSS surveying, and able to delineate a shoreline from processed imagery within 0.04 meters, which also included digitizing error. Gonçalves and Henriques (2015) get even higher accuracy of sandy coastal spits of 0.01–0.02 meters in elevation inside of the boundary of ground control points. Obtaining high-accuracy surface elevations using these SfM methodologies makes volumetric assessments of coastal regions highly feasible.

Drones also have the benefit of being light, cheap, and quick to deploy, making it easier to acquire data before and after episodic events, such as severe storms (*Clark*, 2017; *Colomina and Molina*, 2014; *Gonçalves and Henriques*, 2015). Drone photogrammetric surveying provides the capability to develop high-resolution DSMs to extend shoreline change analysis beyond lateral movement, into a three-dimensional analysis (i.e., to include changes in elevation and volume). *Dohner and Trembanis* (2017) demonstrated the use of sUAV and SfM techniques to analyze changes at a beneficial-use site at Broadkill Beach in Delaware Bay. In their case study, erosional events were identified through the rapid deployment of a sUAV before and after storms. Volume changes were identified on the order of hundreds to tens of thousands of cubic meters of sand and were mainly erosional in nature (*Dohner and Trembanis*, 2017).

## Cockspur Island

Cockspur Island, located in the Savannah River estuary near the river mouth, is an area currently being affected by extensive shoreline change (Figure 1). The island is managed by the

National Park Service as a part of Fort Pulaski National Monument. Fort Pulaski, completed in 1839, is located on the eastern portion of the island, and is best known for its role during the Civil War, when it was first occupied by the Confederate Army and subsequently surrendered to the Union forces after a short battle in April 1862. After the Fort was taken by Union forces, it became a refuge for freed low-country slaves after the Emancipation Proclamation by President Lincoln.

After the Civil War, the fort was abandoned as a defensive structure and transferred to the U.S. Army Corps of Engineers (USACE) in 1884. In 1896, the USACE finished the construction of a jetty that extends from the northeastern tip of island along the Savannah River north channel to improve navigation and reduce shoaling of the north channel (Figure 2). This jetty still exists today. The USACE continued to dredge the Savannah River and deposited dredge spoil on Cockspur Island and to the south of the northeast jetty, increasing its overall extent.

Fort Pulaski was established as a national monument in 1924 and was transferred to the National Park Service (NPS) in 1932. Fort Pulaski's administrative history is documented in *Meader* (2003). By 1959, the national monument included the majority of Cockspur Island. Even after the transfer of the island to the NPS, the USACE continued to deposit dredge spoil on the northern shoreline, destroying salt marsh habitat and threatening the historical structures located there. The NPS ultimately put an end to regular use of Cockspur Island for spoil placement in the 1960s.

The monument includes several historic structures that are threatened by erosion and relevant to this project: the North Pier, a remnant of the original construction village that housed workers while they were building the Fort (Figure 2); Battery Hambright, built in the Spanish-American War, just 50 meters behind the North Pier (Figure 2); and the Cockspur Island

lighthouse, which was originally completed in 1848, destroyed by a hurricane, and rebuilt in 1854. Non-historical structures of note on the island include the Savannah Pilots' facilities and wharf, and the U.S. Coast Guard Station Tybee (Figure 1). The Savannah Pilots lease a 0.7-acre lot along the northern shoreline of the island and provide piloting services to cargo ships entering and leaving the Port of Savannah. Both facilities are fronted by a continuous riprap bulkhead, which was built and backfilled with dredge spoil in the early 1970s (*Alexander*, 2008) (Figure 2). The Savannah Pilots' large, high-displacement vessels regularly transport pilots to and from the cargo ships at sea.

#### 1.2 LITERATURE REVIEW

The Savannah River is currently in the process of being deepened to allow larger, postPanamax cargo ships to enter the Port of Savannah. These ships have a larger draft, width, and length than cargo ships frequenting the Port before deepening. A study by Maynord (2007) concluded that these larger ships would increase bow and stern wakes along the Savannah River's north channel. In response, Houser (2010) studied the wind and vessel-generated wave impacts to the northern shoreline of Cockspur Island to determine whether the potential rise in wave energy would affect erosion rates at Fort Pulaski. The study concluded that the vessel-generated waves were most effectively putting force on the marsh scarp at high tide, in the absence of storm tides, and accounted for 25% of the total wave force actively eroding the scarp on the northern shoreline. They estimated that an increase in the channel depth could lead to an 8% increase in wave force generated by cargo ships, equating to about 0.04 meters of additional retreat marsh per year.

Alexander (2008) used historical imagery and maps to evaluate shoreline change on Cockspur's northern shoreline from 1852 to 2005. The northern shoreline was accretionary up

until the 1940s due to dredge spoil deposition on the island. There was also some accretion in the 1950s and 1960s, which was found to be the result of a dike and ditch construction project that remobilized sediment that then became available for marsh shoreline building. After this point, the northern shoreline became dominantly erosional. The study also found that migration of an oyster shell ridge along the northern shoreline had increased the rates of erosion as the ridge moved alongshore. The shell ridge migrated westward and landward, degrading the marsh over which it moved. As the oyster shells migrated farther west, the emergent, now-denuded marsh edge was again affected by erosion from ship wakes and wind waves. Since the 2008 study, the oyster shell ridge has moved out of the intertidal region near the North Pier, but erosion of the marsh edge continued. In contrast to the dominantly erosional northern shoreline, the *Alexander* (2008) study showed that the southern shoreline was 13% erosional and 87% stable. The eastern shoreline was mostly accretionary; in general, progradation rates increase from south to north along the eastern shoreline.

### 1.3 THESIS OBJECTIVES

With the USACE no longer depositing dredge spoil on the north shoreline of Cockspur Island, extensive erosion has occurred on the shoreline that, in the last few decades, has begun to threaten the North Pier and Battery Hambright (*Alexander*, 2008; *Van Westendorp*, 2005).

Because of this threat, the National Park Service partnered with the USACE to nourish a section of the northern shoreline immediately in front of the North Pier using high-quality dredge spoil to create a defensive berm. The nourishment was performed in September and October 2015 and spanned from the northeastern jetty west to the armored shoreline section in front of the Savannah Pilots' and U.S Coast Guard facilities. The nourishment material was derived from maintenance dredging of the Savannah River shipping channel and would have normally been

placed in an offshore disposal site for dredged material, or on upland disposal sites adjacent to the shipping channel, in the absence of the beneficial-use project (*Bell*, 2019).

This project is part of an examination of the beneficial use of dredge spoil in an effort to reduce dumping of dredge spoil in upland disposal sites, and instead using these high-quality sand resources for community benefit. There is little research to determine the effectiveness and consequences of renourishment efforts in estuarine areas, as most such efforts are focused on ocean-facing sandy beaches. In addition, most work has focused on replenishment efforts of existing resources rather than studying newly-created environments (*Nordstrom*, 2005).

Beneficial-use dredge spoil projects may become more common as one way to effectively manage shoreline erosion, thus research evaluating these exploratory projects is essential to informing the future use of dredge spoil for community benefit.

The purpose of this research, in its broadest sense, is to understand the dynamics of shoreline change on Cockspur Island on both short and long timescales. The character of change in this region is important for future management strategies for the North Pier and Battery Hambright. Considering the low-lying nature of the salt marsh habitat and the proximity of historic structures to the shorelines, management of both is highly dependent on understanding historical, current, and potential future shoreline change trends.

This study used two methods of analyzing shoreline change. First, for the long-term (85-year) analysis of shoreline trends of the northern, southern, and eastern shorelines, historical maps, aerial imagery and pedestrian surveys were used to delineate shorelines and analyze lateral movement from 1933 to 2018. Second, for the short-term (monthly to annual) dynamics of the nourished northern shoreline, an sUAV, or drone was used to collect high-resolution, high-overlap imagery on approximately monthly timescales spanning from July 2018 to March 2019.

This imagery was processed into high-resolution DSMs and compared to topographic and bathymetric data taken before and after the 2015 USACE nourishment, as well as to LiDAR data taken approximately 19 months after the nourishment. This second part of the study analyzed volume and elevation changes as opposed to lateral shoreline movement.

Together, these methods provide insight into both the long and short-term dynamics of change occurring on Cockspur Island's shores, including the performance of the protective berm placed to prevent erosion at the site of the North Pier. Significantly, this study provides information and guidelines for both local and regional agencies that add to their ability to effectively implement the beneficial use of dredge spoil in estuarine habitats.

#### **METHODOLOGY**

#### 2.1 STUDY SITE

Cockspur Island is located in a dynamic environment in the Savannah River estuary. As a low-lying marsh island at the mouth of the Savannah River, it experiences a wide-range of physical energy. The estuary is mesotidal, with semidiurnal tides, and spring high tides up to 2.6 meters above mean lower low water (MLLW)(Clayton et al., 1992). Fetch is limited, except from the Northeast, where wind waves and ocean swell propagate from the Atlantic Ocean, and from the northwest, where wind waves propagate downriver (Clayton et al., 1992). During the period of this study, the island experienced effects from four hurricanes: Hurricane Matthew in 2016; Hurricane Irma in 2017; Hurricanes Florence and Michael in September and October of 2018, respectively; and from 4 other tropical storms (*National Weather Service*, 2019). Hurricane Matthew, which was a Category 1 hurricane when it reached Georgia's coast, impacted Fort Pulaski most significantly. Storm surge inundation for this storm event was recorded at 1.5 meters (5.1 ft) above mean higher high water (MHHW) at the Fort Pulaski National Ocean Survey tide gauge, which was a record high (Stewart, 2017). This event flooded the majority of the low-lying island and caused significant damage and the prolonged closure of the national monument. The North Pier sits at approximately 0.9 meters (3.1 ft) above MHHW, indicating that the North Pier was flooded by approximately 0.6 meters of water during this storm event.

## Cockspur Island Northern Shoreline

The northern shoreline of Cockspur Island comprises the south shore of the north channel of the Savannah River (Figure 1). It is divided into four sections, described from west to east: a natural, marsh-fronted section; an armored, rip-rap section; a nourished, sandy section; and a section fronted by the northeast jetty. The shoreline experiences a variety of physical energy. Wakes from container vessels entering and leaving the Port of Savannah, commercial fishing vessels, the Savannah Pilots' transport vessels, U.S. Coast Guard vessels, and recreational boats impact the shore at all stages of the tide. Further, this shoreline is also exposed to the wind waves and ocean swell generated off the coast which propagate into the lower estuary. The entire shoreline historically consisted of salt marsh but has been anthropogenically modified over time. The northeastern tip of the island is partially protected by a jetty (Meader, 2003). In contrast to the riprap bulkhead in front of the Savannah Pilots' and U.S Coast Guard facilities, the jetty on the northeastern tip of the island has not succeeded in stabilizing the shoreline. The salt marsh directly behind the jetty is still affected by wave energy at high tide and during storm events, and some salt marsh retreat south of the jetty is apparent. The western end of the shoreline is unarmored salt marsh, and is directly exposed to wave, tidal, and wake energy during high tide. Historically, the westernmost tip of the island connected with Long Island, the island immediately upriver from Cockspur Island. The connection between the two islands has narrowed over time by erosion along the north channel until 2008, when the island breached. The channel between Cockspur and Long Islands has been widening since that time and is currently over 300 meters wide.

## Cockspur Island Nourished Northern Shoreline

The section of the northern shoreline nourished by the USACE in September and October 2015 is located between the northeastern jetty and the armored section fronting the Savannah Pilots' and U.S. Coast Guard facilities (Figure 1), and just north of Battery Hambright and the North Pier (Figure 2). In 2005, approximately 50 meters of salt marsh formed a buffer between the North Pier and the channel (*Van Westendorp*, 2005). By 2014, the salt marsh had completely eroded away, leaving the North Pier directly exposed to tidal flooding and wave attack. Further erosion threatened the stability of and access to both the North Pier and Battery Hambright in the absence of human intervention.

To protect these structures, dredge spoil was placed by the USACE in September and October 2015. The dredge spoil was deposited in a shore-parallel berm, providing a barrier between the river and the North Pier. The sand flats that are located west and northeast of the defensive berm flood with each high tide. An ephemeral pond exists in a depression directly in front of the North Pier and behind the berm, and its extent varies with tidal flooding and precipitation. The pond is inundated during high tide through a shore-parallel channel between the sand berm and remaining marsh. The channel was created during the nourishment to provide tidal flow to the remaining salt marsh habitat behind the berm (*personal communication, Laura Waller, Cultural Resources Specialist, Fort Pulaski National Monument,* 2018). The channel floods from the west side of the nourished area, around the western crest of the berm. Between February and March 2019, a smaller, shore-perpendicular channel opened across the berm approximately 50 meters northeast of the North Pier, creating a more direct route to the pond.

## Cockspur Island Southern Shoreline

The southern shoreline of Cockspur Island comprises the northern shore of the south channel of the Savannah River (Figure 1). This channel has not been dredged for navigation since the mid-1800s. Its main use is by recreational and small fishing vessels. A bridge spans from Highway 80 to the southern shore of Cockspur Island. The bridge footings on Cockspur Island's southern shoreline are surrounded by rip-rap. The rest of the shoreline is unarmored but has been modified by drainage channels, which are part of the island's interior dike system.

## Cockspur Island Eastern Shoreline

The eastern shoreline of Cockspur Island faces the Atlantic Ocean and the northern tip of Tybee Island. It consists of expansive, low-lying salt marshes. Dredge spoil was historically deposited immediately south of the northeastern jetty, and sediment has also accreted on the eastern shoreline because the northeastern jetty creates a quiescent, sheltered environment. Thus, the northern section of the shoreline extends farther seaward than the southern section of the shoreline.

## 2.2 HISTORICAL SHORELINE CHANGE

Shoreline change rates were calculated using the AMBUR software package (*Jackson et al.*, 2012). Shoreline change was evaluated independently for the northern, southern, and eastern shorelines (Figure 2). The northern shoreline analysis was divided into three separate groupings to gather information on the behavior of the various shoreline segments: the first analysis included all shorelines and transects; the second included only shoreline transects that were on unstabilized sections of the shore; and the third analysis included only shoreline transects in the stabilized region in front of the Savannah Pilots' and U.S. Coast Guard facilities (Figure 2). The

northeastern jetty was included in the second analysis, but not the third analysis because shoreline retreat has been observed behind the jetty.

This shoreline change analysis has 11 shorelines, ranging in time from 1933 to 2018 (Table 1). Sources include National Ocean Service (NOS) T-sheets and controlled aerial imagery from NOS, the United States Geological Survey, the Savannah Area GIS (SAGIS) program, and the National Aerial Photography Program (NAPP). A geographic positioning system (GPS) ground survey was conducted in this project to provide the shoreline in 2017. All imagery was procured from the Skidaway Institute of Oceanography Coastal Georgia Image Archive.

I used several methods for shoreline delineation depending on the shoreline characterization of the region and the imagery source. For salt marsh areas, I used the vegetation line (typically in images taken at low tides) or the vegetation-water interface (typically in images taken at higher tide) delineated the shoreline (*Romine et al.*, 2009). For sandy areas, the visible wet-dry line delineated the shoreline. On NOS T-sheets, the high water mark (HWM) was used to delineate the shoreline (*Crowell et al.*, 1991). For areas with shoreline armoring, I used the crest of the structure to delineate the shoreline. For the digitized shoreline that includes the northeastern jetty, I used either the jetty's crest as the shoreline delineation if vegetation was directly adjacent to the crest or the visible edge of vegetation if the vegetation line had identifiably retreated back from the jetty (due to jetty disrepair). I digitized the shorelines were at scales ranging from 1:1,500 to 1:500. I then attributed the shorelines with their year and accuracy, and for the northern shoreline of Cockspur Island, with either "stabilized" or "unstabilized" as well.

Analysis of shoreline change is limited by the accuracy and resolution of the shoreline's source data, (i.e. the raw aerial images, maps, or DSMs from which it is derived), as well as the

accuracy of the shoreline digitization itself (*Dolan et al.*, 1991). To evaluate the analysis error of shoreline change using AMBUR with hand-digitized shorelines, the following factors must be considered: accuracy of the rectification of maps and aerial and satellite imagery used to delineate the shoreline; the resolution of the source map or imagery; and the accuracy of the shoreline digitizer (*Crowell et al.*, 1991; *Dolan et al.*, 1991; *Romine et al.*, 2009).

The accuracy of the source data used for shoreline delineation differs between maps and aerial imagery. Maps and NOS T-sheets are subject to plotting error derived from the surveyor's initial plotting of the high water mark (HWM) ( $E_{ts}$ ). The estimated plotting error for maps and tsheets derived from aerial imagery (after 1930) is 5.1 meters (Romine et al., 2009). The aerial and satellite imagery rectification error was determined during georectification in ESRI ArcMap 10. During georectification, 10-15 ground control points (GCPs) (typically manmade, permanent objects such as corners of structures and road intersections) were used to fit the imagery. All images were referenced to 2004 aerial imagery obtained from SAGIS. The root mean square error (RMSE) provided by ArcMap's georectification toolbox was input as the accuracy for aerial and satellite imagery  $(E_r)$ . The pixel resolution of aerial and satellite imagery limits the ability to resolve features less than the pixel size  $(E_p)$  (Dolan et al., 1991; Romine et al., 2009). Lastly, the digitizer error is caused by inconsistencies in interpreting the shoreline's position from the source material ( $E_d$ ). My own digitization accuracy for shorelines from 1970, 1983, 1987, and 2018 was evaluated by digitizing a 1-kilometer length of shoreline for each of the four years five times each and evaluating the standard deviation for each shoreline age based on methods from Romine et al. (2009). Ideally, shorelines for a project should be digitized by only one person for consistency of digitizer error between shorelines. Shorelines from 1972, 1984, 1993, 1999, and 2016 were obtained from the digital archive of shorelines maintained by the

University of Georgia Skidaway Institute of Oceanography Geospatial Laboratory. Some of the archived shorelines did not have full metadata available concerning georectification or digitizer error, and estimates for accuracy from *Crowell et al.* (1991) were used.

These errors are independent of one another according to *Crowell et al.* (1991). The square root of the sum of squares of each independent error value provides the shoreline uncertainty.

$$E = \pm \sqrt{E_{ts}^2 + E_r^2 + E_p^2 + E_d^2}$$
 Equation 1.

The resulting uncertainty (E) was input into AMBUR as the estimated accuracy of the shoreline and was incorporated into the output metrics for shoreline change.

After shoreline shapefiles were created, outer and inner baselines were created channel-ward and inland, encompassing the shorelines (*Jackson*, 2010; *Jackson et al.*, 2012). Transects were then cast perpendicularly from the outer baseline to the nearest point of the inner baseline at a project-specific spacing, in this case, 50 meters. These transects were then filtered or "smoothed" to eliminate gaps or overlapping transects due to the curvature of the shorelines (*Jackson*, 2010; *Jackson et al.*, 2012). Capture points were created where the transects intersect each shoreline, and using those points, AMBUR output data tables and shapefiles that contain statistical calculations as outlined in *Jackson* (2010) and *Jackson et al.* (2012). The statistics used in this study for shoreline analysis included the mean net change, and the mean EPR. In this study, positive values indicate accretion, and negative values indicate erosion.

#### 2.3 SHORT-TERM NOURISHED SHORELINE CHANGE

To evaluate the longevity of the spoil sand berm as an effective defensive mechanism to protect the North Pier and adjacent salt marsh on the northern shoreline, both its vertical and

horizontal extent must be considered. Because the berm is a three-dimensional feature, and not just a simple linear shoreline, the short-term change portion of this study focused on elevation and volume changes for assessing the nourished material's erosion and accretion patterns. The shore profile was surveyed by the U.S. Army Corps of Engineers (USACE) previous to the shoreline nourishment, in April 2015, and right after the nourishment, in November 2015. These surveys are a combination of hydrographic single-beam sonar surveys and RTK-GPS terrestrial topographic surveys to cover both subaerial and subaqueous regions. Bathymetric transects were spaced 25 to 30 meters apart; individual points on each transect were about 0.15 meters apart. The USACE data was collected in NAD83 Georgia State Plane East coordinate system in feet using the Mean Lower Low Water (MLLW) vertical datum. The surveys were transformed into Universal Transverse Mercator Zone 17N and the North American Vertical Datum of 1988 (NAVD88) in meters. The latter datums were used for all data in this analysis.

Digital surface models were interpolated from these topographic and bathymetric surveys using the Natural Neighbor method in ArcMap 10's 3D Analyst toolbox. Natural Neighbor was chosen due to it best representing the nature of the survey data once interpolated, compared to surfaces interpolated using Inverse Distance Weighting, Kriging, Topo to Surface and Spline methods. This was determined using a surface error analysis of the interpolated surfaces using randomly selected points from the USACE topographic and bathymetric survey that were excluded from the surface interpolation.

The USACE National Coastal Mapping Project collected aerial LiDAR of the study site in June 2017, intermediate between the November 2015 USACE data and the monthly drone survey data collected starting July 2018. This LiDAR survey provided a bare-earth DSM, interpolated into a 1x1-meter cell raster.

#### 2.4 DRONE SURVEYING AND PROCESSING

Starting in July 2018, I conducted monthly drone surveys over the northern nourished shoreline of Cockspur Island, using a DJI Phantom 4 Professional sUAV. Each flight required a crew of two people: a pilot-in-command, and a visual observer. Low tides, preferably close to spring low tides, were selected to get maximum exposure of the study area. During the summer and early fall, we were constrained to surveying during low tides that were early in the morning to avoid overheating the drone electronics and to avoid frequent afternoon thunderstorms. It took two (infrequently three) days to cover the whole study area; the western portion of the nourished shoreline was surveyed on the first day in the field, and the eastern portion was surveyed on the subsequent day. Infrequently, flight missions were separated by one or two days due to equipment availability and weather restrictions.

During each survey period, 20-24 GCPs made of 60x60-cm acrylic or corrugated plastic squares, painted with a checkerboard black-and-white pattern, were placed around the study area. Approximately half were distributed around the edges of the study area, and half were distributed within the study area. The GCPs' approximate locations were established in July 2018; GCPs were replaced in the same general location for each subsequent survey using visual cues. Locations were not exactly reoccupied because of time constraints and variability in vegetation, tides, and beach debris. After being placed for each survey, the current GCP coordinates and elevation were measured using a Trimble RTK-GPS, with an approximate accuracy of  $\pm 2$  cm (*Trimble*, 2013). Precision of the RTK-GPS was evaluated for each survey day using a United State Geological Survey permanent benchmark on Fort Pulaski before and after measuring the GCPs. The RMSE of the benchmark measurements were used as the estimated accuracy of the GCPs for the processing software.

After placement of the GCPs, the nourished shoreline was flown using the DJI Phantom 4 Pro. Flights began approximately one hour before low tide and extended approximately one hour after low tide. I chose flight parameters to provide the smallest ground sampling distance (GSD) within the limitations of the tide and the time provided by our drone batteries (Table 2). Drone batteries lasted between 25—35 minutes each and we had four batteries. Battery longevity was shorter during days with higher wind speeds.

For each monthly survey, approximately 2,000 images were collected to cover the whole study area. The image capture settings were optimized for processing using photogrammetric techniques, which require images to be taken with high overlap and about 50% at an oblique angle to achieve a wide variety of angles of the berm. I used Pix4Dmapper for the processing of all drone-acquired imagery in this study (Pix4D SA, 2018). Pix4Dmapper is a photogrammetric software used specifically for transforming drone imagery into DSMs and orthomosaics, among other outputs. Pix4Dmapper projects require the input of the exchangeable image file format (EXIF) data associated with each image. Images are arranged spatially using the EXIF coordinate data recorded by the drone's internal GPS. I input GCPs into the initial processing to georeference and transform the point cloud. Pix4Dmapper used a bundle block adjustment to identify "key points", which are points that are identified in two or more overlapping images. These key points were processed into three-dimensional points that populated a dense point cloud. While the majority of the processing is automatic, manual corrections were made throughout the three steps of processing. Before initial processing, I manually identified GCPs in a 4 to 6 images per point, to train the software to identify the points during initial processing. I also visually checked and adjusted the GCP identifications after the initial processing and bundle block adjustment, to verify and increase accuracy of the point cloud and DSM. After

densification, I manually trimmed the point cloud exclude noise and inaccuracies in the point cloud caused by water, heavy vegetation, or human presence. I then interpolated the point cloud to a DSM using an inverse-distance-weighting interpolation. The DSMs and orthomosaics can be exported as a geoTiff at specified resolutions coarser than the initial ground sampling distance. For comparison of volumes and elevations, I exported all drone DSMs at a 1x1-meter cell grid size, as I had to take into consideration the lower resolution of data taken before drone surveying for comparison.

All DSMs were imported into ESRI ArcMap 10.4 for additional analysis (*ESRI*, 2018). Error for each surface was derived from accuracy check points taken using the RTK-GPS in the field during surveys. Approximately 30 to 50 points were taken randomly around the survey area and compared with the under-lying surface elevation. The error was represented by the RMSE of all of the errors of the check points within the area of analysis (*James et al.*, 2017).

#### 2.5 AREAL ELEVATION CHANGE

Spatial trends in surface elevation change were quantified between all DSMs using the ArcGIS RasterMath tool to subtract each sequentially older DSM from the one subsequent to it in time. DSM elevation change was also analyzed for the whole period of study, November 2015 to March 2019, to determine the net change since the initial sediment placement.

The area of analysis was trimmed to exclude areas with heavy vegetation and areas that were inundated in some surveys, neither of which provides a true surface elevation because of varying vegetation heights and density, and sun glint off the water.

### 2.6 SHORELINE PROFILE CHANGE

Elevation profile transects were sampled from the DSMs to visualize shoreline profile changes in representative regions of the study area. Elevations were derived from all DSMs

along transects using the Stack Profiles tool in ESRI ArcMap 10.4. Elevation data tables for each profile were then exported and plotted in R using the ggplot2 package (*Wickham*, 2016). Transects were not limited by the boundary of the elevation change polygon but did continue to exclude heavily vegetated regions near the upland. Transect distance was measured from the low-water channel edge and extended inland. Transect profiles were also compared to mean high water (MHW), mean higher high water (MHHW), approximate spring tide levels, and extreme water levels provided in Table 3 (*Clayton et al.*, 1992; *National Oceanic and Atmospheric Administration*, 2018b). All comparisons to water levels values are in reference to 0 meters in NAVD88.

#### 2.7 VOLUME CHANGE

Volume comparisons were performed using the successive DSM elevation change rasters. Raster cells were sampled using the 3D analyst toolbox in ESRI ArcMap 10, and the elevation change cell values for each interval were exported into a data table. The elevation changes were converted into volume changes by multiplying the cell value by the cell area. The sum of all volume changes for each interval were calculated, resulting in the *interval volume change*. The errors for the volume changes were calculated by taking the RMSE for the corresponding elevation change surface and multiplying it by the volume change analysis area. The *interval percent change* was calculated using the percent volume change in the interval in comparison to the volume remaining at the start of the interval. *Monthly interval percent change* was calculated by dividing the interval percent change by the number of months in the interval.

Volume change analysis was conducted over the entire study area. Because an analysis over the whole study area can mask important dynamics occurring with it, volume change was also assessed over three individual subsections of the study area. Subsections A, B, and C were

calculated separately to identify variations in volume change that were occurring in different areas of the nourished shoreline (Figure 3). Subsections A, B, and C had areas of 11,288 m<sup>2</sup>, 28,042 m<sup>2</sup>, and 14,325 m<sup>2</sup>, respectively, within the full study area polygon (Figure 2). Subsection A is located at the western end of the nourished shoreline and includes what are currently the western sand flats. Subsection B covers the extent of the defensive berm from channel to shore as of March 2019. Subsection C includes the eastern sand flats north of and to the east of the berm crest. Each subsection's analysis followed the same workflow as the analysis for the entire area.

# 2.8 SEDIMENT GRAIN SIZE

Surficial sediment samples were collected from the upper 2 centimeters of the sediment body along eight cross-shore transects. Each transect had six sediment samples (A—F) ranging from the low tide line to the upland, with coordinates of each sample location recorded with an RTK-GPS during the first sampling in January 2018. In all cases, Sample A was taken near the low tide line; Sample B was taken at the mid-beach slope; Sample C was taken at the crest of the berm; Sample D was taken on the mid-back-slope of the berm, Sample E was taken in the channel behind the berm, and Sample F was taken past the extent of sand intrusion into the vegetated marsh. The sample locations were reoccupied in December 2018 to determine change in grain size distribution at the original sample locations. Sand was separated from silt and clay by wet sieving with a 63-micron sieve. The sand fraction was dried overnight and sieved at quarter-phi intervals from -2 phi to 4 phi (4 mm to 0.063 mm) (*Griffiths*, 1967). The silt and clay fractions were determined using the settling rate methodology and Stoke's Law as outlined in *Griffiths* (1967) and *Selley* (2000).

Sediment statistics used to characterize grain size distributions were determined using the method of moments as outlined in *Griffiths* (1967). Sediment grade scales were defined by the Wentworth scale (*Wentworth*, 1922). Changes in these statistics between the first sampling in January 2018 and the sampling in December 2018 were also calculated. The mean ( $\bar{X}$ ) is calculated as the first moment, defined as the position of the center of gravity of the distribution. Sorting ( $\sigma$ ), the second moment, is defined as the standard variance of the grain size distribution. The changes in mean grain size and sorting between January and December 2018 were also evaluated to investigate associations between parameters and erosional and accretionary regions of the nourished shoreline.

#### RESULTS

#### 3.1 HISTORICAL SHORELINE CHANGE

# <u>Cockspur Island Northern Shoreline</u>

The northern shoreline was examined for shoreline change using three different analyses (Table 4). The first analysis includes the entire northern shoreline and all shoreline ages, which will be referred to henceforth as the "All" shorelines analysis. The second analysis includes only sections and years of the shorelines that were not stabilized through armoring and will be referred to as the "Unstabilized" shorelines analysis. This analysis includes the section currently armored, but only for the years before the armoring (i.e., 1930 and 1970; Table 4). The third analysis includes only the section of shoreline that was stabilized through armoring, utilizing shorelines from years only after the armoring occurred (i.e., 1970 through 2018; Table 4). This section consists of the span of riprap revetment in front of the U.S. Coast Guard Station Tybee and Savannah Pilots' facilities and will be referred to as the "Stabilized" shoreline analysis. Not all shorelines cross through all transects due to availability of imagery, creating differences in EPR errors between transects.

When evaluating "All" shorelines, 83 % of the 81 transects exhibit net erosion, and the remaining 17 % of transects exhibit net accretion between 1933 and 2018 (Figure 4a, Table 4). The mean net change is -27.67 m, and the mean EPR is -0.35 m yr<sup>-1</sup>. The EPR error for this analysis ranges between  $\pm$  0.07 m yr<sup>-1</sup> and  $\pm$  0.20 m yr<sup>-1</sup>. EPRs by transect can be found in Figure 5a. The accretionary transects are clustered around two locations: the nourished section of the shoreline and the eastern end of the stabilized section in front of the U.S. Coast Guard Station Tybee and Savannah Pilots' facilities. The most western end of the shoreline exhibits erosional

net change that is two to three times higher than other erosional regions on this shoreline.

Magnitudes of accretion are similar to magnitudes of erosion in the analysis.

The "Unstabilized" shorelines analysis exhibits net erosion, with 86% of the 81 transects exhibiting net erosion, and the remaining 14% of transects exhibiting net accretion (Figure 4b, Table 4). The mean net change is -32.30 m, and the mean EPR is -0.47 m yr<sup>-1</sup>. EPRs by transect can be found in Figure 5b. The EPR error is  $\pm$  0.08 m yr<sup>-1</sup> for transects analyzed from 1933 to 2018 and is  $\pm$  0.28 m yr<sup>-1</sup> for the transects that were analyzed from 1933 to 1970. A few accretionary transects are located in front of the North Pier. The transects that include the armored section of the shoreline are no longer accretionary as they are in the "All" shorelines analysis. This section is now characterized as erosional because it was erosional before the shoreline stabilization occurred.

The "Stabilized" shoreline analysis exhibits net erosion, with 64% of the 22 transects net erosional, and the remaining 36% of transects exhibiting net accretion from 1970 to 2018 (Figure 4c, Table 4). The mean net change is -27.67 m, and the mean EPR is -0.04 m yr<sup>-1</sup>. EPRs by transect can be found in Figure 5c. The mean EPR error for this analysis is estimated at ±0.10 m yr<sup>-1</sup>, showing that the mean EPR for this section of the shoreline is not greater than the error and is not substantially different from zero. The erosional transects and the accretionary transects are clustered in four alternating sets, starting with accretionary at the west end of the revetment and ending with accretion at the east end of the revetment.

# Cockspur Island Southern Shoreline

Results for the southern shoreline change analysis are presented in Table 4. The southern shoreline is mainly erosional. Of the 89 transects, 81 % are erosional, and the remaining 19% are accretionary (Figure 6). The mean net change is -12.91 m. The mean EPR is -0.16  $\pm$  0.08 m yr<sup>-1</sup>.

EPRs by transect are shown in Figure 7. The southern shoreline shows accretion around manmade creek inlets, mainly on the most eastern end of the shoreline, which prograded as the eastern shoreline advanced seaward. The accretionary transects on the eastern end of the shoreline, overlain on 2018 aerial imagery, show that the accretionary areas are near a region with visible sand deposition into the salt marsh. Another accretionary transect is located at the foot of the bridge spanning from I-80 to Cockspur Island. The southern shoreline's EPRs show a general pattern of increasing erosion with distance away from creek inlets.

# Cockspur Island Eastern Shoreline

Results for the eastern shoreline change analysis are presented in Table 4. The eastern shoreline of Cockspur Island is accretionary in all 21 transects (Figure 8). The mean net change is +321.7 m, and the maximum net change is +839.7 m. The northern end of the shoreline (transects 12-22) has a mean EPR (+6.5 m yr<sup>-1</sup>), which is over eight times higher than the southern end mean EPR (+0.8 m yr<sup>-1</sup>) (transects 1-11). The least amount of accretion occurred at transect 5, which is the central transect of the embayed portion of the southern end of the shoreline. The mean EPR for the eastern shoreline is +3.79 m yr<sup>-1</sup> and the maximum EPR is +9.90 m yr<sup>-1</sup> with an error of  $\pm0.07$  to  $\pm0.08$  m yr<sup>-1</sup>. EPRs are plotted by transect in Figure 9.

# 3.2 SHORT-TERM NOURISHED SHORELINE ELEVATION CHANGE

Elevation change between the ten survey periods for the nourished shoreline are shown in Figures 10 through 19. The area of the polygon common to all surveys was 53,652 m<sup>2</sup> after trimming of vegetated and inundated areas. Elevation change characterizations by interval are shown in Table 5.

From April 2015 to November 2015, the time period which encompasses the USACE sediment placement, the study area had an average elevation gain of +2.00 meters (Figure 10).

The sediment was deposited in a berm parallel to the shore. The greatest elevation gain was approximately 4.5 meters, at the crest of the berm, located centrally in the area of analysis, directly in front of the North Pier and extending west approximately 100 meters. The study area had 0.2 % erosional cells and 97.5 % accretionary cells for this interval. The remaining 2.3% of cells showed change that was less than the calculated elevation error (± 0.07 meters).

From November 2015 to June 2017 (the LiDAR survey), the area had an average elevation change of -0.20 meters (Figure 11). The cells were 42.1% erosional, 19.0% accretionary, with the remaining 38.9% showing elevation change less than the calculated elevation error ( $\pm$  0.16 meters).

From June 2017 to July 2018, the area had an average elevation change of -0.08 meters (Figure 12). Erosion was slightly greater than accretion, with 30.8% erosional cells compared with 29.1% accretionary cells. The majority of cells (40.1%) had elevation changes within the error ( $\pm$  0.16 meters).

Monthly surveying began in July 2018 and continued through March 2019, with interruptions in November 2018 and January 2019 for survey data processing issues and the U.S. federal government shutdown, respectively. In comparing subsequent surveys, the mean elevation changes for these analyses ranged between -0.02 meters and + 0.01 meters. Cell elevation changes were dominantly within the range of calculated errors ( $\pm$  0.05 to  $\pm$  0.09 meters; Figures 13—17). The percentage of erosional cells ranged from 3.5% to 24.2% and were always greater than the percentage of accretionary cells with the exception of the December 2018 to February 2019 comparison, which showed 12.8% erosional cells and 26.0% accretionary cells. The percentages of cells with no significant change ranged from 57.2% to 83.8%, always greater than the percentage of erosional and accretionary cells combined.

In contrast, the February 2019 to March 2019 surface comparison analysis exhibited a return to dominantly erosional conditions (Figure 18). The average elevation change was -0.07 meters. The cells were 49.4% erosional and 2.6% accretionary, with the remaining 48.0% of the area exhibiting elevation changes less than the error ( $\pm$  0.06 meters).

From November 2015 to March 2019, from immediately after placement to the end of the study period, the nourished shoreline was dominantly erosional (Figure 19). The average loss of elevation was -0.41 meters. For the area, 52.8% of cells were erosional, 22.3% were accretionary, and 24.8% were within the error of the analysis ( $\pm$  0.16 meters).

### 3.3 SHORT-TERM NOURISHED SHORELINE PROFILE CHANGE

Transect locations for cross-sectional profiles are shown in Figure 20. Profiles for transects 1 through 7 are represented in Figures 21 through 27. Transects were numbered from west (transect 1) to east (transect 7). All transects showed some deposition of sediment from April 2015 to November 2015 from the USACE nourishment event, but not all show a definitive berm structure.

Transect 1 was outside the main project area for the dredge spoil placement, but still showed some deposition in the nourishment period (Figure 21). This transect inundated at MHW for all DSMs analyzed. Transect 1 shows that after November 2015, the surface elevation continued to accrete until June 2017 in the first 25 meters of the transect (the extent of the November 2015 data). However, farther inland along the transect, the June 2017 profile showed a decreasing slope and erosion to below the April 2015 surface. The limited extent of the data for November 2015 prevented us from documenting the patterns before placement to June 2017 for the landward portion of the transect. After June 2017, the channelward slope of the berm became

steeper and lost elevation, but then built elevation and decreased in slope after the 30-meter mark.

Transect 2 is the westernmost transect to show a definitive berm structure from the USACE placement (Figure 22). At this location in November 2015, the crest of the berm was only approximately +1.3 meters high NAVD88, the lowest elevation of all the transects where the berm was present. As of November 2015, the berm was not overtopped at MHHW, but was inundated by spring tides. By June 2017, the berm had been eroded and the area had flattened to a gentle slope at just below 0.0 meters NAVD 88. After the deflation of the berm, the elevation of the sandy slope continued to decrease between June 2017 and July 2018 and onwards; the slope angle showed little change. As of March 2019, the slope was inundated by MHW levels. The marsh edge behind the berm showed very little change in this location.

In transect 3, the crest of the berm in November 2015 was higher than at transect 2, at approximately +1.7 meters NAVD88 elevation (Figure 23). During this period, the berm would have been overtopped by the extreme water levels in October 2015 and October 2016 associated with perigean tides and Hurricane Matthew. The berm persisted through June 2017, longer than it did in transect 2. Between the initial placement and June 2017, the berm's crest shifted inland. The back slope also steepened, and the channel slightly undercut the November 2015 channel's surface. After June 2017, the berm would have been overtopped by extreme water levels in September 2017 associated with Hurricane Irma. By July 2018, the berm was completely flattened, similar to what was observed at transect 2. From July 2018 onwards, transect 3's profile was a gently sloping beach face just above 0 meters NAVD 88, with little change in elevation after July 2018, similar to transect 2. The slope was inundated by MHW levels. The

landward end of the transect leading from sand to marsh showed little change throughout the time period.

Transect 4 is located at the western extent of the ephemeral pond. Here, the crest of the berm was approximately +1.9 meters NAVD88 in elevation in November 2015 (Figure 24).

Unlike transects 2 and 3, in transect 4 the crest of the berm was maintained through March 2019 at this height. It would not have experienced regular overtopping with spring tides but would have been overtopped during the extreme water level events in October 2015, October 2016, and September 2017. Erosion was ongoing at the channel-facing slope, and the front of the berm steepened. The channel behind the berm gained 0.5 meters in elevation from November 2015 to March 2019.

Transect 5 is at the eastern extent of the ephemeral pond and is the closest transect to the North Pier. The crest of the berm in November 2015 was approximately +1.9 meters NAVD88 in elevation and was located at approximately 19 meters along the transect (Figure 25). At +1.9 meters, the berm would have inundated with the extreme water level events in October 2015, October 2016, and September 2017. Between November 2015 and June 2017, the only change occurred was an approximate -0.2-meter loss in elevation at the crest. However, between June 2017 and March 2019 the berm underwent further erosion and scarping. During this period, the berm was overtopped by the extreme water level event in September 2017, and the slope of the erosional scarp was decreased. The crest of the berm lost an additional 0.1 meters in elevation, and the toe of the berm also retreated inland almost 20 meters. The area behind the crest of the berm has neither gained nor lost elevation throughout the entire study period.

Transect 6 includes the eastern sand flats and the berm behind them. In November 2015, the toe of the berm extended to the channelward limit of the transect, and at its crest was

approximately +2.8 meters NAVD88 in elevation (Figure 26). At this elevation, the crest of the berm was not overtopped by extreme water levels occurring in October of 2015 and 2016.

Throughout the profile comparisons, the berm at this location did not lose more than 0.1 meters in elevation, but the toe of the berm eroded landward substantially throughout the study period. The toe of the berm eroded 59 meters from November 2015 to June 2017, for an average rate of 2.58 m mo<sup>-1</sup>. The rates of retreat slowed for later periods, with an average retreat rate of 1.21 m mo<sup>-1</sup> from June 2017 to August 2018, and 0.57 m mo<sup>-1</sup> from August 2018 to March 2019, with a total retreat of 80 meters for the toe of the berm by March 2019. This retreat left expansive, low-lying sand flats between the north channel and the toe of the berm at low tide. The elevation of the sand flats in front of the escarpment generally gained almost half a meter of elevation between June 2017 and July 2018. Between July 2018 and March 2019, the elevation of the sand flats remained unchanged. The environment behind the crest of the berm neither gained nor lost elevation throughout the entire study period.

Transect 7 is beyond the eastern extent of the placement area of the defensive berm. This region is inundated during spring high tides and was inundated during extreme water levels in 2015, 2016 and 2017 (Figure 27). The profile showed some elevation gain from November 2015 to July 2018, mainly closer to the channel. However, between July 2018 and March 2019, the transect profiles showed little change in elevation.

# 3.4 SHORT-TERM NOURISHED SHORELINE VOLUME CHANGE

Volume change of the USACE nourishment was analyzed within the study area polygon and within three subsections of the study area polygon. Interval volume changes over the entire polygon are shown in Table 6. From April 2015 to November 2015, the full study area polygon gained  $114,668 \pm 4,000 \text{ m}^3$  of sediment. Subsection A, located on the west side of study area, had

a volume gain of  $16,799 \pm 841 \text{ m}^3$  (Table 7). Subsection B, the central section of the study area, showed almost five times higher volume gain, with a gain of  $83,221 \pm 2,090 \text{ m}^3$  of sediment (Table 8). Subsection C had the smallest total volume gain, with a gain of  $14,562 \pm 1,068 \text{ m}^3$  of sediment (Table 9).

From November 2015 to June 2017,  $10.2 \pm 7.5\%$  of the total volume of material placed was lost over the entire area. This represents a loss rate of  $-0.5 \pm 0.4\%$  per month, over a total of 19 months. Analyses by subsections show that significant volume change only occurred in subsections A and B, with a loss of  $-2,469 \pm 1,815$  m<sup>3</sup> ( $-14.7 \pm 12.7\%$ ) and  $-7,534 \pm 4,510$  m<sup>3</sup> ( $-9.1 \pm 6.0\%$ ), respectively. Subsection C's volume loss of  $-1,631 \pm 2,304$  m<sup>3</sup> ( $-11.2 \pm 17.8\%$ ), was less than the error term, indicating no significant change in this region. Subsection B lost the greatest volume of sediment in this time period.

Comparing June 2017 to July 2018 did not indicate significant volume change beyond the analysis error when looking at the full polygon area. However, when analyzing by subsections, B and C had significant losses of volume. Subsection B showed a loss of -6,648  $\pm$  4,587 m<sup>3</sup>, and subsection C showed a loss of -3,500  $\pm$  2,343 m<sup>3</sup>, equating to a loss of -8.8  $\pm$  6.6% and -27.1  $\pm$  14.3% of the material remaining in June 2017.

Between July 2018 to February 2019, month-to-month analyses did not show any volume changes that were beyond the volume error for either analysis of the entire area or any of the subsections with the exception of one interval: October 2018 to December 2019. During this period, subsection A showed a small volume loss on the western end of the area of  $-564 \pm 510$  m<sup>3</sup>.

In comparing the volumes from February to March 2019, significant volume change is found both for the entire area and within subsections A and B. The entire area showed a loss of

 $-3,846 \pm 3,282$  m<sup>3</sup>. Subsection A had a volume loss of  $-1,238 \pm 691$  m<sup>3</sup>, or  $-10.2 \pm 6.3\%$  of the volume remaining in the subsection at the beginning of this interval. Subsection B lost  $-2,251 \pm 1,715$  m<sup>3</sup>, or a loss of  $-3.4 \pm 2.7\%$  of the volume remaining in the subsection during this interval. Subsection C exhibited change of -355 m<sup>3</sup>  $\pm 876$  m<sup>3</sup>, not significant with respect to the analysis error.

Over the complete study period, spanning from November 2015 to the last data collection in March 2019,  $-21,973 \pm 8,343$  m<sup>3</sup> of sediment was lost. This equates to a  $-19.2 \pm 7.3\%$  loss of the placed material. Three quarters of this loss occurred within subsection B, and the remaining was lost in subsection A. The rate of loss when considering just those two surfaces is  $-0.5 \pm 0.2\%$  per month, or  $-549 \pm 209$  m<sup>3</sup> per month.

# 3.5 SEDIMENT GRAIN SIZE

Sediment samples from January 2018 had mean grain size for individual samples ranging from coarse to fine sand, with grain sizes of 0.19 phi to 2.00 phi (0.88 mm to 0.25 mm) (Figure 28). The mean of all samples was 1.30 phi, or medium sand. On the west end of the nourished shoreline, sediment became finer towards the upland. The top of the berm was dominated by medium and coarse sands. Behind the berm and closer to the marsh and upland, sediment became finer, although the classification remained medium sand. Samples taken at the marsh edge were also classified as medium sand, as were samples C through F taken at the most eastern transect. Only one sample, (4f) was characterized as fine sand.

January sorting descriptions ranged from well sorted to poorly sorted, with sorting values from 0.38 to 1.40. Average sorting for all January sediment samples was 0.90, corresponding to moderately sorted (Figure 29). Three samples were considered well-sorted: on the channelward slope of the berm for transects 5 and 6 (sample b); and in the marsh for transect 2 (sample f).

Moderately sorted samples were located throughout the nourished shoreline and were typically found on the sand flats and behind the berm. Sediments on the berm crest were poorly sorted, as were samples 6a and 6b and 7a, on the eastern sand flats.

December 2018 samples had mean grain size ranging from very coarse to fine sand, with values spanning -0.29 phi to 2.18 phi (1.22 mm to 0.22 mm) (Figure 30). The mean of all the samples was 1.15 phi, or medium sand. The top of the berm was still dominated by medium and coarse sand but had a greater proportion of coarse sand samples compared with January 2018. The majority of the western end of the berm retained its trend of becoming finer towards the upland, starting with coarse sand near the channel. Sample 4a was the only sample to be classified as very coarse sand. Sample 4f was again the only sample that is classified as fine sand.

December sorting values ranged from 0.56 to 1.44, which corresponded to moderately well sorted to poorly sorted distributions (Figure 31). Average sorting for all December samples was 0.97 (moderately sorted), but close to the boundary between moderately and poorly sorted. The west end of the nourished shoreline was generally poorly sorted, while the western sand flats were moderately to poorly sorted. Sediments on top of the berm remain poorly sorted, as did the eastern sand flats' low tide areas for sample 6a, 6b, and 7a.

In figure 32, January 2018 mean grain sizes are plotted against the corresponding sample from December 2018 mean grain size. A line with the slope of 1 is plotted, and samples falling below that line experienced a coarsening over time, and samples above the line became finer over time. Samples were color coded in blue if the samples were in erosional regions from July 2018 to December 2018. Of the 48 samples, 13 were located in areas that had experienced erosion from July 2018 to December 2018 (Figure 32). Only two samples were located in areas

of accretion (3a and 8b). The rest of the samples were located in areas of no significant change beyond the elevation change analysis error or were outside of the elevation analysis study area. Eleven of the 13 samples located in erosional regions on the nourished beach became coarser from January to December of 2018. The greatest changes in mean grain size were observed at sites that were nearest to the toe of the protective berm, with the exception of 7a and 8c, which were located near the low tide line at the east end of the shoreline and at the mouth of a shallow washover channel at the east tip of the berm, respectively (Figure 33). Samples 4a, 5a, 6b, and 8c all became more than 0.75 phi coarser from January to December. Sample 7a became 0.8 phi finer.

Sorting increased considerably at samples 4c, 4d, and 5d. All three samples were located at the crest or on the back slope of the protective berm and increased in sorting value by  $0.25\,\sigma$  or more (Figure 34). In figure 35, January 2018 sorting values are plotted against the corresponding sample from December 2018 sorting values. A line with the slope of 1 is plotted, and samples falling below that line became more well sorted over time, and samples above the line became more poorly sorted over time. Samples were color coded in blue if the samples were in erosional regions from July 2018 to December 2018. Approximately 70 % of all samples became more poorly sorted from January 2018 to December 2018 (Figure 35). There was no distinct trend in grain size sorting associated with erosional or accretional elevation change.

#### **DISCUSSION**

This research analyzed long term and short term changes in shoreline location and sediment volume using two GIS-based methods of analysis: lateral shoreline movement for the entirety of Cockspur Island, split into the three distinct shorelines (northern, southern, and eastern) using historical maps and imagery; and vertical and volumetric change occurring at the beneficial-use, dredge spoil project site on the northern shoreline using digital surface models derived from monthly drone surveying.

The long-term analysis revealed similarities and differences between the three shorelines of Cockspur Island. The northern and southern shorelines were dominantly erosional, with erosion rates of -0.47 m yr<sup>-1</sup> and -0.16 m yr<sup>-1</sup> respectively, and the eastern shoreline was dominantly accretionary, with a rate of ±3.79 m yr<sup>-1</sup>. With both the northern and the southern shorelines eroding on the west end of the island, the western tip of the island is narrowing and retreating eastward as the shorelines converge. Of the two erosional shorelines, the northern shoreline had the highest erosional EPR. This was true for the "all" shoreline analysis, and the "unstabilized" shoreline analysis. Previous studies have found that erosion of the marsh edge is strongly driven by wave attack, and therefore more powerful and higher density of waves would indicate the most erosional environment (*Cowart et al.*, 2010; *Marani et al.*, 2011; *Schwimmer*, 2001). The greater erosion of the northern shoreline compared with the southern shoreline reflects the higher energy environment in which it exists, which includes a longer fetch and increased wave energy from larger and more frequent vessel wakes. The southern shoreline's

less erosional nature reflects the more limited-fetch environment of the southern channel, with smaller wind driven waves, and smaller wakes from recreational and fishing vessels.

For all three shorelines, regions of accretion were associated with anthropogenically modified areas. These modified areas included man-made inlets to the interior dike system and areas adjacent to the recent bridge construction on the southern shoreline. Accretionary modified regions also include the armored and backfilled region on the northern shoreline, built to protect the Savannah Pilots' and U.S Coast Guard's facilities in the 1970s. For the eastern shoreline specifically, its net accretionary nature is the combined result of sediment trapping from the presence of the northeastern jetty and the dredge spoil deposition that occurred in the early to mid-20th century.

The analysis of "All" shorelines underestimated the mean rates of change of unstabilized shoreline sections. Segmenting the northern shoreline analysis into areas of stabilized and unstabilized shorelines was done to evaluate the effects the armored shoreline had on decreasing the mean rates of shoreline change for the entire shoreline. Comparison of the "All" shorelines analysis versus the unstabilized shoreline analysis shows that the northern shoreline unstabilized section's mean erosion rate was being underestimated by over 25% when calculated with stabilized shorelines included. Future analysis should consider the history of shoreline activity when evaluating future changes in shoreline location based on extrapolations of current trends.

The AMBUR method of evaluating shoreline change and differentiating shorelines with change from those without change was verified by the analysis of the armored region of the northern shoreline. This section showed no net change beyond the analysis error, as the mean EPR was -0.04 m yr<sup>-1</sup>, and the analysis error was  $\pm$  0.10 m yr<sup>-1</sup>. This section of the shoreline was

armored for all iterations of the stabilized analysis. This also validates that the stabilization of this region of the shoreline has been effective.

In general, shoreline change rates for northern and southern Cockspur Island shorelines were found in this current study to be similar to rates found in the Alexander (2008) study, although eastern shoreline rates were higher in the current study than in the Alexander (2008) study. The northern shoreline erosion rates for the 1953 to 2005 analysis in Alexander (2008) are  $-0.31 \pm 0.15$  m yr<sup>-1</sup> for regions not stabilized by anthropogenic modification. This current study found northern shoreline erosion rates in the same regions to be  $-0.47 \pm 0.28$  m yr<sup>-1</sup>. This is a slight rise in apparent rate but ultimately is not a significant increase due to the overlapping errors of the shoreline metric. This result could indicate that the increase in frequency and force of vessel wakes from larger-draft, post-Panamax freight vessels in the past decade was not enough to increase the erosional EPR when averaged over the 85-year period of analysis. The prediction by the *Houser* (2010) study of an additional retreat of 0.04 m yr<sup>-1</sup> of the northern shoreline of Cockspur Island is such a small number that it would be difficult to detect over the short time period by which this current study expands upon the timeframe in Alexander (2008). The predicted net retreat would have been 0.4 meters over the decade period between studies, which is equal to the error of the 2018 shoreline, and therefore, the additional retreat is indiscernible using these methods.

The southern shoreline also exhibited similar EPRs in this study ( $-0.16 \pm 0.08 \text{ m yr}^{-1}$ ) with the *Alexander* (2008) study (EPR:  $-0.22 \pm 0.06 \text{ m yr}^{-1}$ ). The southern shoreline would not have experienced an increase in vessel-wake frequency and forcing in recent years in contrast to the northern channel, leaving the only significant erosion-inducing factors as storm events.

Interestingly, the *Alexander* (2008) shoreline change rates from 1953 to 2005 would have included the effects of several hurricanes and tropical storms, including from Hurricane David in 1979. That the rates for the northern and southern shorelines were similar for both studies indicates that the recent hurricanes in 2016, 2017, and 2018 did not cause enough erosion to increase the shoreline change rate beyond rates that already included the effects from several tropical cyclones. This could be due to the fact the during extreme storm events, water levels were typically elevated beyond the marsh edge, flooding past the typical marsh inundation levels. Houser (2010) found in his study that marsh edge erosion on the northern shoreline was most effective when water levels were even with the elevation of the marsh edge, distributing the majority of the wave force directly onto the marsh scarp. Therefore, if water levels indicated flooding of the island during these extreme storm events, wave force was most likely was not directed at the marsh scarp but rather farther inland from the marsh edge.

The eastern shoreline accretionary rates of  $+3.79 \pm 0.08$  m yr<sup>-1</sup> in this analysis were +0.60 m yr<sup>-1</sup> higher than those in *Alexander* (2008), which had an accretionary rate of  $+3.19 \pm 0.15$  m yr<sup>-1</sup>, respectively. These rates substantially differ, attesting to an increase in accretion on the eastern shoreline since 2008. The hurricanes in 2016, 2017, and 2018 could have been a source of the increased sediment accumulation. Strong storms can be a delivery method for sediment to coastal wetlands through resuspension of sediment into the water column, which can then deposit on the marsh surface, increasing marsh elevation and possibly seaward extent (*Cahoon et al.*, 1995).

As might be expected given the progression of most nourished shorelines, the nourished section of the northern shoreline is net erosional in both elevation and volume from the placement in November 2015 to March 2019. This section of the northern shoreline has

ultimately lost almost 20% of the nourished volume over the 40-month period. The average elevation change across the nourished shoreline was approximately -0.41 meters. In comparison, a similar study at Broadkill Beach in Delaware Bay found a loss of approximately 5% of nourished material with just one hurricane and one winter storm within a 3-month period (*Dohner and Trembanis*, 2017). During our study, the highest loss we saw in a similar time period was about 3% of the total volume of the nourishment (December to March 2019).

Sediment sampling revealed that coarsening of grain size distribution was associated with erosional patterns on the shoreline, as was further verified through field observations of pebble and shell lags at the erosional toe of the berm. Changes in sorting were not associated with any volume or elevation change patterns on or around the protective berm.

The transect profile comparisons and volumetric analysis by subsections further showed that the erosional affects are not occurring equally across the nourished shoreline section.

Subsection B experienced the greatest volume loss of the three sections, losing three times more volume than subsection A. This equates to a loss of -0.12 meters more elevation on average throughout section B than section A. Subsection C was slightly accretionary, but the amount of volume gained was close to the error, indicating any volume gain was minor. Subsection C's results were unexpected considering that the bulk of the protective berm on the east side had been eroded to sand flats by July 2018. However, it appears that much of this sediment was just redistributed from the berm itself to across the eastward edge of the subsection and study area, significantly increasing elevation in that region and extending the sand flats farther north and east.

Areas where the berm elevation was lower than or near the water levels during spring high tide were the quickest to be eroded into sand flats, as regular inundation with wave energy

allowed for reworking of the berm crest and redistribution of the berm sand into the western sand flats. Comparatively, areas where the berm height was well above water levels occurring at spring high tides maintained their heights longer but experienced more erosion and scarping of the channel-facing slope of the berm. This is common in nourished beaches where berms are built too high for wave run up to wash over the top of berms regularly (*Jackson et al.*, 2010b). This causes the majority of wave force to be concentrated on the berm face. Scarping will most likely continue to occur until the berm crest height decreases to the extent that regular overwash becomes possible, and the berm slope face will become more gradual. Shoreline nourishments are typically mechanically regraded after the creation of a scarp for public safety and to enhance turtle nesting (*Jackson et al.*, 2010b). No anthropogenic grading has occurred at the study site since the original placement of material.

The USACE, Georgia Department of Natural Resources, Georgia Coastal Management Program, and Fort Pulaski National Monument are all keenly interested in the sustainability of dredge-spoil beneficial-use artificial berms for the protection of cultural and natural resources in coastal habitats. Assuming that the rate of volume loss calculated over the 40-month study period is consistent in the future, the nourishment on the northern shoreline will have an estimated longevity of approximately 14 years until the placed material is completely depleted, based on the volume remaining in March 2019.

However, a 14-year estimated longevity of the nourished material does not translate to the length of time that the berm will effectively protect the North Pier and adjacent salt marsh from erosion. Sea level is estimated to rise only 0.05 meters in this 14-year period based on the 3.5 mm yr<sup>-1</sup> rate given by the *National Oceanic and Atmospheric Administration* (2018a), not enough to seriously affect the range of tidal inundation of the nourished shoreline.

Current trends in erosion could accelerate the rate at which the berm loses its defensive capabilities, shortening the *effective* longevity. Retreat rates calculated using shoreline profiles near the North Pier indicate instead a more likely effective longevity estimate of 8 years, due to the decrease in elevation of the berm crest and berm width as the berm face continues to retreat inland. These retreat rates have slowed over the study period, decreasing from an average retreat rate of 2.58 m mos<sup>-1</sup> during the first 19 months to 0.57 m mos<sup>-1</sup> over the last 7 months of the study (August 2018 to March 2019). While the first 19 months included effects from Hurricane Matthew, the last 7 months of the study did not include any extreme storm events, suggesting that the retreat rate could increase in the event of another hurricane or tropical storm.

Additionally, the continued reworking of the western end of the berm and its retreat eastward may allow for a larger opening at high tide which would enhance wave energy received from the west. Waves derived from northwest winds or from eastward traveling vessels would be able to propagate behind the berm and erode the marsh. Furthermore, the opening of a second channel across the berm almost directly in front of the North Pier presents a new pathway for inundation and wave attack behind the berm at high tide. If this channel widens and deepens, erosion could possibly accelerate in this section of the berm and allow for a more direct route for wave energy towards the North Pier and the marsh.

The estimated 8-year effective longevity for the berm past March 2019 combined with the 40-month study interval in which the berm effective defended the North Pier from erosion suggests a total *effective* lifetime of about 11 years from placement. This timeline is much longer than the nearby ocean-facing beach on Tybee Island, which as of 2007, was on a 7-year renourishment schedule, but has needed intermediate renourishment due to storm damage (*Elfner*, 2005; *Angell & Robertson*, 2018). This longer effective longevity allows for flexibility

in the renourishment schedule to align with dredging timelines, which occur much more frequently in the lower Savannah River shipping channel, on an annual basis (*Bell*, 2019). This also gives options to nourish the berm in small sections, focusing on erosional hotspots, rather than attempting a full renourishment when the berm nears depletion.

In future surveying efforts, drone survey intervals need to be modified to maximize monitoring efficiency. The shoreline monthly and bimonthly survey intervals for this analysis were often too short to quantify significant change, as volume changes on these timescales were typically small enough over the study site to be within the error. Volume analysis errors for the entire study area ranged from approximately 2,400 to 4,500 m<sup>3</sup> over the approximately 54,000 m<sup>2</sup> nourished area. To quantify significant volume change using current drone survey techniques, the average elevation change across the study area would need to be  $\pm 0.05$  - 0.10 meters. Most surface comparisons for drone surveying had less than  $\pm 0.03$  meters of average elevation change for one- to two-month periods. Further monitoring at this site would be more efficient at three- to four-month intervals, supplemented by additional surveys in anticipation of, and right after, extreme events.

An alternative option for creating a more efficient surveying process would be to lower the error of the DSMS. This could be accomplished using smaller raster cell sizes for analysis, potentially lowering error caused by exporting rasters at almost 70 times greater cell size than the ground sampling distance. The averaging of the elevation within the 1x1-meter cell allows for greater error to be calculated in areas where an accuracy point was taken near an area of high relief. I attempted to verify this method to lower the surface errors by exporting the drone-derived DSMs at 0.5x0.5-meter cell grid size and reassessed the error and volume calculations. However, none of the intervals that showed no significant change in volume in the 1x1-meter

cell grid size changed to showing significant change using the 0.5mx0.5-meter cell grid size. Ultimately, the option of exporting at a finer cell grid size was limited in downscaling by the non-drone data sources as well. This option would only be available when comparing drone surveys, as the sampling distance for the USACE surveys were too large to be interpolated to a similar size. The LiDAR survey, with an error of 0.15 meters, would also need to be removed from the study data in order to limit error as much as possible.

The limitations of identifying small-scale processes in different regions of the nourished shoreline using just the changes in surface elevation and volume highlighted the importance of also assessing shoreline profiles throughout the study area. Identifying topographical features and areas of vulnerability, such as the steep berm scarps north of the North Pier, through the use of shoreline profiles, was of key importance to creating a more realistic estimation of the effective longevity of the berm, which was less than 60% of the longevity of the total placement material. I recommend that this method be coupled with surface elevation and volume change assessments in future monitoring efforts.

As sea-level rise and predicted increase in storm events become the future of our nation's coastlines, monitoring our shorelines for the purpose of adapting management strategies will become increasingly necessary to maintain not just recreational environments and crucial coastal habitats, but also human safety. This study demonstrates the implementation of new and efficient drone surveying methods for shoreline change. The results indicate that the northern shoreline of Cockspur Island will need continued monitoring, especially at the nourished section of the northern shoreline to follow the erosional trajectory of the protective berm. Shoreline nourishment is an effective, mid-term solution to the shoreline erosion occurring in front of the

North Pier, and this volume change assessment will inform future methods and needs for further exploration of this beneficial-use project.

#### CONCLUSIONS

- 1. Cockspur Island is at risk from continued shoreline erosion and inundation due to natural and anthropogenic phenomena; two of the three shorelines are dominantly erosional. The island is continuing to narrow at the western end of the island, from the southern and northern shorelines converging inland. The northern shoreline on average is retreating at a rate of -0.47 m yr<sup>-1</sup>. The western end of the northern shoreline is retreating 2 3.5 times faster than the average at rates of -0.94 to -1.68 m yr<sup>-1</sup>. The southern shoreline is retreating at -0.16 m yr<sup>-1</sup>. As the two shorelines converge, the western tip of the island will regress farther east. The eastern shoreline, in contrast, has accreted seaward, and that rate of accretion has increased from +3.19 m yr<sup>-1</sup> to +3.79 m yr<sup>-1</sup>.
- 2. The nourished northern shoreline has lost just under 20% of the volume placed in 2015 and is decreasing in volume at a rate that will deplete the nourishment material within approximately 14 years. The central-east toe of the berm is retreating at a rate that could decrease the longevity of the effectiveness of the protective berm to 8 years. Erosion is shortening the western extent of the berm and decreasing the width of the eastern area of the berm. These areas should be the focus of future monitoring and possible renourishment. The second, recently created channel across the berm should also be monitored closely for increased erosion and wave intrusion behind the berm at high tides.
- 3. The drone surveying methodology was effective in identifying changes in shoreline location and volume change on an inter-annual scale and could be applied for future monitoring of beneficial-use renourishment sites. However, the continued monitoring of the nourished shoreline will be more cost and time effective if conducted over longer time intervals. Using

monthly drone monitoring for changes in the volume and location of the shoreline at the nourished site on the northern shoreline was beneficial to becoming familiar with the newly established shoreline's environment and small-scale changes. However, the changes occurring within this study area were generally too small to identify significant changes on a one or two-month interval. A better way to capture change would be to continue surveys at intervals of three months or more, and to supplement this surveying schedule with flights in anticipation of, and after, storm events with potential for significant shoreline change. Assessment of shoreline profiles are also necessary to accompany areal elevation and volume change assessments in order to gain better understanding of changes occurring in vulnerable regions within the study area.

5. The beneficial-use dredge spoil placement has effectively preserved the North Pier and Battery Hambright for the public and park administrators for the past 4 years. Similarly, the erosion occurring to the marsh directly adjacent to the North Pier has been stabilized. Going forward, the nourished shoreline needs to be routinely monitored to determine the changing needs of this section of shoreline as natural and anthropogenic phenomena threaten the shoreline with continued erosion.

#### REFERENCES

Alexander, C. (2008). Rates and Processes of Shoreline Change at Ft. Pulaski National Monument. Final Report to Georgia Department of Natural Resources, Coastal Resources Divison, Brunswick, Georgia, 58 pp.

Alexander, C. (2016), Geospatial Characterization Studies for Advancing Estuarine Restoration and Management in Georgia. Final Report to Georgia Department of Natural Resources, Coastal Resources Divison, Brunswick, Georgia, 19 pp.

Angell, T., & Robertson, A. (2018), Tybee Island Dune Restoration 2018. Presentation to Georgia Department of Natural Resources Coastal Resources Division, Brunswick, Georgia, 17 pp. Date retrieved: August 17, 2019. Retrieved from: https://coastalgadnr.org/sites/default/files/crd/MarshandShore/PublicNotice/Tybee/2.TybeeProje ctDescription.pdf

Bell, J., (2019), Savannah Harbor Maintenance Dredging. Savannah, GA: U.S. Army Corps of Engineers, Corporate Communications Office. Date retrieved: August 17, 2018. Retrieved from https://www.sas.usace.army.mil/Media/News-Stories/Article/1807044/24-7-365-savannah-harbor-maintenance-dredging/.

Boak, E. H., & Turner, I. L. (2005). Shoreline Definition and Detection: A Review. *Journal of Coastal Research* 21(4), 688-703.

Burns, C., (2018). Historical Analysis Of 70 Years of Salt Marsh Change at Three Coastal LTER Sites. *Unpublished Master's Thesis*, 200 pp, Athens, Georgia, USA: University of Georgia.

Cahoon, D., Reed, D., Day, J., Steyer, G., Boumans, R., Lynch, J., *et al.* (1995). The Influence of Hurricane Andrew on Sediment Distribution in Louisiana Coastal Marshes. *Journal of Coastal Research*, 21, 280-294.

Carter, R. W. G. (1988). Coastal Environments: An Introduction to the Physical, Ecological, and Cultural Systems of Coastlines. 617 pp., Great Britain: Academic Press.

Casella, E., Rovere, A., Pedroncini, A., Stark, C. P., Casella, M., Ferrari, M., & Firpo, M. (2016). Drones as Tools For Monitoring Beach Topography Changes In The Ligurian Sea (NW Mediterranean). *Geo-Marine Letters*, 36(2), 151-163.

Clark, A. (2017). Small Unmanned Aerial Systems Comparative Analysis for the Application to Coastal Erosion Monitoring. *GeoResJ*, 13, 175-185.

Clayton, T. D., Taylor, L. A., Cleary, W. J., Hosier, P. E., Graber, P., Neal, W. J., & Pilkey, O. H. (1992). Living with the Georgia Shore. 145 pp., *Duke University Press*, Durham, North Carolina.

Colomina, I., & Molina, P. (2014). Unmanned Aerial Systems for Photogrammetry and Remote Sensing: A Review. *ISPRS Journal of Photogrammetry and Remote Sensing*, 92, 79-97.

Cowart, L., Walsh, J. P., & Corbett, D. R. (2010). Analyzing Estuarine Shoreline Change: A Case Study of Cedar Island, North Carolina. *Journal of Coastal Research*, 26(5), 817-830.

Crowell, M., Leatherman, S. P., & Buckley, M. K. (1991). Historical Shoreline Change: Error Analysis and Mapping. *Journal of Coastal Research*, 7(3), 839-852.

Davis, R. A., & Fitzgerald, D. M. (2009). Beaches and Coasts. John Wiley & Sons.

Dohner, S., & Trembanis, A. (2017). Broadkill Beach Delaware: Case study of a Beneficial Use of Dredged Material Project. *Atti della Società Toscana di Scienze Naturali Memorie Serie A*, 124, 83-92.

Dolan, R., Fenster, M., & Home, S.J. (1991). Temporal Analysis of Shoreline Recession and Accretion. *Journal of Coastal Research*, 7(3), 723-744.

Doody, J. P. (1996), Management and Use of Dynamic Estuarine Shorelines, in Nordstorm, K. F., et al. (Eds.), *Estuarine Shores: Evolution, Environments, and Human Alterations* (pp. 421-434). Great Britain: John Wiley & Sons.

Elfner, M. A., (2005), Tybee Island Beach Management Plan. Final Report to City of Tybee Island, GA, 83 pp. Date retrieved: August 17, 2019. Retrieved from https://www.cityoftybee.org/DocumentCenter/View/402/Beach-Management-Plan-PDF.

Environmental Systems Research Institute (2018). ArcMap 10.4. Redlands, California.

Fagherazzi, S., Mariotti, G, Wiberg, P. L., & McGlathery, K. J. (2013). Marsh Collapse Does Not Require Sea Level Rise. *Oceanography*, 26(3), 70-77.

Gonçalves, J. A., & Henriques, R. (2015). UAV Photogrammetry for Topographic Monitoring of Coastal Areas. *ISPRS Journal of Photogrammetry and Remote Sensing*, 104, 101-111.

Goossens, H., & Zwolsman, J. J. G. (1996). An Evaluation of the Behavior of Pollutants during Dredging Activities, *Terra et Aqua*, 62, 20-28.

GRASS Development Team, (2017). Geographic Resources Analysis Support System (GRASS) Software, Version 7.2. Open Source Geospatial Foundation. Retrieved June 26, 2019 from http://grass.osgeo.org.

Griffiths, J. C. (1967). Scientific Method in Analysis of Sediment, 508 pp., USA: McGraw-Hill.

Hoeke, R. K., Zarillo, G. A., & Synder, M. (2001). A GIS-Based Tool for Extracting Shoreline Positions from Aerial Imagery (BeachTools). Vicksburg, MS: Engineer Research and Development Center, Coastal and Hydraulics lab.

Houser, C. (2010). Relative Importance of Vessel-Generated and Wind Waves to Salt Marsh Erosion in a Restricted Fetch Environment. *Journal of Coastal Research*, 26(2), 230-240.

Jackson, C. W. (2010). AMBUR package for R: Basic User Guide (Windows). p. 44, *The AMBUR Project*, R-Forge. Retrieved July 10, 2016 from http://ambur.r-forge.r-project.org/.

Jackson, N. L., Nordstrom, K. F., Saini, S., & Smith, D. R. (2010) Effects of Nourishment on the Form and Function of an Estuarine Beach. *Ecological Engineering*, 36, 1709-1718.

Jackson, C. W., Alexander, C. R., & Bush, D. M. (2012). Application of the AMBUR R Package for Spatio-temporal Analysis of Shoreline Change: Jekyll Island, Georgia, USA. *Computers and Geosciences*, 41, 199 - 207.

James, M. R., Robson, S., d'Oleire-Oltmanns, S. & Niethammer, U. (2017). Optimizing UAV Topographic Surveys Processed with Structure-From-Motion: Ground Control Quality, Quantity and Bundle Adjustment. *Geomorphology*, 280, 51-66.

Juliean, P. Y. (1995). *Erosion and Sedimentation*, 280 pp., Cambridge, Great Britain: Cambridge University Press.

Kirwan, M. L., & Megonigal, J. P. (2013). Tidal Wetland Stability in The Face of Human Impacts and Sea-Level Rise. *Nature*, 504(7478), 53-60.

Lillesand, T. M., Kiefer, R. W., & Chipman, J. W. (2007). *Remote Sensing and Image Interpretation*, 6th ed., 756 pp. New Jersey: John Wiley & Sons.

Marani, M., d'Alpaos, A., Lanzoni, S., & Santalucia, M. (2011). Understanding and Predicting Wave Erosion of Marsh Edges. *Geophysical Research Letters*, 38(21), 5 pp.

Maynord, S. T. (2007). Ship Forces on the Shoreline of the Savannah Harbor Project. *Final Report*, 62 pp. Vicksburg, MS: Engineer Research and Development Center, Coastal and Hydraulics Laboratory, U.S. Army Corps of Engineers.

McVeigh, B. (2018). Ecological and Economic Viability of Beneficially Using Dredged Materials for Reclamation Projects. *Unpublished Thesis*, 242 pp, Aberdeen, Scotland, U.K.: Robert Gordon University.

Meader, J. F. (2003). Fort Pulaski National Monument: Administrative History, Cultural Resources Division, Southeast Regional Office, National Park Service. 136 pp.

National Oceanic and Atmospheric Administration (2018). Datums for 8670870 Fort Pulaski, GA, *NOAA Tides and Currents*. Retrieved February 26, 2019 from https://tidesandcurrents.noaa.gov/sltrends/sltrends\_station.shtml?id=8670870

National Oceanic and Atmospheric Administration (2018). Relative Sea Level Trend: Fort Pulaski, Georgia, *NOAA Tides and Currents*. Retrieved November 13, 2018 from https://tidesandcurrents.noaa.gov/datums.html?id=8670870

National Research Council (1995). *Beach Nourishment and Protection*, 352 pp., Washington, D.C.: The National Academies Press.

National Weather Service (2019). Tropical Cyclone History for Southeast South Carolina and Northern Portions of Southeast Georgia. *Weather.gov*. Retrieved March 20, 2019 from https://www.weather.gov/chs/TChistory

Nordstrom, K. (2005). Beach Nourishment and Coastal Habitats: Research Needs to Improve Compatibility. *Restoration Ecology*, 13(1), 215-222.

Pix4D (2018). Pix4Dmapper. SA, Switzerland.

Pye, K., & Allen, J. R. L. (2000). Past, Present, and Future Interactions, Management Challenges, and Research Needs in Coastal and Estuarine Environments. In Pye, K., & Allen, J. R. L. (Eds.) *Coastal and Estuarine Environments: sedimentology, geomorphology and geoarcheology*, London: The Geological Society, 1-4.

QGIS Development Team (2019). QGIS Geographic Information System. Open Source Geospatial Foundation Project. Retrieved June 26, 2019 from http://qgis.osgeo.org

Romine, B. M., Fletcher, C. H. Frazer, L. N., Genz, A. S., Barbee, M. M., & Lim, S. C. (2009). Historical Shoreline Change, Southeast Oahu, Hawaii: Applying Polynomial Models to Calculate Shoreline Change Rates. *Journal of Coastal Research*, 25(6), 1236-1253.

Schwimmer, R. A. (2001). Rates and Processes of Marsh Shoreline Erosion in Rehoboth Bay, Delaware, USA. *Journal of Coastal Research*, 17(3), 672-683.

Selley, R. C. (2000). Applied Sedimentology. 2nd ed., 523 pp., USA: Academic Press.

Stewart, S. R. (2017), Hurricane Matthew. *Tropical Cyclone Report*. 96 pp, United States: National Hurricane Center. Retrieved March 20, 2019 from https://www.nhc.noaa.gov/data/tcr/AL142016\_Matthew.pdf

Thieler, E. R., Himmelstoss, E. A., Zichichi, J. L., & Ergul, A. (2009). The Digital Shoreline Analysis System (DSAS) version 4.0-an ArcGIS Extension for Calculating Shoreline Change. 2331-1258, US Geological Survey. Retrieved May 21, 2019 from https://pubs.er.usgs.gov/publication/ofr20081278

Trimble (2013), Trimble R8 Model 4, R6 Model 4, and R4 Model 3 GNSS Receivers User Guide. Retrieved September 19, 2017 from http://trl.trimble.com/docushare/dsweb/Get/Document-666220/R8-R6-R4-5800M3\_v411A\_UserGuide.pdf

U.S. Census Bureau (2010), GCT-PH1 - Population, Housing Units, Area, and Density: 2010 - State -- County / County Equivalent, generated by Colby Peffer (2019). Retrieved May 21, 2019 from http://factfinder.census.gov.

U.S. Environmental Planning Agency, U.S. Army Corps of Engineers (2007), Identifying, Planning, and Financing Beneficial Use Projects Using Dredged Material, 114 pp., Final Report EPA842-B-07-001.

van Maren, D. S., van Kessel, T., Cronin, K., & Sittoni, L. (2015), The Impact of Channel Deepening and Dredging on Estuarine Sediment Concentration, *Continental Shelf Research*, 95, 1-14.

Van Westendorp, C. H. (2005), Impacts of Physical Processes on a Coastal Georgia Estuary: Fort Pulaski National Monument Oyster Shell Ridge. *Unpublished Master's Thesis*, 109 pp, Savannah, Georgia, USA: Savannah State University.

Wentworth, C. K. (1922), A Scale of Grade Class Terms for Clastic Sediments. *Journal of Geology*, 30, 377-392.

Westoby, M.J., Brasington, J., Glasser, N.F., Hambrey, M.J., Reynolds, J.M., (2012), 'Structure-from-Motion' Photogrammetry: A Low Cost, Effective Tool for Geoscience Applications, *Geomorphology*, 179, 300-314.

Wickham, H. (2016), ggplot2: Elegant Graphics for Data Analysis, New York: Springer-Verlag.

# TABLES AND FIGURES

Table 1. Digitized shoreline information for Cockspur Island, including imagery types, imagery source, digitizing and total shoreline error values.

Shoreline Year	Imagery Type	Source	Digitizer	Total Estimated Error (m)
1933	NOS T-sheets (from aerial photographs)	National Ocean Survey	National Ocean Survey	6.1
1970	Controlled aerial photograph	National Ocean Service	Colby Peffer	8.5
1972	Controlled aerial photograph	unknown	Colby Peffer	3.4
1987	NOS Chart	National Ocean Service	Colby Peffer	3.0
1993	Controlled aerial photograph	National Aerial Photography Program	Alexander lab archives	3.4
1999	Controlled aerial photograph	<b>USGS DOQQ</b>	Alexander lab archives	3.4
2004	Controlled aerial photograph	SAGIS	Alexander lab archives	3.2
2013	Controlled aerial photograph	National Ocean Service	Colby Peffer	3.4
2016	Controlled aerial photograph	National Ocean Service	Alexander lab archives	3.2
2017	Pedestrian survey with Trimble GeoXT	Alexander, UGA SkIO	Colby Peffer	0.4
2018	Controlled aerial photograph	National Ocean Service	Colby Peffer	3.4

Table 2. UAV flight parameters used in Pix4D capture iOS application for Apple  $^{\circ}$  iPad.

Flight Parameter	Value		
Altitude (Above Ground Level)	53 m		
Image Size	5472 x 3648 pixels		
Forward Overlap	85 %		
Side Overlap	75 %		
Camera Angle (% of images)	Nadir: 50%; Oblique: 50%		
Planned Ground Sampling Distance	~1.5 cm		
Image Capture Methods	During flight		

Table 3. Results for shoreline change analysis using AMBUR transect data showing percent erosional and accretionary transects and shoreline change statistics. For net change and EPR, positive values indicate accretion and negative values indicate erosion.

Shoreline	Number of Transects	Percent Erosional	Percent Accretionary	Mean Net Change (m)	Max. Net Change (m)	Mean EPR (my <sup>-1</sup> )	Max. EPR (my <sup>-1</sup> )	EPR Error (my <sup>-1</sup> )
Northern - All	81	83 %	17 %	-27.67	-143.84	-0.35	-1.68	$\pm 0.07 \text{-} 0.20$
Northern - Unstabilized	81	86 %	14 %	-32.30	-143.84	-0.47	-1.69	$\pm 0.08$ -0.28
Northern - Stabilized	22	64 %	36 %	-1.80	-10.55	-0.04	-0.23	± 0.10
Southern - All	89	81 %	19 %	-12.91	-40.40	-0.16	-0.54	$\pm 0.08$
Eastern - All	22	0 %	100 %	+321.70	+839.68	+3.79	+3.24	± 0.07-0.08

Table 4. Tidal Datums and Extreme Water Levels observed at Fort Pulaski National Monument. \*All tidal datum conversions retrieved from NOAA Tides and Currents for Fort Pulaski, GA tidal gauge were retrieved from https://tidesandcurrents.noaa.gov/datums.html?id=8670870

Water Level	Elevation (NAVD88) (m)	Source
Mean Sea Level	-0.07	NOAA Tides and Currents*
Mean High Water	+0.94	NOAA Tides and Currents*
Mean Higher High Water	+1.05	NOAA Tides and Currents*
Spring High Tide	+1.37	(Clayton et al., 1992)
Extreme Water Level: October 2015	+1.94	NOAA Tides and Currents*
Extreme Water Level: October 2016	+2.58	NOAA Tides and Currents*
Extreme Water Level: September 11, 2017	+2.40	NOAA Tides and Currents*

Table 5. Areal elevation change of the nourished northern shoreline of Cockspur Island from April 2015 to March 2019

Interval	Accretional (% of cells)	Erosional (% of cells)	No Change (% of cells)	Combined Surface Error (m)
April '15 to November '15	95.2	0.2	4.6	± 0.07
November '15 to June '17	19.0	42.1	38.9	± 0.16
June '17 to July '18	29.1	30.8	40.1	± 0.16
July '18 to August '18	2.7	3.5	93.8	$\pm 0.08$
August '18 to September '18	2.0	8.3	89.7	± 0.09
September '18 to October '18	3.3	6.4	90.3	$\pm 0.08$
October '18 to December '18	18.6	24.2	57.2	± 0.05
December '18 to February '19	26.0	12.8	61.2	± 0.05
February '19 to March '19	2.6	49.4	48.0	± 0.06
November '15 to March '19	24.8	52.8	22.3	± 0.16

Table 6. Volume change of the nourished northern shoreline of Cockspur Island from April 2015 to March 2019. Intervals highlighted in grey indicate intervals with volume change greater than the interval volume error.

Interval	Interval Volume Change (m³)	Interval % Volume Change	Interval % Monthly Volume Change	Months in Interval
April '15 to November '15	$+114,669 \pm 4,000$	100 %		N/A
November '15 to June '17	$-11,716 \pm 8,630$	-10.2 ± 8.4 %	$\text{-}0.5 \pm 0.4 \; \%$	19
June '17 to July '18	$-4,583 \pm 8,777$	-4.5 ± 8.9 %	$-0.3\pm0.7~\%$	13
July '18 to August '18	$-105 \pm 4{,}054$	-0.1 $\pm$ 4.1 %	-0.1 $\pm$ 4.1 %	1
August '18 to September '18	$-1,199 \pm 4,597$	$-1.2 \pm 4.7 \%$	$-1.2 \pm 4.7 \%$	1
September '18 to October '18	$+88 \pm 4{,}494$	$+0.1\pm4.6~\%$	$+0.1\pm4.6~\%$	1
October '18 to December '18	$-1,148 \pm 2,452$	$-1.2 \pm 2.5 \%$	$-0.6\pm1.3~\%$	2
December '18 to February '19	$+259 \pm 2,929$	$+0.3\pm3.0~\%$	$+0.1\pm1.5~\%$	2
February '19 to March '19	$-3,847 \pm 3,282$	-4.0 ± 3.6 %	-4.0 ± 3.6 %	1
November '15 to March '19	$-21,973 \pm 8,343$	-19.2 ± 7.3 %	$\text{-}0.48 \pm 0.2 \; \%$	40

Table 7. Subsection A volume change of the nourished northern shoreline of Cockspur Island from April 2015 to March 2019. Intervals highlighted in grey indicate intervals with volume change beyond the interval volume error.

Interval	Interval Volume Change (m³)	Interval % Volume Change	Interval % Monthly Volume Change	Months in Interval
April '15 to November '15	$+16,799 \pm 842$	+100 %		N/A
November '15 to June '17	$-2,470 \pm 1,816$	-14.7 ± 12.7 %	$\text{-}0.8 \pm 0.7 \%$	19
June '17 to July '18	$-1,450 \pm 1,847$	-10.1 ± 14.3 %	$\text{-}0.8 \pm 1.1 \; \%$	13
July '18 to August '18	$-401 \pm 853$	$-3.1 \pm 6.8 \%$	$-3.1 \pm 6.8 \%$	1
August '18 to September '18	$-720 \pm 967$	$\text{-}5.8 \pm 8.2 \ \%$	$\text{-}5.8 \pm 8.2 \ \%$	1
September '18 to October '18	$+436 \pm 945$	$+3.7\pm7.8$ %	$+3.7\pm7.8$ %	1
October '18 to December '18	$-564 \pm 510$	-4.6 ± 4.4 %	-2.3 ± 2.2 %	2
December '18 to February '19	$+484 \pm 616$	$+4.2 \pm 5.1 \%$	$+2.1 \pm 2.5 \%$	2
February '19 to March '19	$-1,238 \pm 691$	-10.2 ± 6.3 %	-10.2 ± 6.3 %	1
November '15 to March '19	$-6,022 \pm 1,755$	-35.8 ± 10.4 %	$-0.9\pm0.3~\%$	40

Table 8. Subsection B volume change of the nourished northern shoreline of Cockspur Island from April 2015 to March 2019. Intervals highlighted in grey indicate intervals with volume change beyond the interval volume error.

Interval	Interval Volume Change (m³)	Interval % Volume Change	Interval % Monthly Volume Change	Months in Interval
April '15 to November '15	$+83,222 \pm 2,091$	+100 %		N/A
November '15 to June '17	$-7,534 \pm 4,511$	-9.1 ± 6.0 %	$-0.5 \pm 0.3 \%$	19
June '17 to July '18	$-6,649 \pm 4,587$	$-8.8 \pm 6.6 \%$	$\text{-}0.7 \pm 0.5 \ \%$	13
July '18 to August '18	$-28 \pm 2{,}119$	$0.0\pm3.1~\%$	$0.0 \pm 3.1 \%$	1
August '18 to September '18	$-780 \pm 2{,}403$	-1.1 ± 3.5 %	$-1.1 \pm 3.5 \%$	1
September '18 to October '18	$-306 \pm 2{,}349$	-0.4 ± 3.5 %	$-0.4\pm3.5~\%$	1
October '18 to December '18	$-954 \pm 1,267$	-1.4 ± 1.9 %	$\text{-}0.7 \pm 0.9 \ \%$	2
December '18 to February '19	$-62 \pm 1{,}531$	$\text{-}0.1 \pm 2.3 \ \%$	$0.0\pm1.1~\%$	2
February '19 to March '19	$-2,251 \pm 1,715$	$-3.4 \pm 2.7 \%$	$-3.4 \pm 2.7 \%$	1
November '15 to March '19	$-18,261 \pm 4,361$	-21.9 ± 5.2 %	$\text{-}0.6 \pm 0.1 \; \%$	40

Table 9. Subsection C volume change of the nourished northern shoreline of Cockspur Island from April 2015 to March 2019. Intervals highlighted in grey indicate intervals with volume change beyond the interval volume error.

Interval	Interval Volume Change (m³)	Interval % Volume Change	Interval % Monthly Volume Change	Months in Interval
April '15 to November '15	$14,563 \pm 1,068$	100 %		N/A
November '15 to June '17	$-1,631 \pm 2,304$	-11.2 ± 17.8 %	$\text{-}0.6 \pm 0.9 \ \%$	19
June '17 to July '18	$+3,501 \pm 2,343$	27.1 ± 14.3 %	$+2.1 \pm 1.1 \%$	13
July '18 to August '18	$+321 \pm 1,083$	$+2.0\pm6.5~\%$	$+2.0 \pm 6.5 \%$	1
August '18 to September '18	$+299 \pm 1,227$	$+1.8\pm7.2~\%$	$+1.8 \pm 7.2 \%$	1
September '18 to October '18	$-41 \pm 1{,}200$	-0.2 ± 7.1 %	-0.2 ± 7.1 %	1
October '18 to December '18	$+368 \pm 647$	$+2.2\pm3.7~\%$	$+1.1 \pm 1.9 \%$	2
December '18 to February '19	$-166 \pm 782$	$\text{-}1.0 \pm 4.5 \%$	$-0.5 \pm 2.3 \%$	2
February '19 to March '19	$-355 \pm 876$	-2.1 ± 5.2 %	$-2.1 \pm 5.2 \%$	1
November '15 to March '19	$+2,372 \pm 2,228$	+16.3 ± 15.3 %	$+0.4 \pm 0.4\%$	40



Figure 1. Map of Cockspur Island. Inset map (bottom left) shows relative location of Cockspur Island (white box) to Georgia coast. The red box on the northern shoreline of Cockspur Island indicates the nourished region of the shoreline.

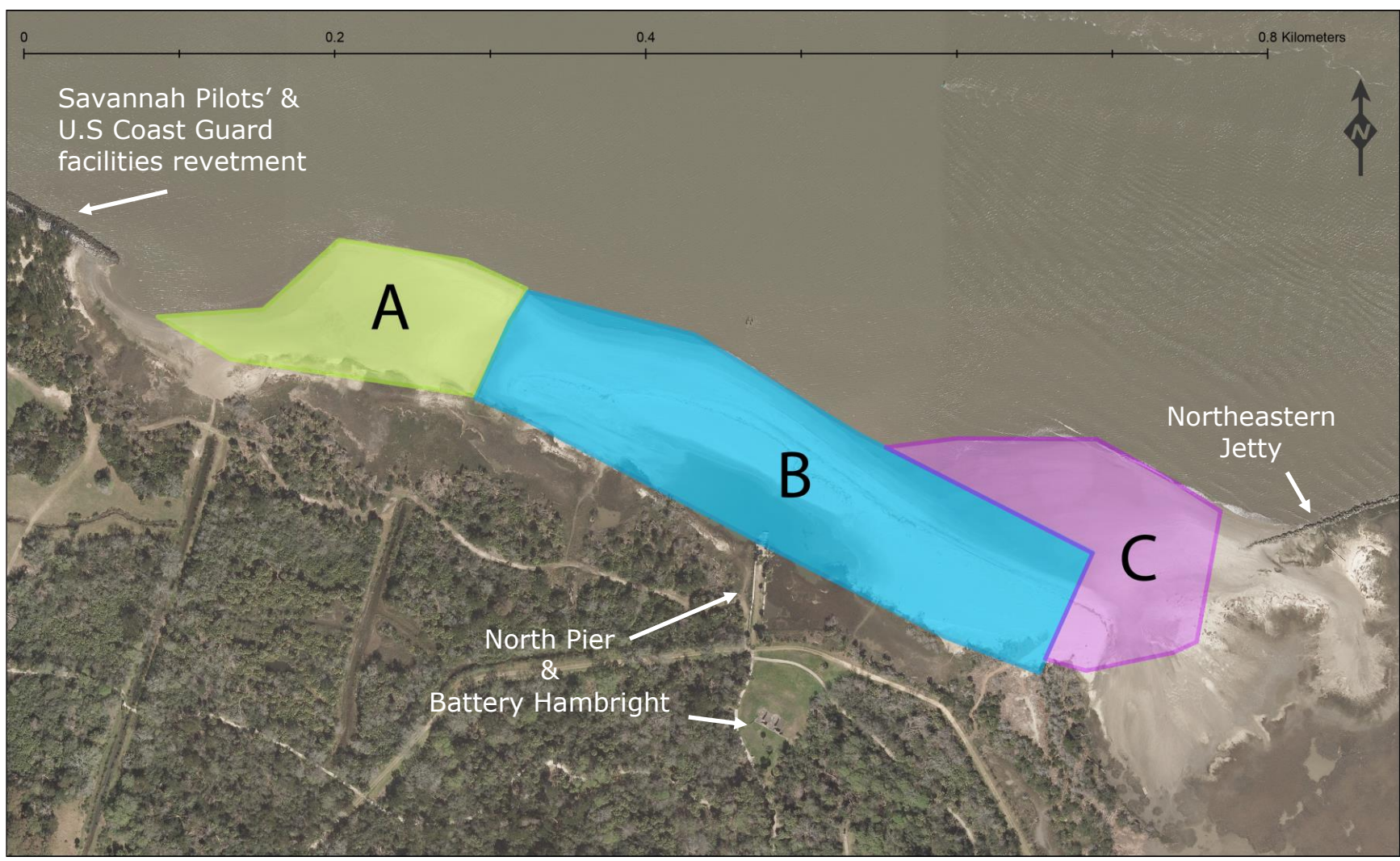


Figure 2. Map of Cockspur Island's nourished northern shoreline, with overlaid analysis, divided into subsections A (in green), B (in blue), and C (in purple). The North Pier and Battery Hambright are shown south of subsection B, and the area is bordered by a revetment to the west and a jetty to the east.

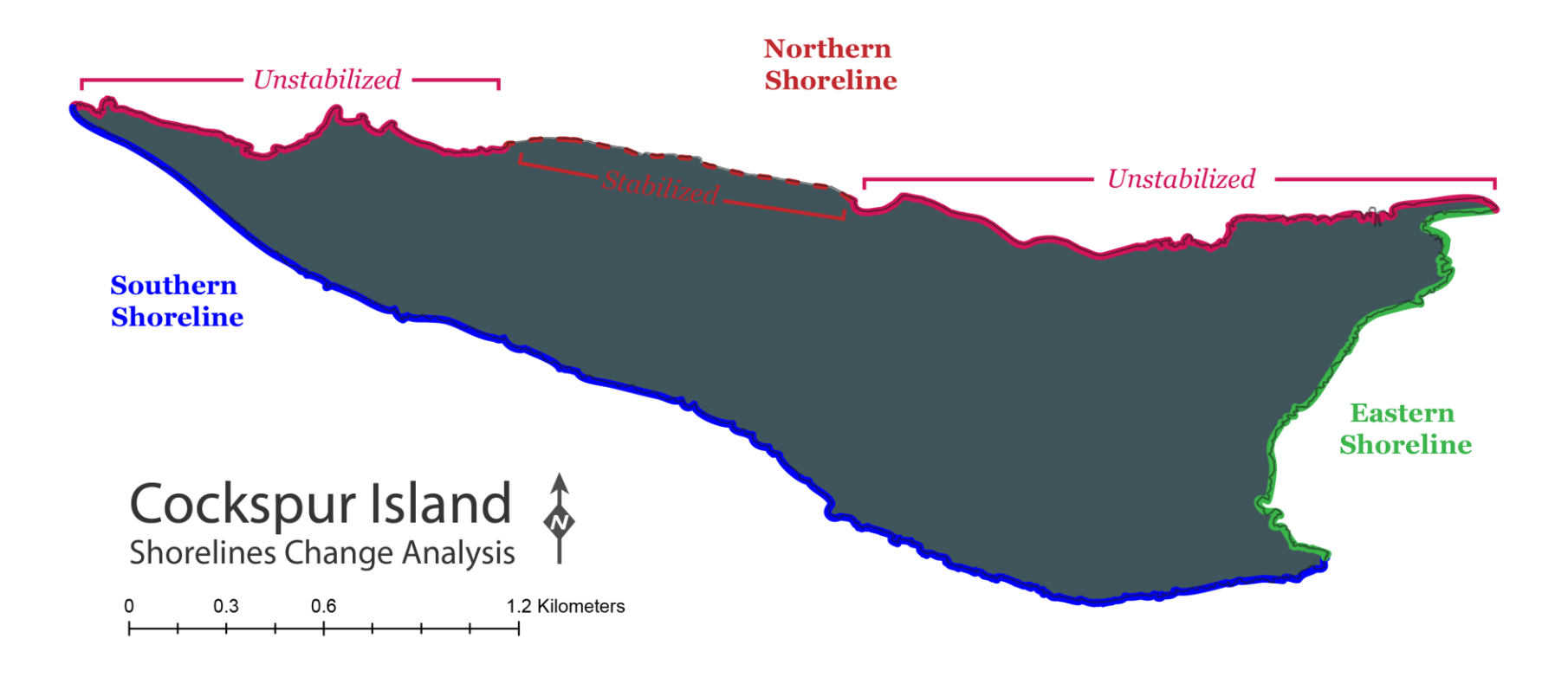


Figure 3. Map of Cockspur Island AMBUR shoreline regions. The red line indicates the northern shoreline, the purple line indicates the southern shoreline, and the blue line indicates the eastern shoreline as of 2018. The solid red line indicates sections of the northern shoreline included in the Unstabilized analysis. The dashed red line indicates the section of the northern shoreline included in the Stabilized analysis.

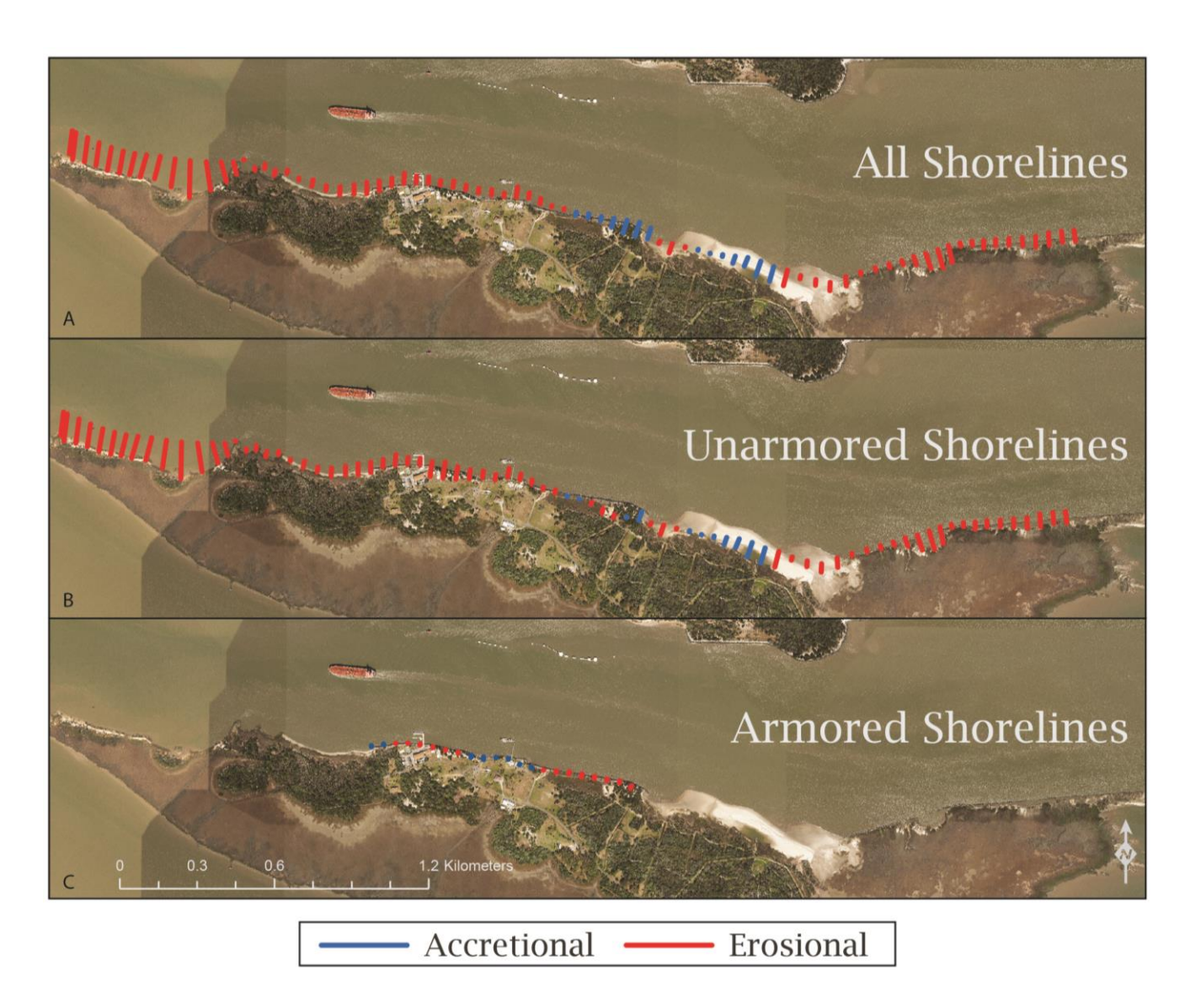


Figure 4. AMBUR produced transects of Cockspur Island northern shoreline. Length of transects represent the magnitude of change. A) Analysis performed with all shoreline transects, from 1933 to 2018. B) Analysis performed with only unstabilized shorelines transects. C) Analysis performed with only stabilized shoreline transects and years. Blue transects indicate net accretion, red transects indicate net erosion.

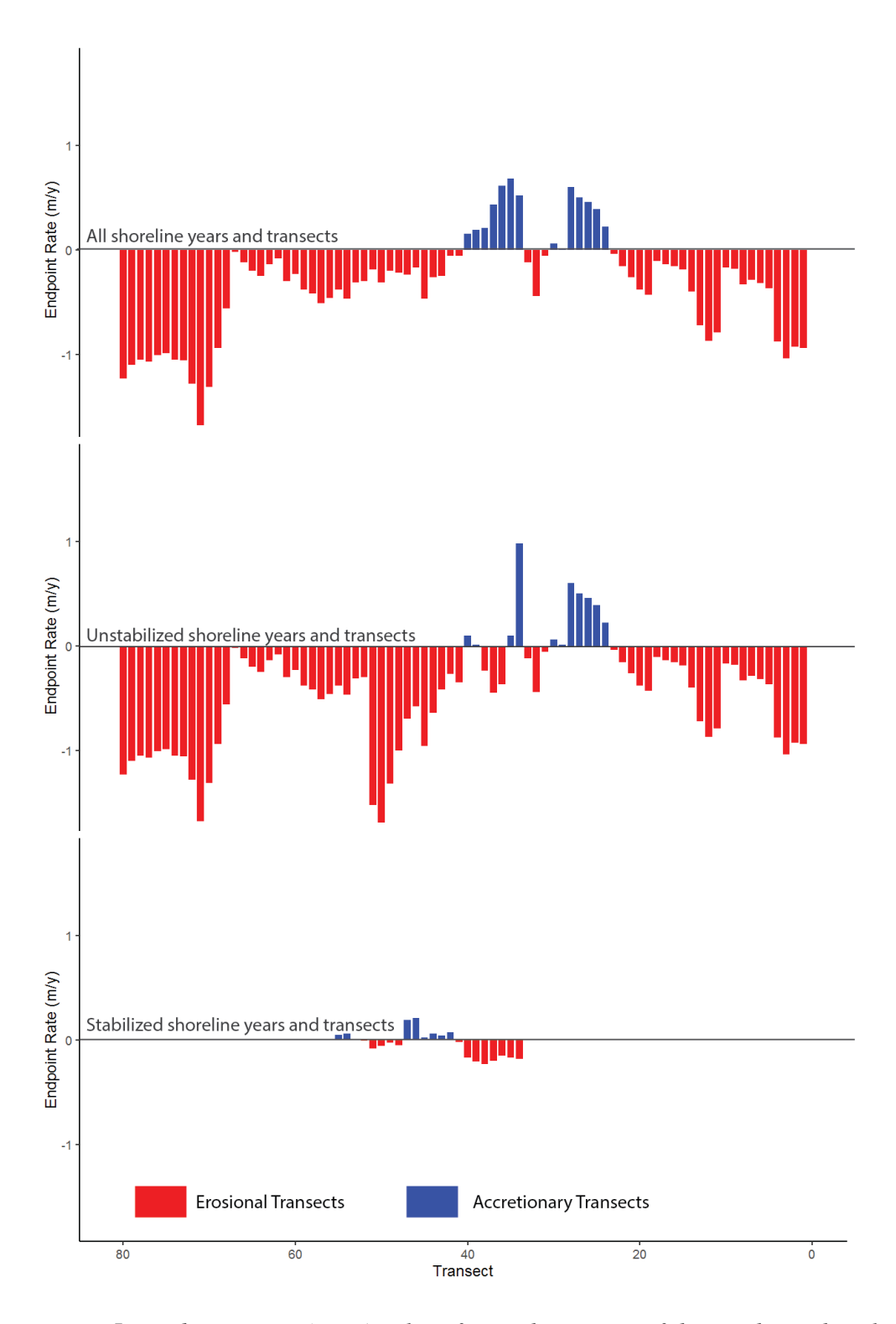


Figure 5. End point rate (EPR) values for each transect of the northern shoreline, plotted by shoreline analysis group. The top graph is All shorelines, middle graph is Unstabilized shorelines, and bottom graph is Stabilize shorelines. The y-axis is identical for each plot. Red bars are erosional, blue bars are accretional.

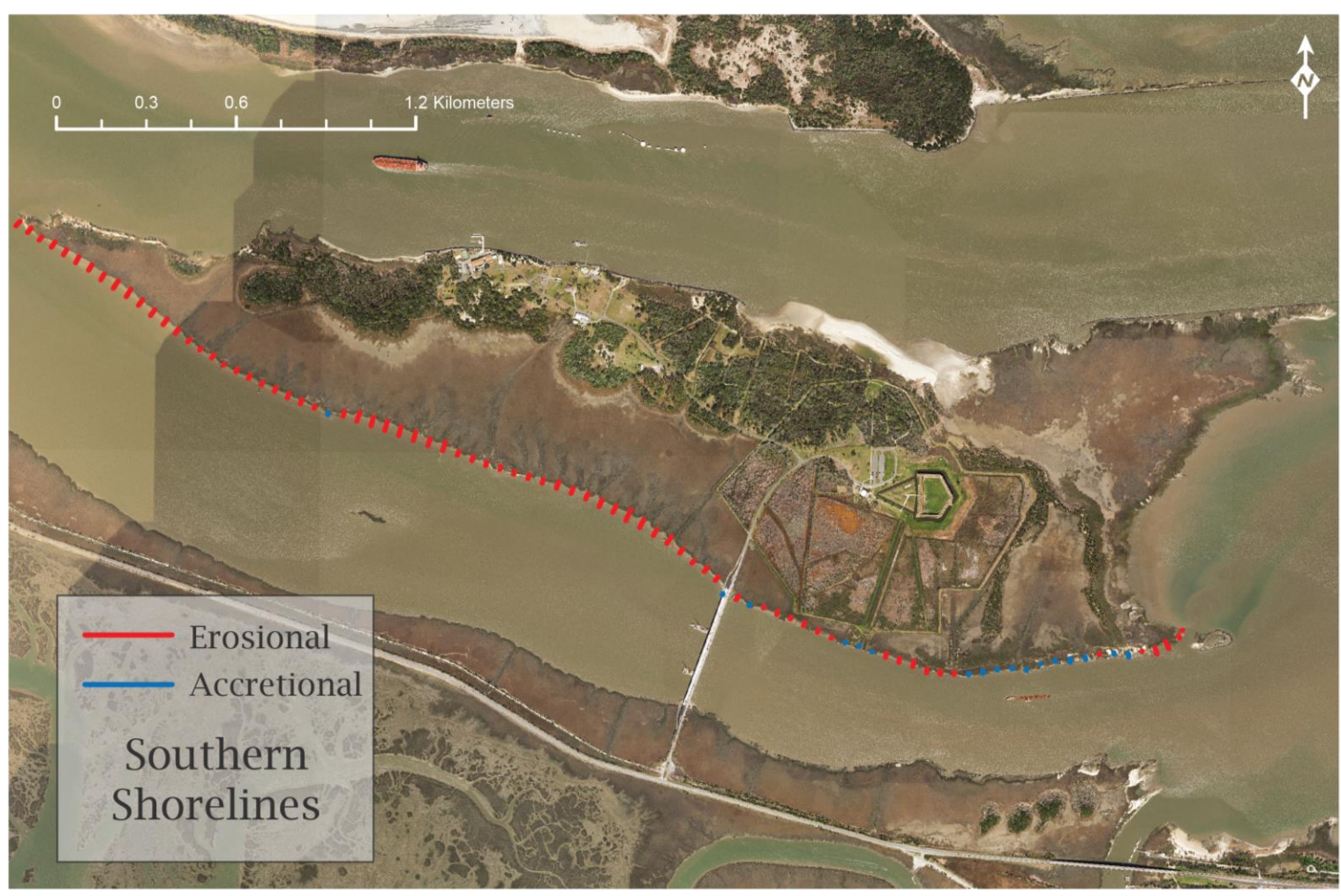


Figure 6. AMBUR produced transects of Cockspur Island southern shoreline. Length of transects represent the magnitude of change. Analysis performed with all shoreline transects, from 1933 to 2018. Blue transects indicate net accretion, red transects indicate net erosion.

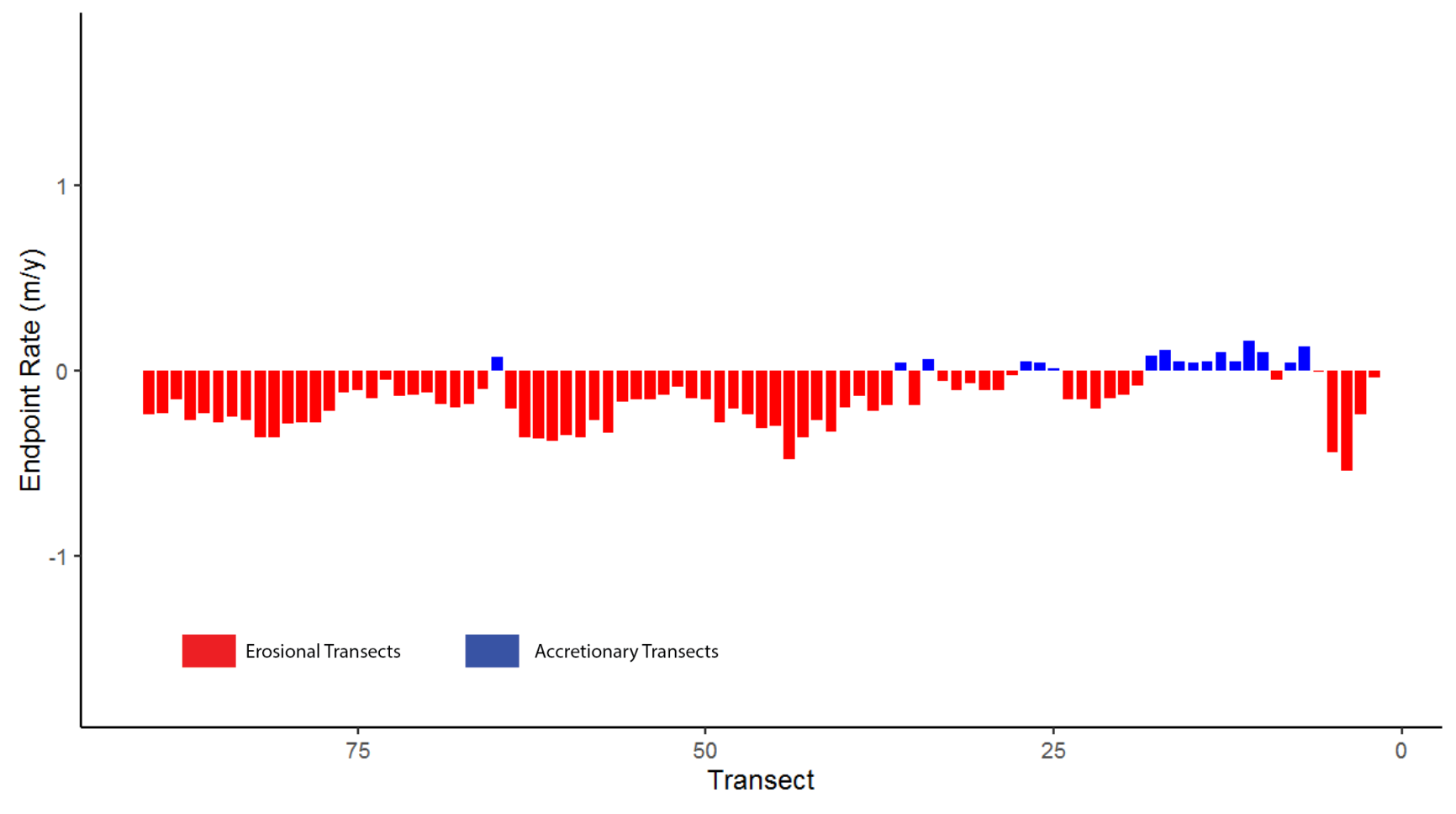


Figure 7. AMBUR produced end point rate (EPR) values for each southern shoreline transect from 1933 to 2018. Red bars are erosional, blue bars are accretional.



Figure 8. AMBUR produced transects of Cockspur Island eastern shoreline. Length of transects represent the magnitude of change. Analysis performed with all shoreline transects, from 1933 to 2018. Blue transects indicate net accretion, there are no erosional transects.

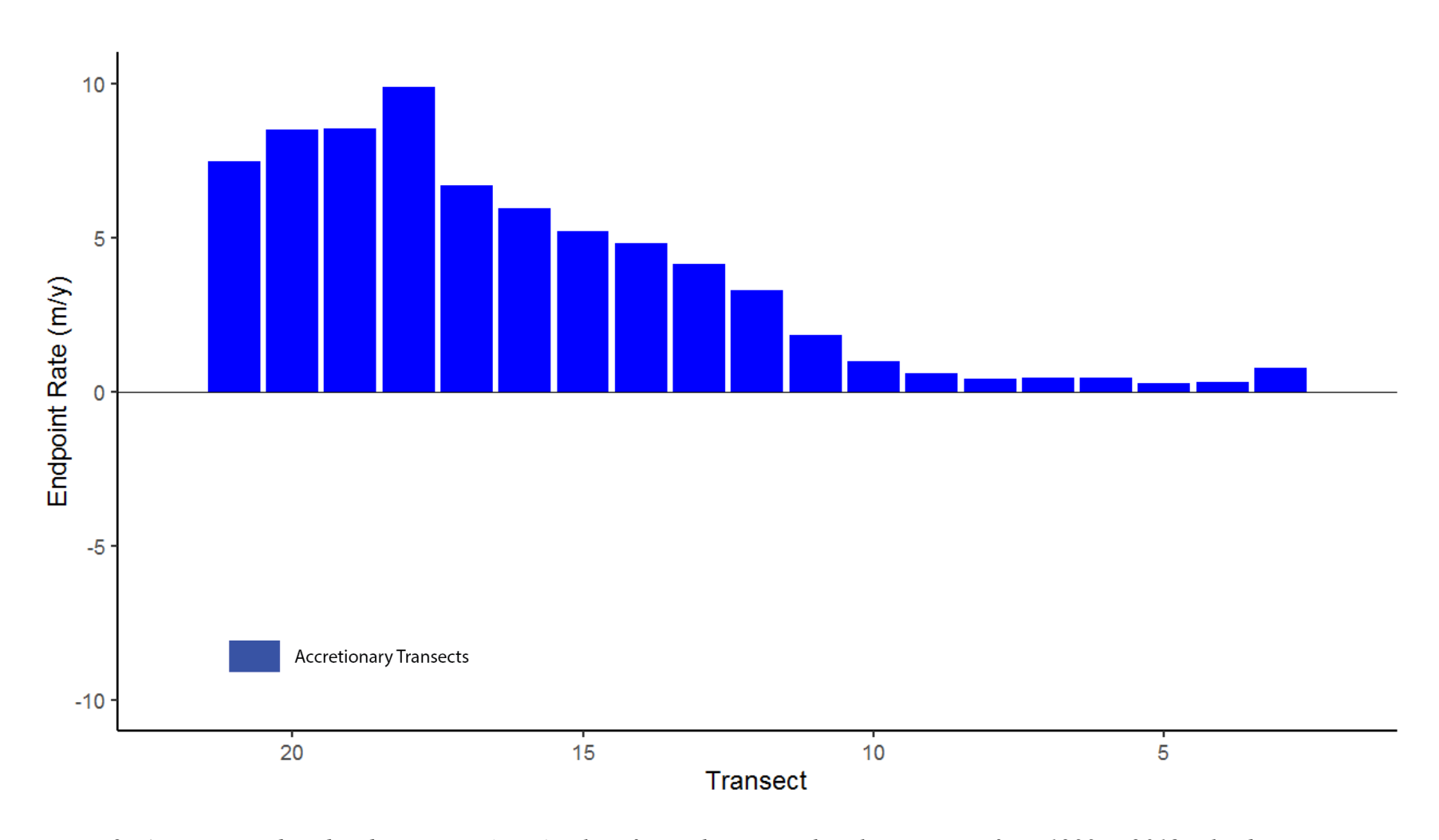


Figure 9. AMBUR produced end point rate (EPR) values for each eastern shoreline transect from 1933 to 2018. Blue bars are accretional, there are no erosional bars.

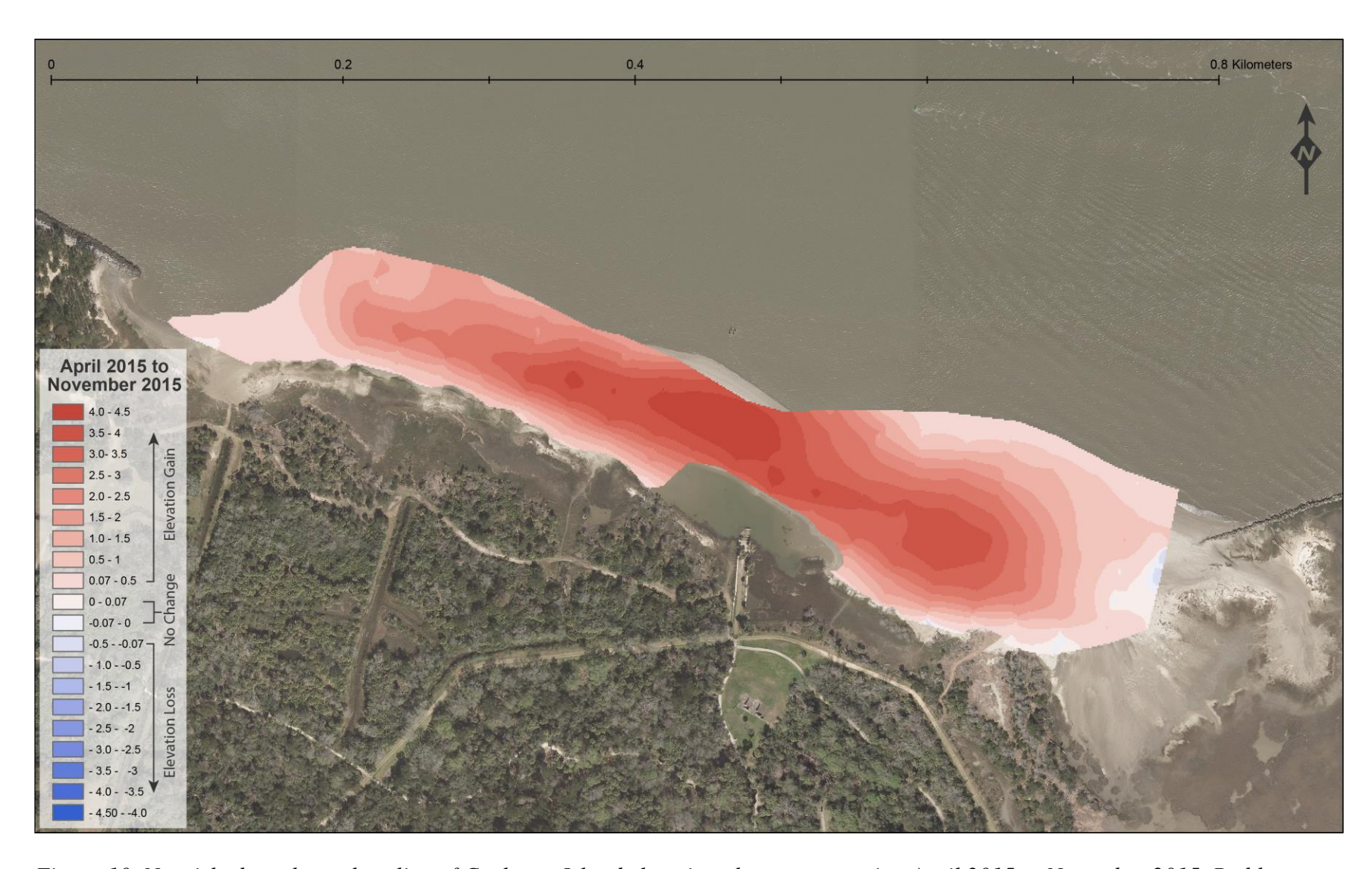


Figure 10. Nourished northern shoreline of Cockspur Island elevation change comparing April 2015 to November 2015. Red hues indicate elevation gain, blue hues indicate elevation loss. More saturated colors indicate greater elevation change.

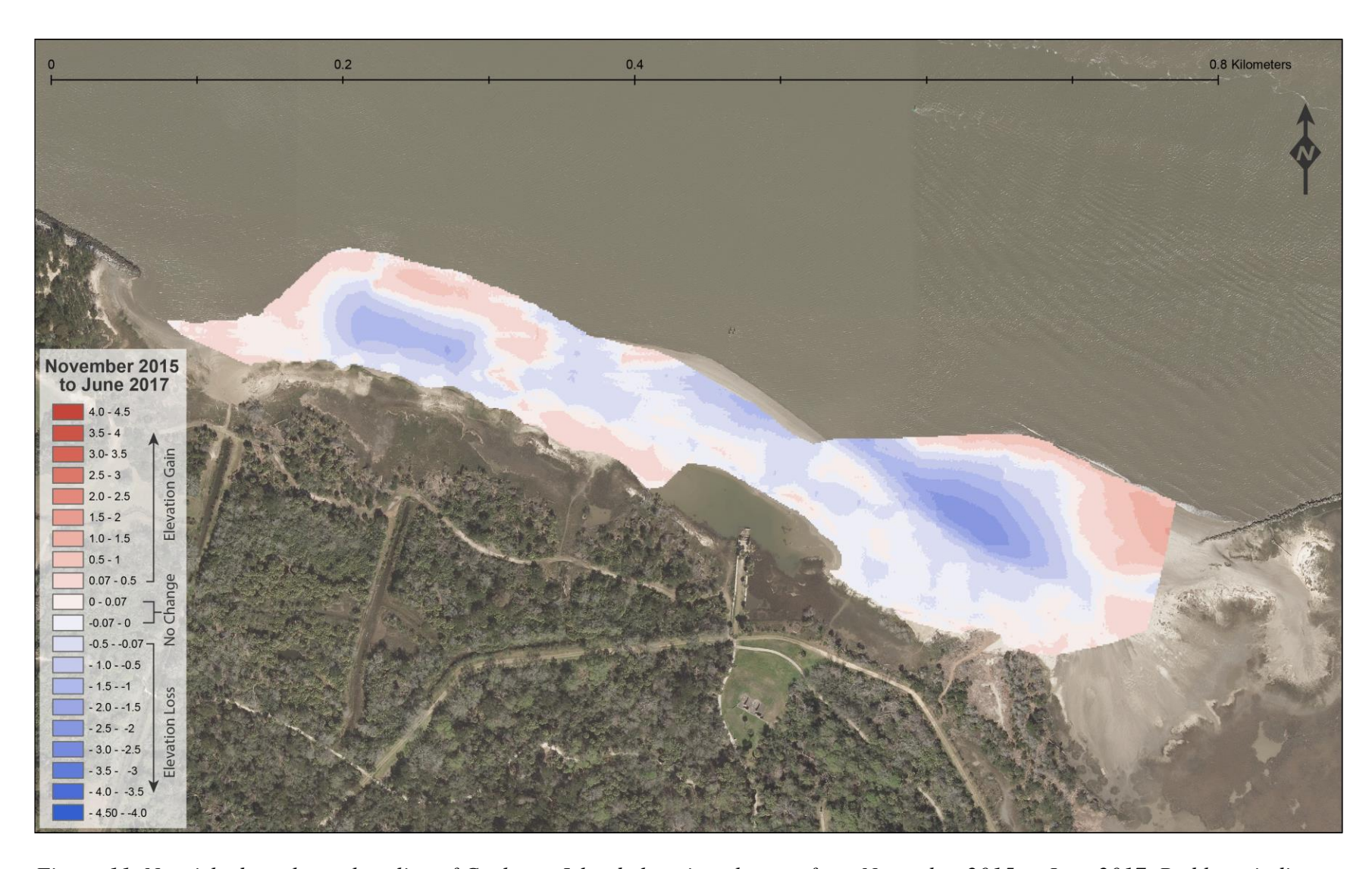


Figure 11. Nourished northern shoreline of Cockspur Island elevation changes from November 2015 to June 2017. Red hues indicate elevation gain, blue hues indicate elevation loss. More saturated colors indicate greater elevation change.

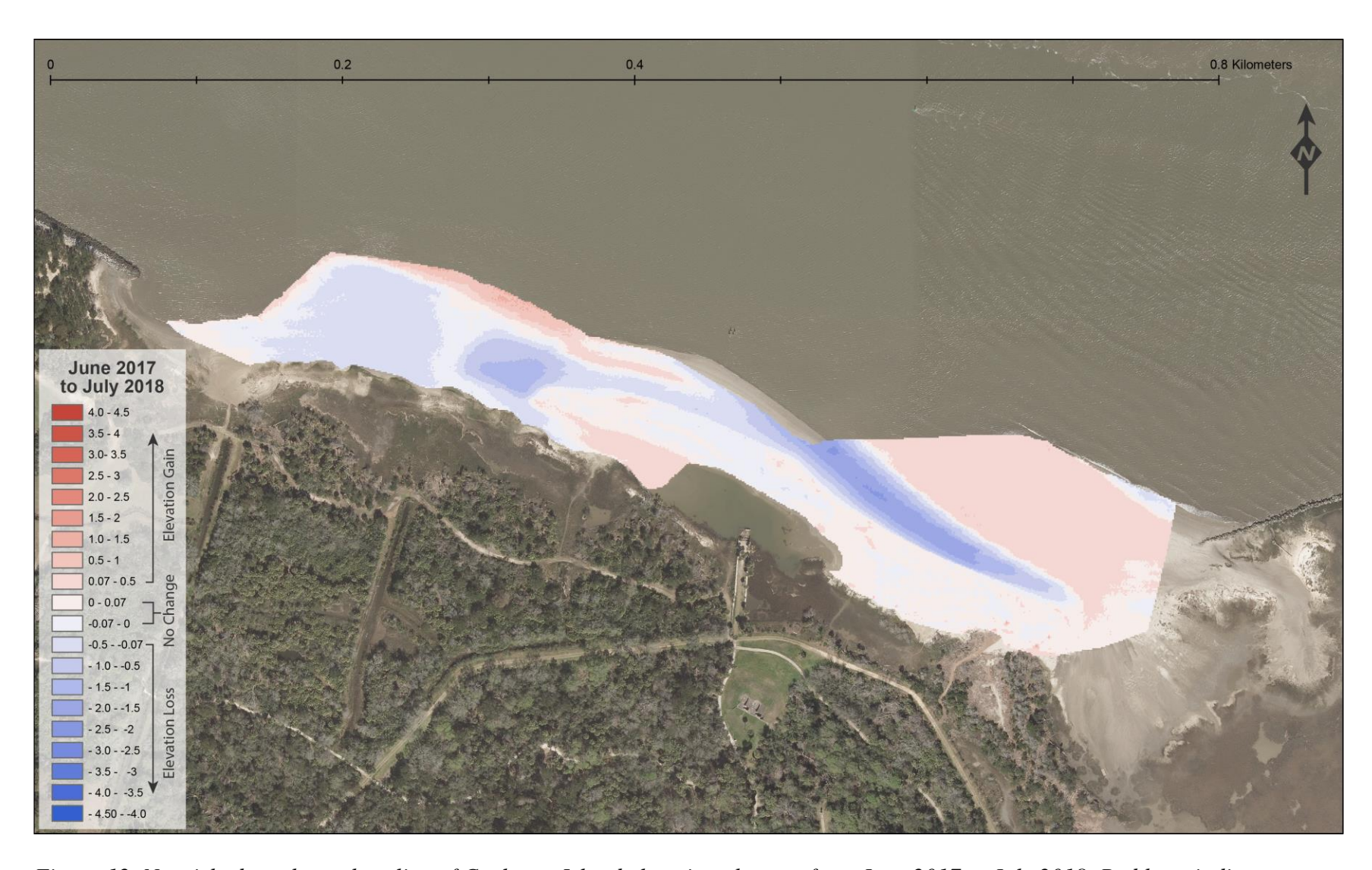


Figure 12. Nourished northern shoreline of Cockspur Island elevation changes from June 2017 to July 2018. Red hues indicate elevation gain, blue hues indicate elevation loss. More saturated colors indicate greater elevation change.

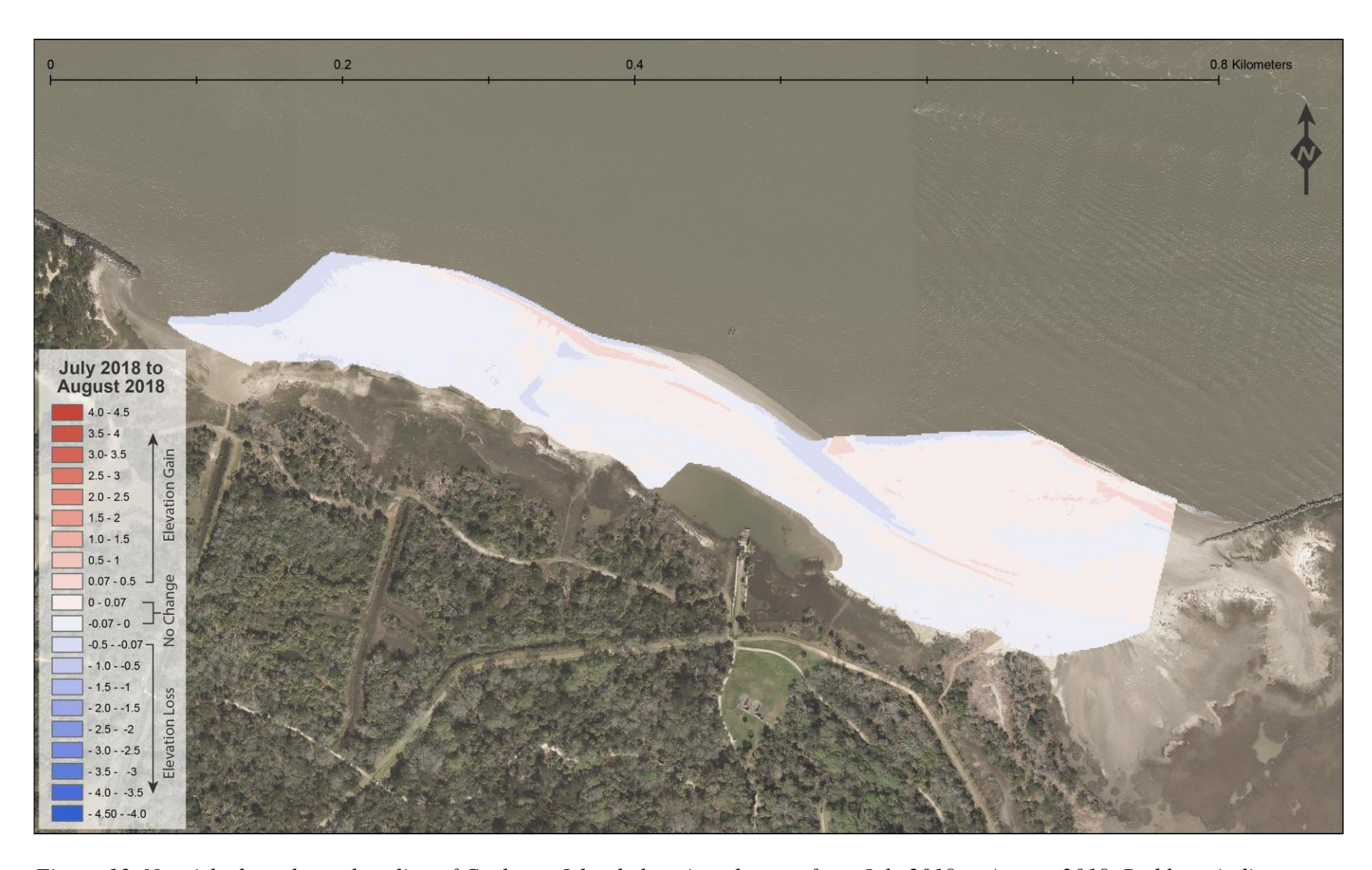


Figure 13. Nourished northern shoreline of Cockspur Island elevation changes from July 2018 to August 2018. Red hues indicate elevation gain, blue hues indicate elevation loss. More saturated colors indicate greater elevation change.

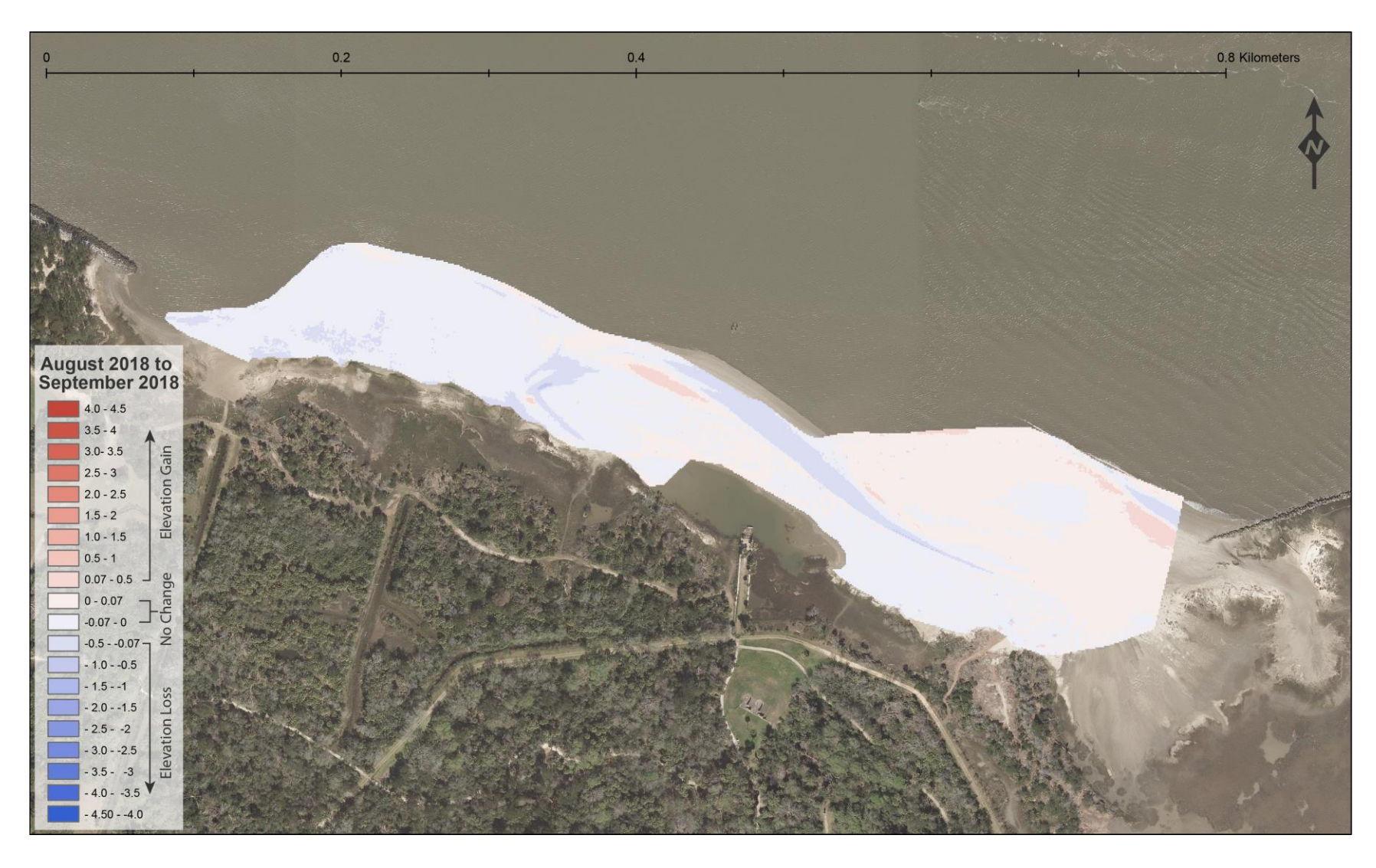


Figure 14. Nourished northern shoreline of Cockspur Island elevation changes from August 2018 to September 2018. Red hues indicate elevation gain, blue hues indicate elevation loss. More saturated colors indicate greater elevation change.

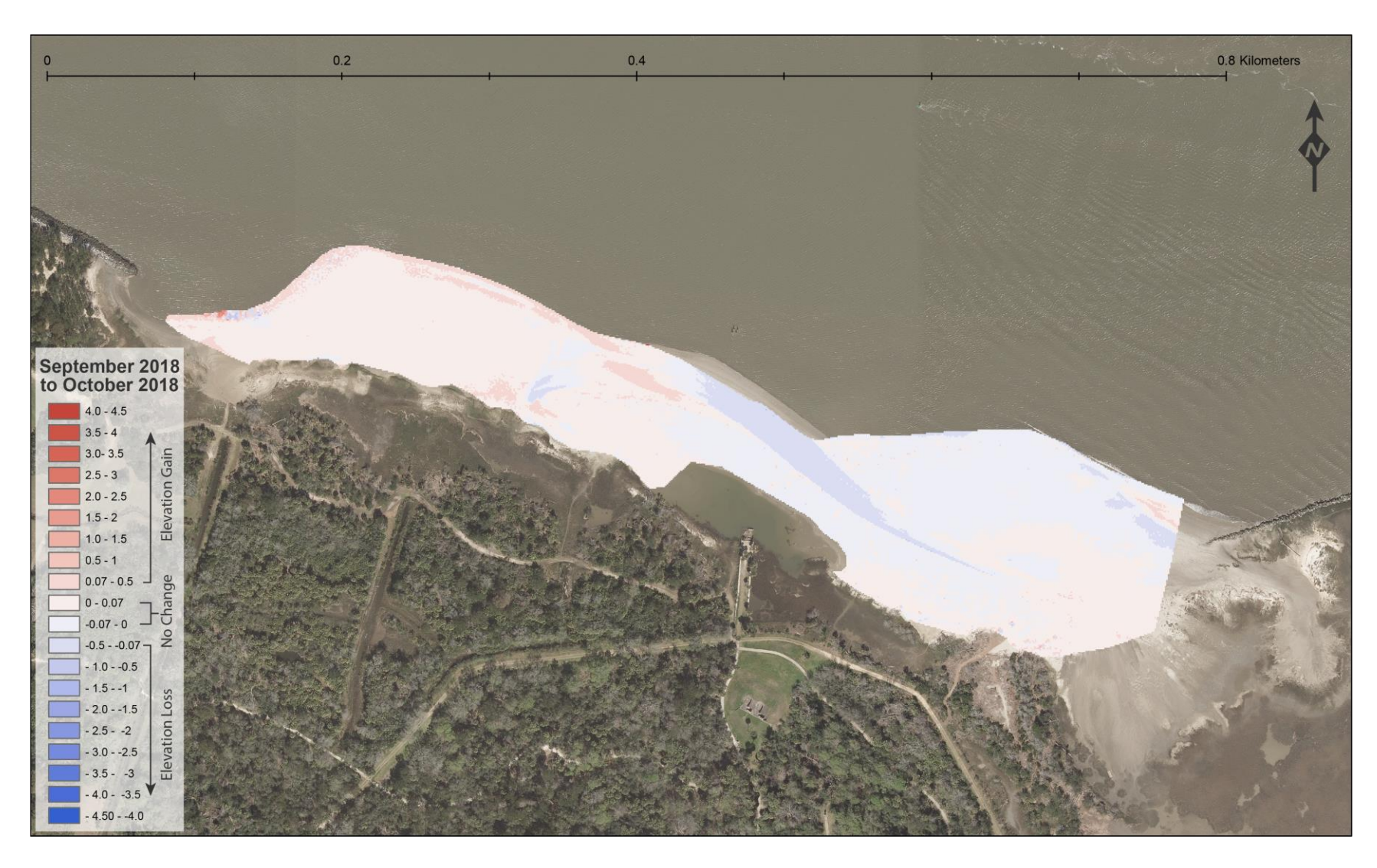


Figure 15. Nourished northern shoreline of Cockspur Island elevation changes from September 2018 to October 2018. Red hues indicate elevation gain, blue hues indicate elevation loss. More saturated colors indicate greater elevation change.

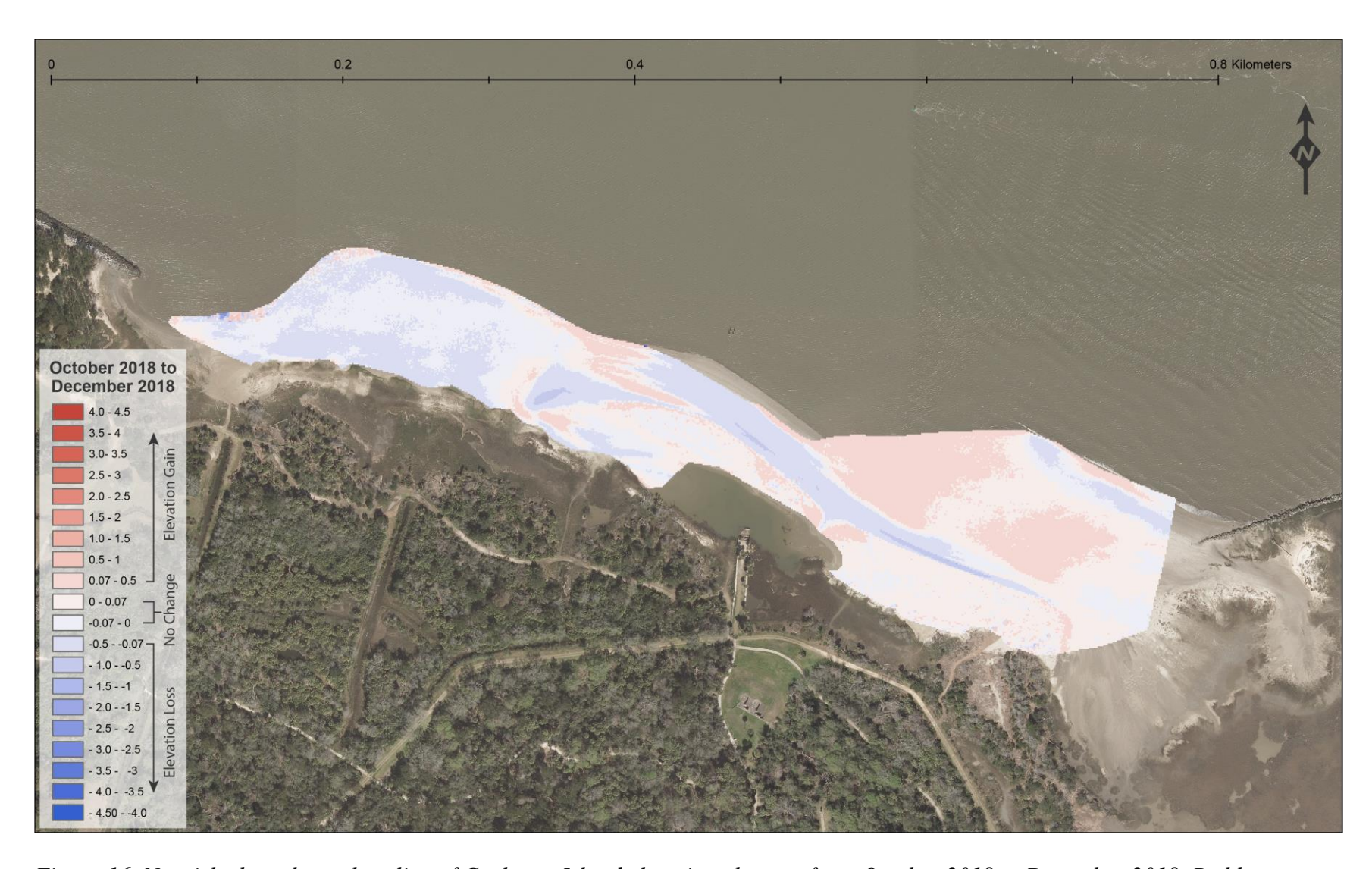


Figure 16. Nourished northern shoreline of Cockspur Island elevation changes from October 2018 to December 2018. Red hues indicate elevation gain, blue hues indicate elevation loss. More saturated colors indicate greater elevation change.

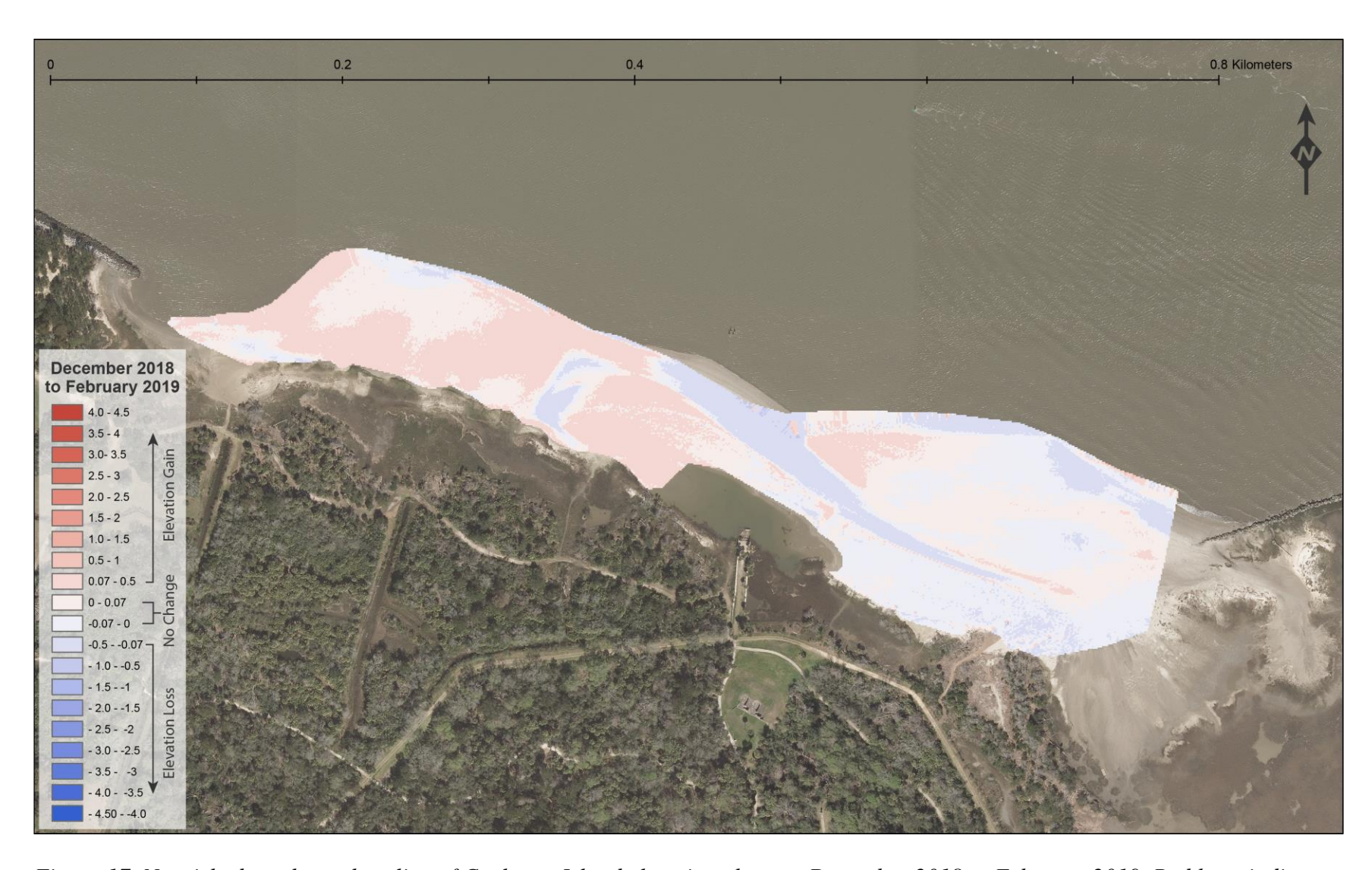


Figure 17. Nourished northern shoreline of Cockspur Island elevation changes December 2018 to February 2019. Red hues indicate elevation gain, blue hues indicate elevation loss. More saturated colors indicate greater elevation change.

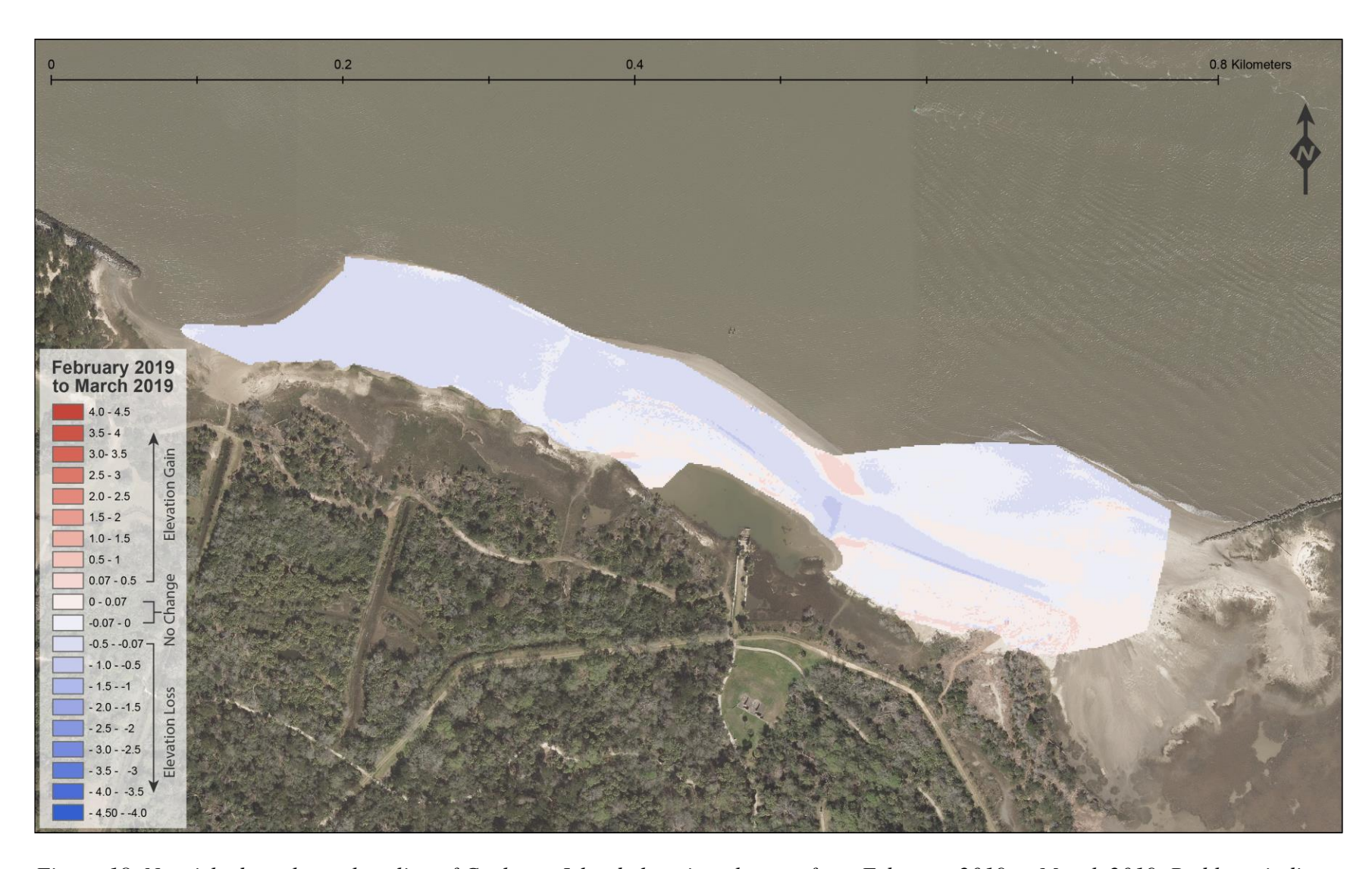


Figure 18. Nourished northern shoreline of Cockspur Island elevation changes from February 2019 to March 2019. Red hues indicate elevation gain, blue hues indicate elevation loss. More saturated colors indicate greater elevation change.

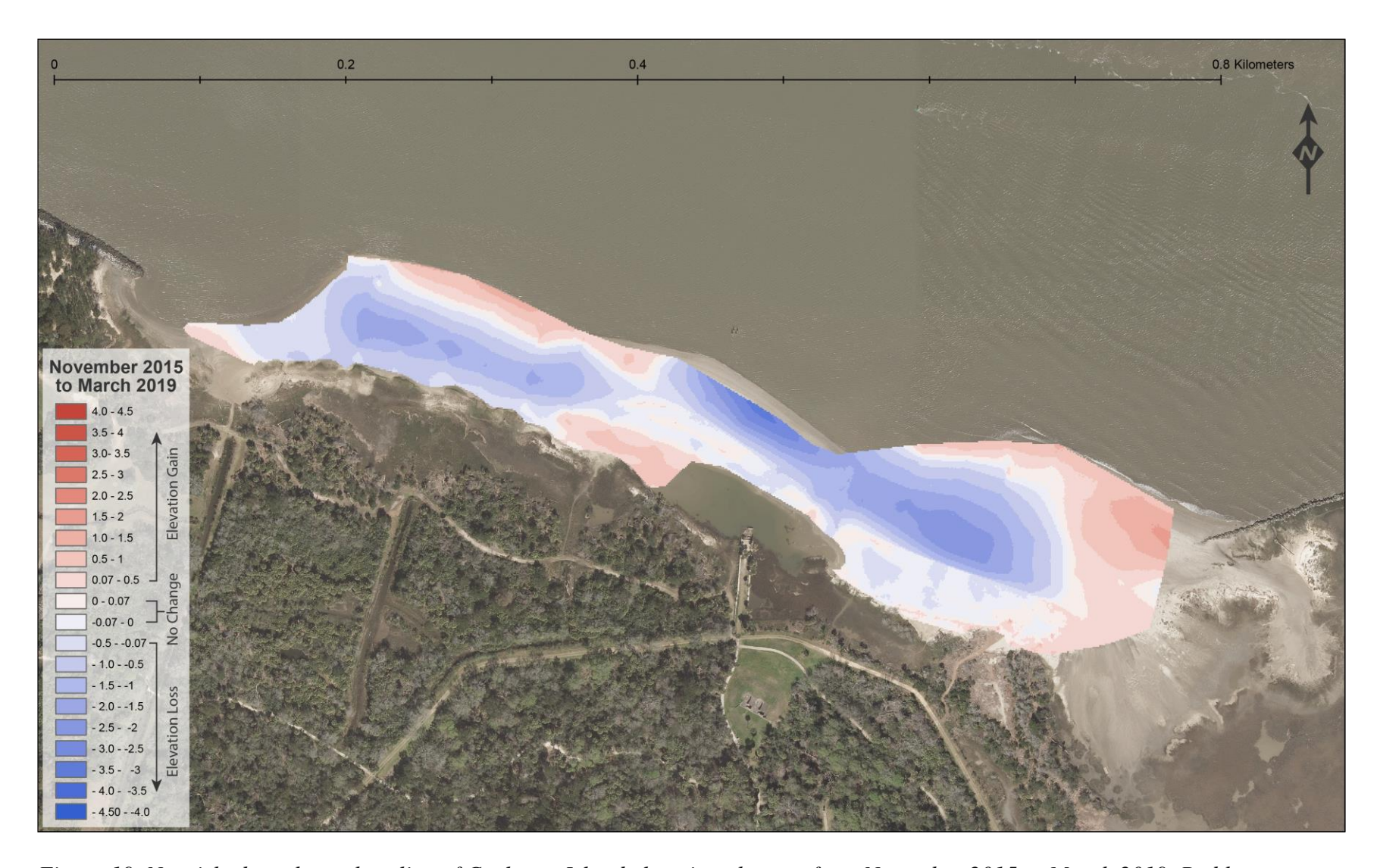


Figure 19. Nourished northern shoreline of Cockspur Island elevation changes from November 2015 to March 2019. Red hues indicate elevation gain, blue hues indicate elevation loss. More saturated colors indicate greater elevation change.



Figure 20. Map of transect locations for elevation profile comparisons on Cockspur Island's nourished northern shoreline. Transects are labeled from the western end to the eastern end of the shoreline. Transects are measured from the channelward edge to the landward edge.

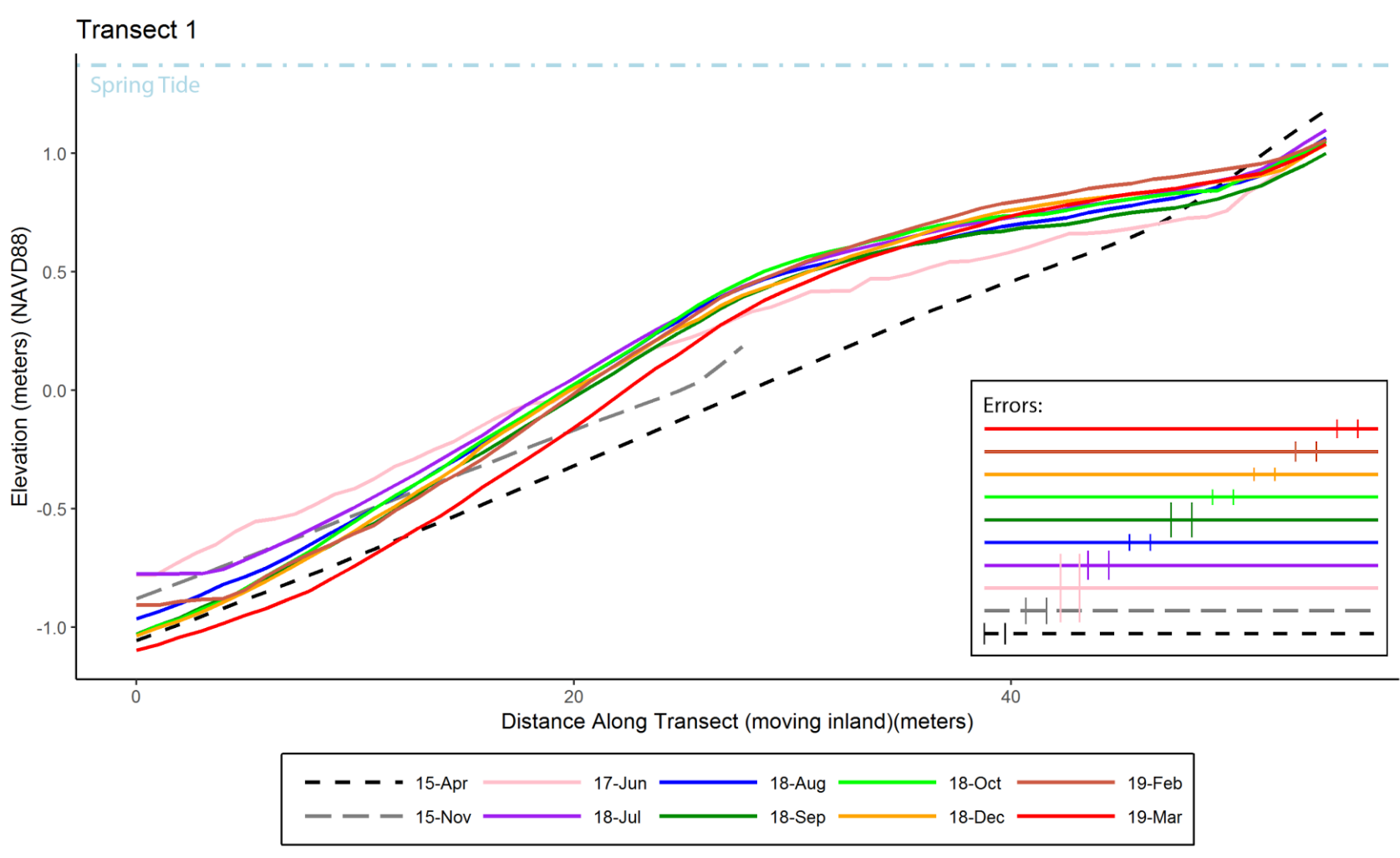


Figure 21. Elevation Profile Transect 1. Elevations are in NAVD88 datum in meters. Distance along transect is measured meters, starting at the channelward edge moving towards the landward edge of the transect. Black long dashed line indicates April 2015 elevation. Gray dashed line indicates November 2015 elevation. Pink through red lines progress in a gradient for June 2017 through March 2019 elevations. Errors are shown in the legend inset.

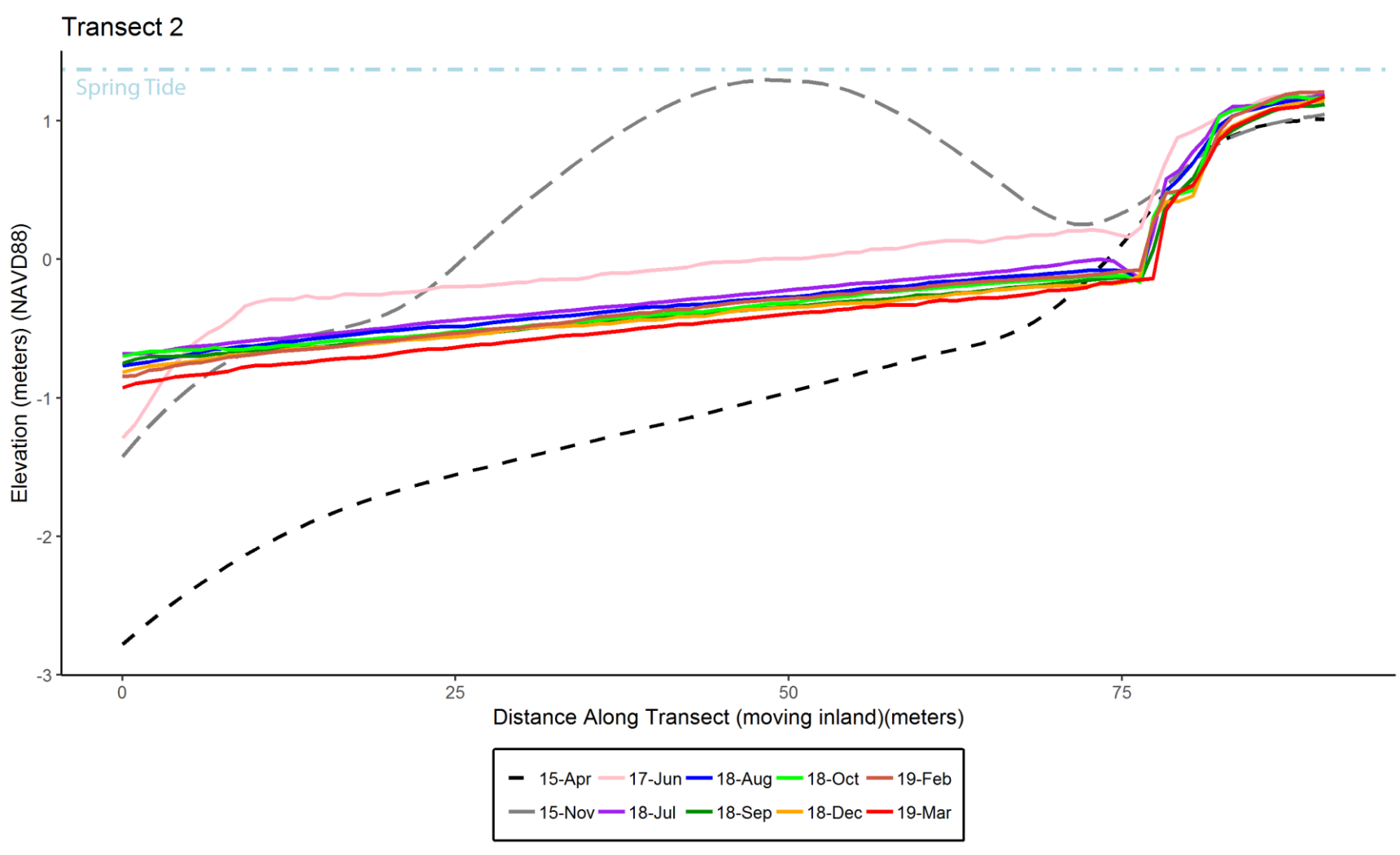


Figure 22. Elevation Profile Transect 2. Elevations are in NAVD88 datum in meters. Distance along transect is measured meters, starting at the channelward edge moving towards the landward edge of the transect. Black long dashed line indicates April 2015 elevation. Gray dashed line indicates November 2015 elevation. Pink through red lines progress in a gradient for June 2017 through March 2019 elevations.

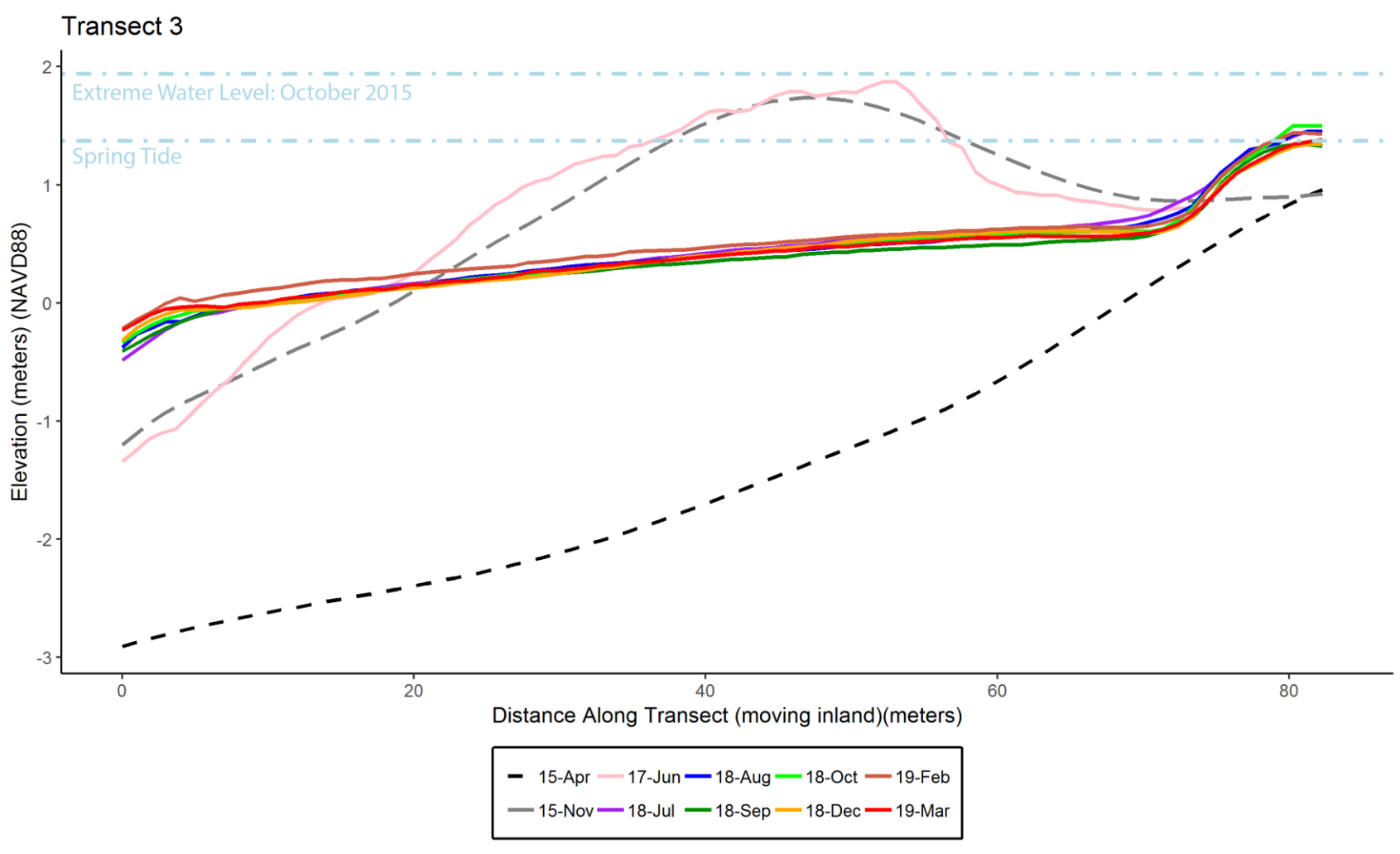


Figure 23. Elevation Profile Transect 3. Elevations are in NAVD88 datum in meters. Distance along transect is measured meters, starting at the channelward edge moving towards the landward edge of the transect. Black long dashed line indicates April 2015 elevation. Gray dashed line indicates November 2015 elevation. Pink through red lines progress in a gradient for June 2017 through March 2019 elevations.

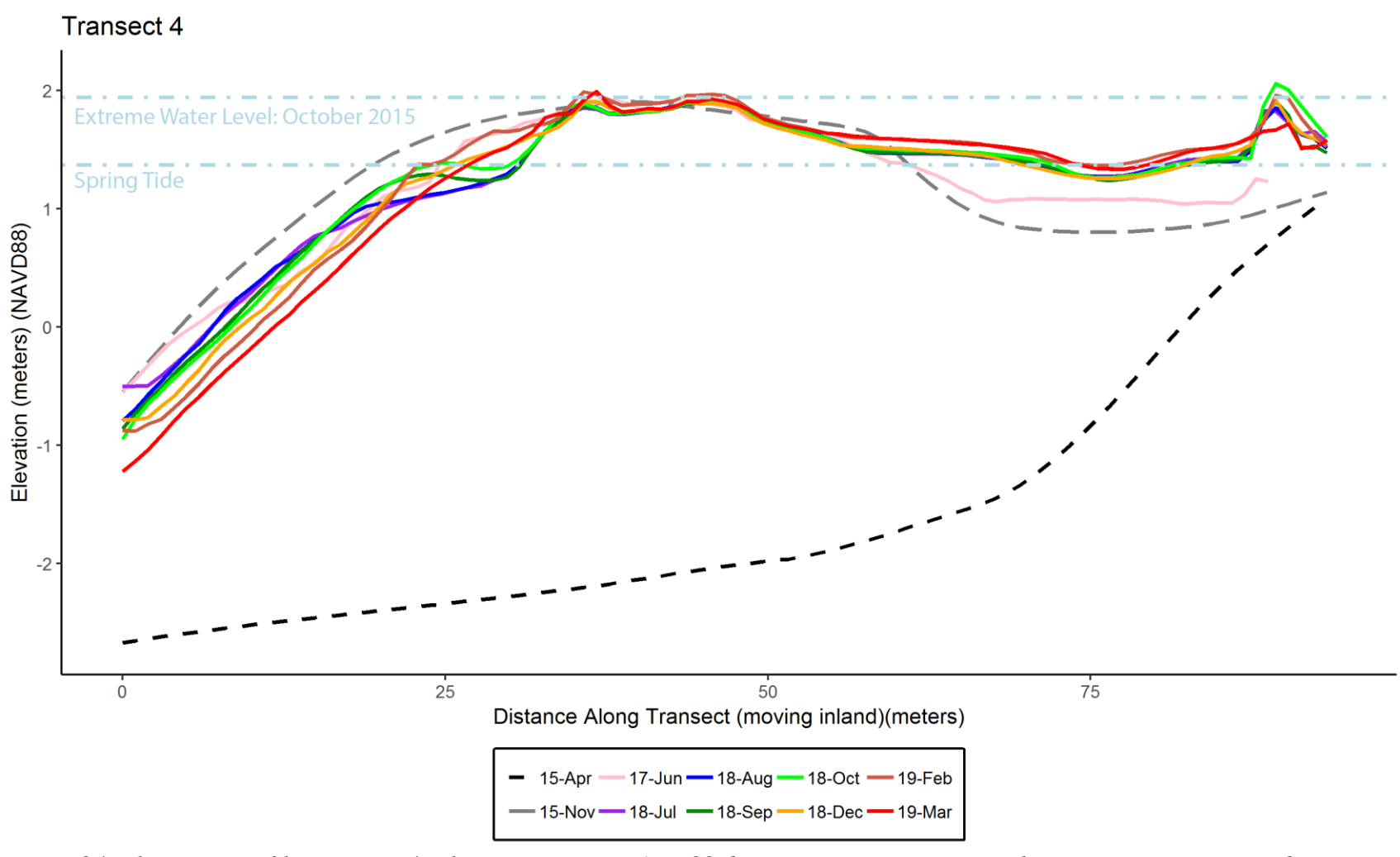


Figure 24. Elevation Profile Transect 4. Elevations are in NAVD88 datum in meters. Distance along transect is measured meters, starting at the channelward edge moving towards the landward edge of the transect. Black long dashed line indicates April 2015 elevation. Gray dashed line indicates November 2015 elevation. Pink through red lines progress in a gradient for June 2017 through March 2019 elevations.

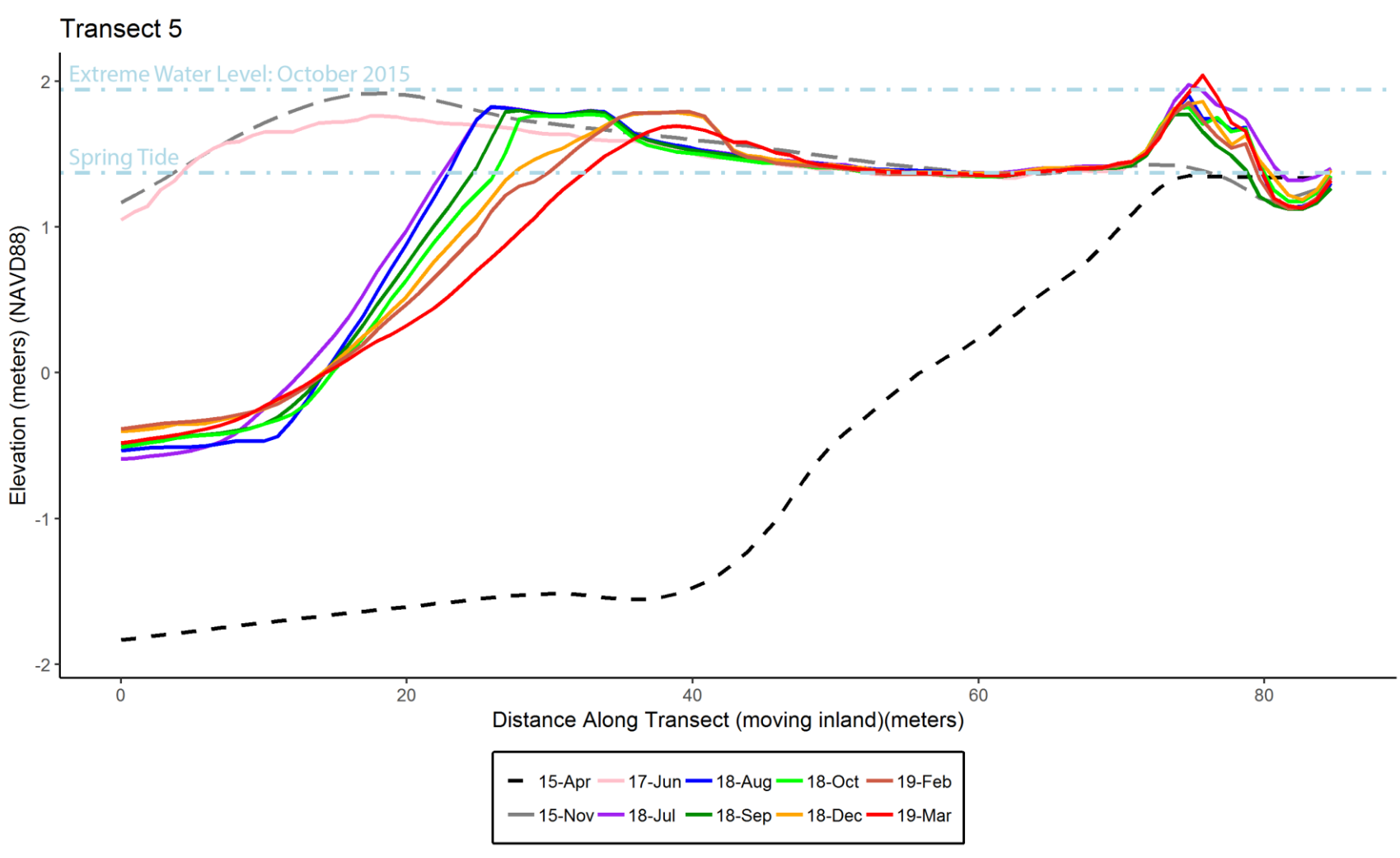


Figure 25. Elevation Profile Transect 5. Elevations are in NAVD88 datum in meters. Distance along transect is measured meters, starting at the channelward edge moving towards the landward edge of the transect. Black long dashed line indicates April 2015 elevation. Gray dashed line indicates November 2015 elevation. Pink through red lines progress in a gradient for June 2017 through March 2019 elevations.

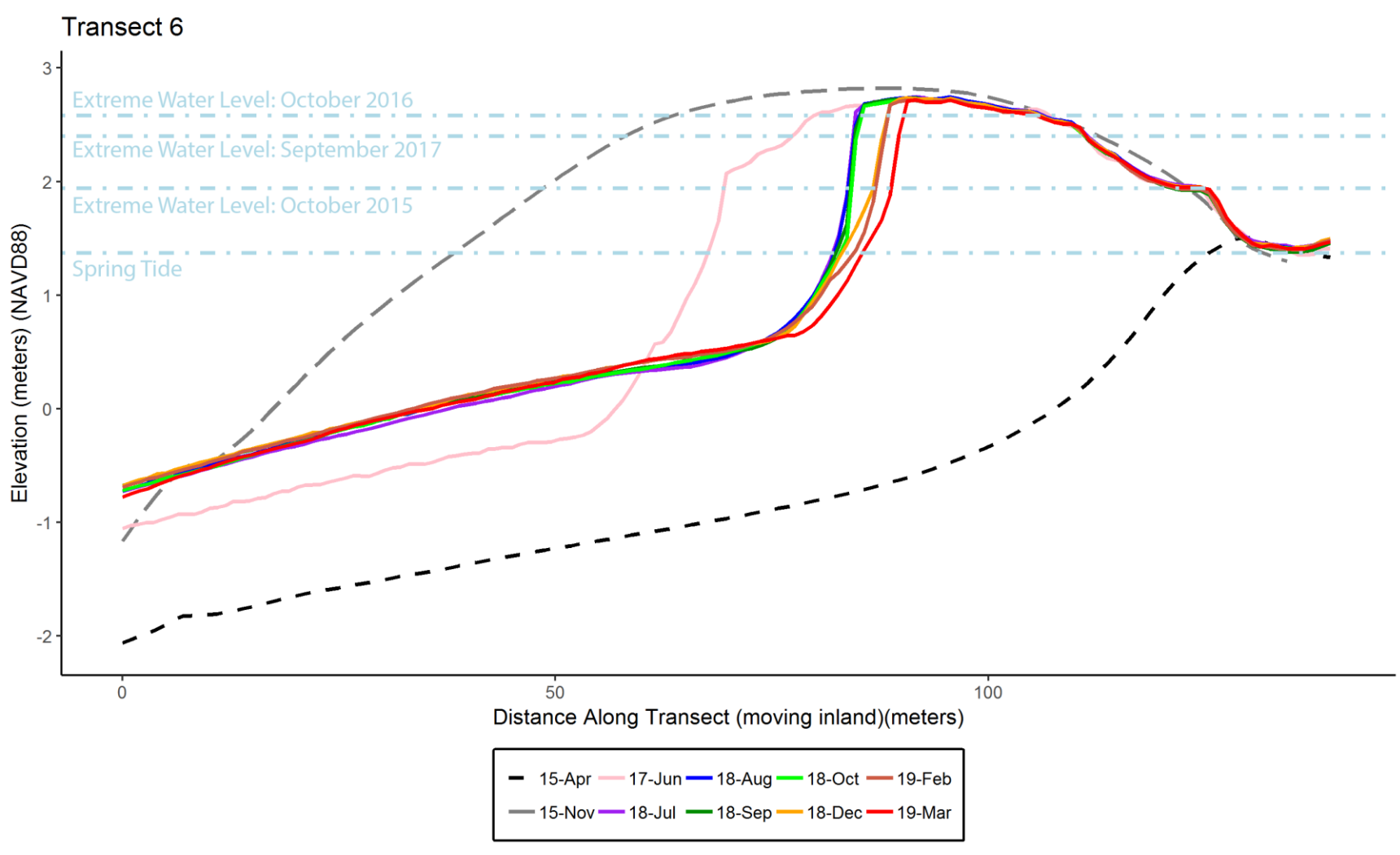


Figure 26. Elevation Profile Transect 6. Elevations are in NAVD88 datum in meters. Distance along transect is measured meters, starting at the channelward edge moving towards the landward edge of the transect. Black long dashed line indicates April 2015 elevation. Gray dashed line indicates November 2015 elevation. Pink through red lines progress in a gradient for June 2017 through March 2019 elevations.

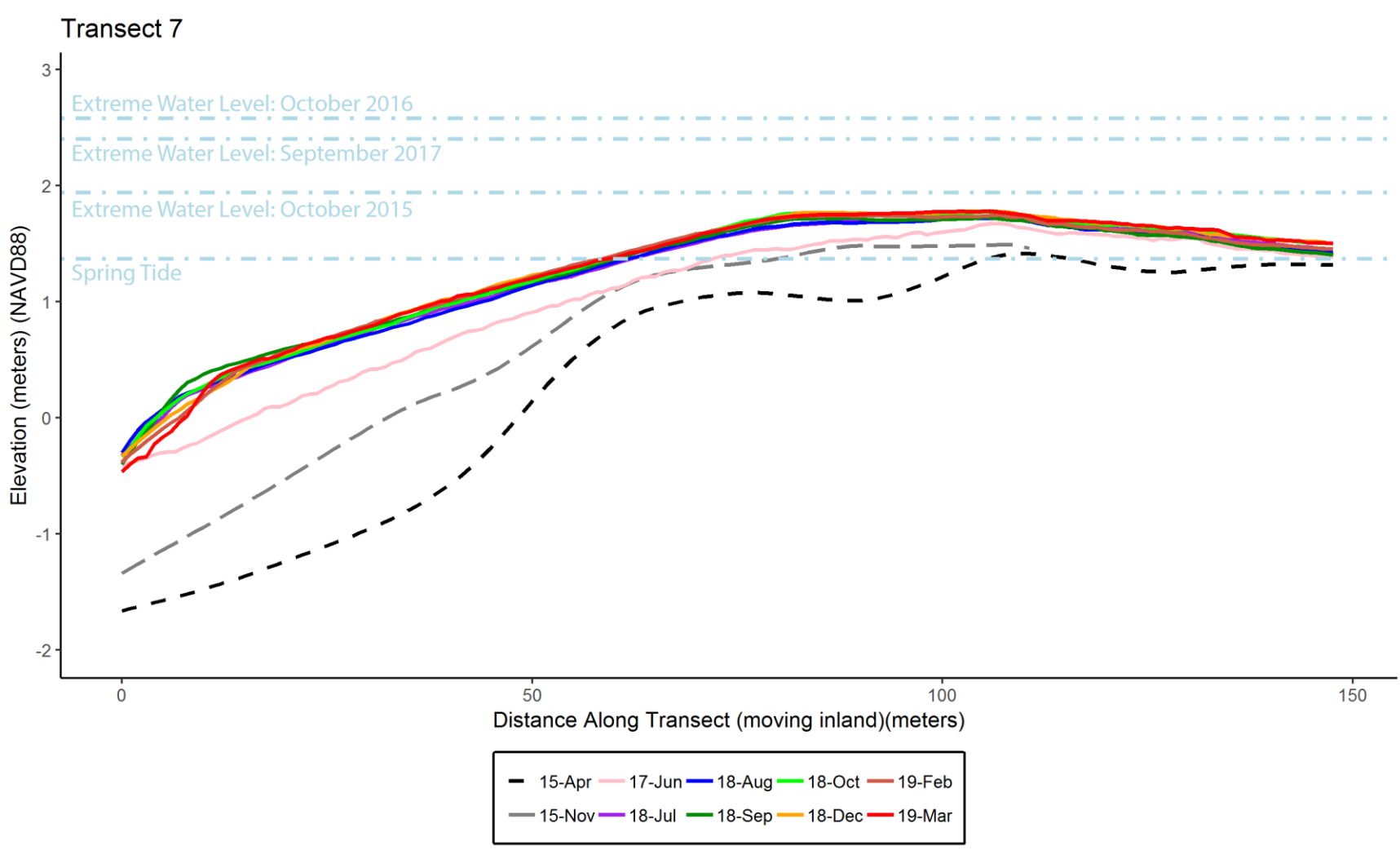


Figure 27. Elevation Profile Transect 7. Elevations are in NAVD88 datum in meters. Distance along transect is measured meters, starting at the channelward edge moving towards the landward edge of the transect. Black long dashed line indicates April 2015 elevation. Gray dashed line indicates November 2015 elevation. Pink through red lines progress in a gradient for June 2017 through March 2019 elevations.



Figure 28. Map of mean grain size, in phi, of the nourished northern shoreline on Cockspur Island, for January 2018. Light hues indicate finer sediment grain size; darker hues indicate coarser sediment grain size.



Figure 29. Map of grain size sorting of the nourished northern shoreline on Cockspur Island, for January 2018. Light hues indicate poorer sediment grain size sorting; darker hues indicate more well-sorted sediment grain size



Figure 30. Map of mean grain size, in phi, of the nourished northern shoreline on Cockspur Island, for December 2018. Light hues indicate finer sediment grain size; darker hues indicate coarser sediment grain size.



Figure 31. Map of grain size sorting of the nourished northern shoreline on Cockspur Island, for December 2018. Light hues indicate poorer sediment grain size sorting; darker hues indicate more well-sorted sediment grain size.

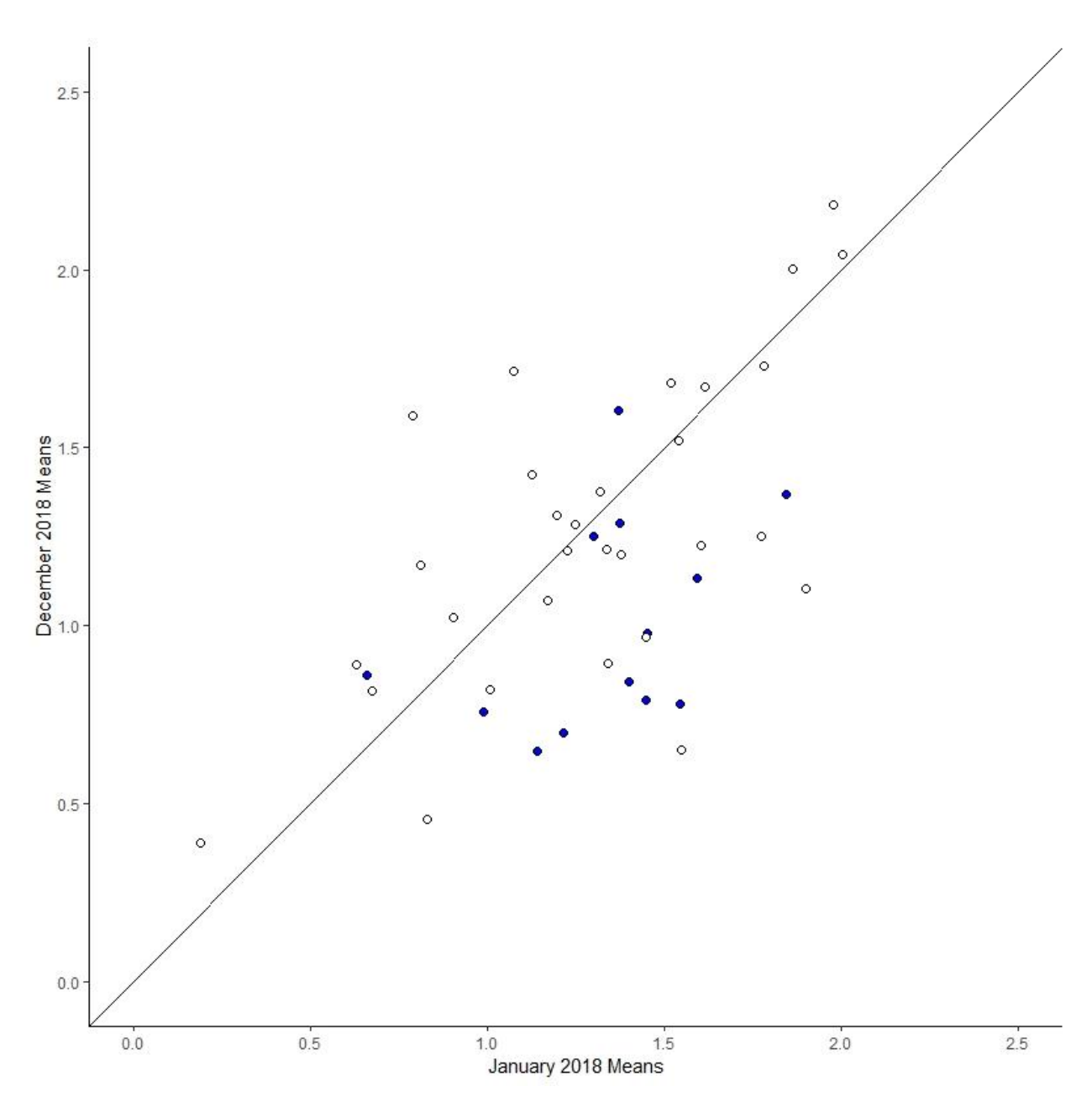


Figure 32. January 2018 sediment sample means plotted against December 2018 sediment sample means at the same location. Blue filled dots indicate samples that were located in erosional areas when comparing the July 2018 digital surface model to the December 2018 digital surface model. Samples that became coarser are located below the one-to-one sloped line, samples that became finer are above the one-to-one sloped line.



Figure 33. Map of change in Mean Grain Size, in phi, on Cockspur Island, on the nourished northern shoreline. Cool colors indicate mean grain size becoming finer, warm colors indicate mean grain size becoming coarser.



Figure 34. Map of change in Grain Size Sorting on Cockspur Island, on the nourished northern shoreline. Cool colors indicate grain size becoming less well-sorted, warm colors indicate grain size becoming more well-sorted.

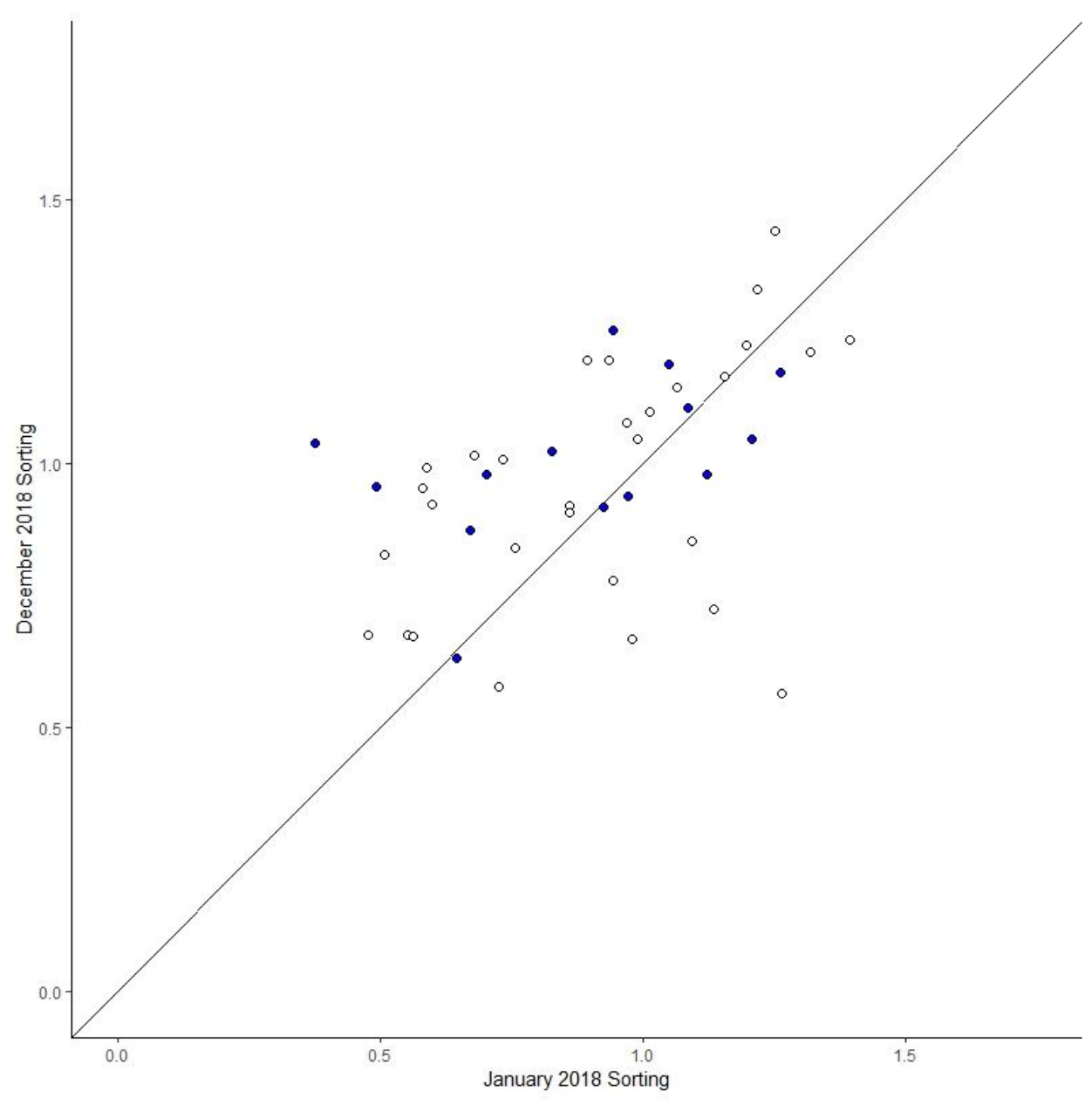


Figure 35. January 2018 sediment sample sorting values plotted against December 2018 sediment sample sorting values at the same location. Blue filled dots indicate samples that were located in erosional areas when comparing the July 2018 digital surface model to the December 2018 digital surface model. Samples that became more well sorted are located below the one-to-one sloped line, samples that became more poorly sorted are above the one-to-one sloped line.